

https://dspace.org/

Mineralogical - Geochemical Investigation of two sections across the Permian-Triassic Boundary in the Continental Realm of the Southern Karoo Basin, South Africa

Coney, Louise

2006-11-17T06:21:34Z
http://hdl.handle.net/10539/1819

Downloaded from a DSpace repository. https://dspace.org/

MINERALOGICAL - GEOCHEMICAL INVESTIGATION OF TWO SECTIONS ACROSS THE PERMIAN-TRIASSIC BOUNDARY IN THE CONTINENTAL REALM OF THE SOUTHERN KAROO BASIN, SOUTH AFRICA

Louise Coney

A dissertation submitted to the Faculty of Science, University of the Witwatersrand, Johannesburg, in fulfillment of the requirements for the degree of Master of Science.

Johannesburg, 2005

DECLARATION

I declare that this dissertation is my own, unaided work. It is being submitted for the Degree of Master of Science in the University of the Witwatersrand, Johannesburg. It has not been submitted before for any degree or examination in any other university.

_____.
Louise Coney

_____day of_____2005

Abstract

The Late Permian (251.0 ± 0.4 Ma) mass extinction is universally acknowledged as the most consequential of the five major Phanerozoic mass extinctions. More than 90% of marine species, ~70% of terrestrial vertebrates, and ~90% of plant life were lost in a very short interval. The nature of the Permian-Triassic (P-Tr) boundary and the cause of the mass extinction associated with it have been the subject of extensive international debate. Possible causes for the P-Tr extinction include asteroid/comet impact, oceanic anoxia, volcanism, methane clathrate dissociation, or combinations of these causes.

Geochemical studies of the P-Tr boundary have traditionally been focused on the marine realm, as the boundary in continental sections is typically difficult to pinpoint. One continental setting of the P-Tr boundary that has, however, received much attention is that in the main Karoo Basin, South Africa.

The Karoo Basin is a large retro-arc foreland basin which accumulated sediment from the Carboniferous (300 Ma) through to the Early Jurassic (180 Ma) in southwestern Gondwana. Mineralogical and geochemical investigations across two palaeontologically well-constrained continental P-Tr boundary sections at Commando Drift Dam and Wapadsberg in the southern Karoo Basin of South Africa have been undertaken in order to aid in our understanding of this extinction event. The Commando Drift Dam section is also constrained palaeomagnetically.

There is a change in paleosol colour across the P-Tr boundary from green-grey to red-brown, which is believed to reflect a change of oxidizing conditions at the P-Tr boundary.

Quartz grains were examined for possibly impact-produced microdeformation features, but these were not found. Iridium concentrations are below the detection limit (by instrumental neutron activation analysis) and the sections could not be evaluated as to whether any significant enrichment has taken place at the P-Tr boundary.

Major element chemical profiles are dominated by the signatures of carbonate nodular horizons in both sequences. Iron contents (and accompanying siderophile element abundances) increase across the palaeontologically-defined P-Tr boundary, followed by a decrease thereafter. The major element concentrations, together with the effects of weathering, largely control trace element distribution.

Carbon isotopic results from the Commando Drift Dam section show a gradual decrease in values before the P-Tr boundary, with a larger negative excursion at the P-Tr boundary. Above the boundary, gradual recovery to initial ratios is observed, followed by another gradual decrease in values to the palaeomagnetically defined boundary.

No evidence supporting an extraterrestrial impact extinction mechanism has been found. Rather, the carbon isotope data from this study support two gradual palaeoclimatic changes separated by a sudden change in the carbon isotopic content of the atmosphere. The size and nature of these excursions support the addition of large amounts of anoxic material into the atmosphere. This is proposed to have been caused by the multiple influx of carbon dioxide, methane and other greenhouse gases at various times and by different mechanisms. Such a release of carbon dioxide, methane and other greenhouse gases could have been caused by the coincident volcanic event (the formation of the Siberian Traps) and the episodic release of methane clathrates.

DEDICATION

For my parents, Marylyn and Ron Coney,
who have made everything possible.

Acknowledgements

I would like to thank the following individuals for help, motivation and support in this project.

Firstly, funding has been generously provided by the following sponsors:
The Palaeo-Anthropology Scientific Trust; the National Research Foundation; the Geological Society of South Africa; and the Barringer Family Fund for Meteorite Impact Research. Without this funding, this project would not have been realized.

Prof. Uwe Reimold: not only have you been a fantastic "hands-on" supervisor, but also a mentor and a friend. Dr John Hancox: thank you for the mental stimulation, particularly in the field. John has really taught me the meaning of living and breathing my project at all times of the day and night!

Prof. Christian Koeberl: who provided unparalleled assistance and instruction in INAA analysis and stable isotope geochemistry. I would like to thank both you and Dona for being the perfect hosts to my two months in Vienna, Austria.

Dr Bernd Bodiselitsch: who analysed my samples for both sulphur and carbon in Vienna.

Mrs Sharon Turner and Mr Bheki Makhatini, who assisted in preparing and analyzing the samples by X-Ray Fluorescence and X-Ray Diffraction.

Mr Alex Mathebula who made my thin sections.

Mr Mitch Miles and Mr Matt Kitching for technical assistance.

Prof. Kevin Burke and Dr Peter Ward provided some interesting input into the project at the Lunar and Planetary Science Conference.

The Impact Geologists: Dr Cristiano Lana, Martin Tuchscherer and Frank Wieland.

The other Geologists: Libby Sharman Harris, Robyn Pickering, Lynnette Greyling, Tom Clarke, Charlie Seabrook, James Roberts and Richard Hornsey.

Fiona Stevens, who was a better office-mate than anyone else could have been.

My boyfriend, Luke Longridge, who kept me sane in the last 6 months of this project.
Thank you.

CONTENTS **PAGE**

DECLARATION……ii
ABSTRACT……...iii
ACKNOWLEDGEMENTS……..……..vi
LIST OF FIGURES…….…….…...x
LIST OF TABLES……....xvi

CHAPTER ONE – INTRODUCTION

1.1 Background……1
1.1.1 The "Big Five" Phanerozoic Mass Extinctions……..2
1.2 Proposed Causes of the P-Tr Mass Extinction Event…….....9
1.2.1 Asteroid/Comet Impact……..10
1.2.2 Oceanic Anoxia or Overturn……..14
1.2.3 Volcanism……..15
1.2.4 Methane Clathrate Dissociation Events…….17
1.2.5 Synergistic Mechanisms……19
1.3 Non-marine P-Tr Sections…….....22
1.3.1 The Karoo Basin……24
1.3.2 Placement of the P-Tr Boundary in the Karoo Basin……26
1.3.3 Previous Work on the P-Tr Boundary in the Karoo Basin……..33
1.4 Objectives of this Study……...…….....36

CHAPTER TWO – METHODOLOGY

2.1 Sample Collection……39
2.2 Thin Section Preparation……..39
2.3 Geochemical Analyses…….39
2.3.1 X-Ray Fluorescence Spectrometry……....40
2.3.2 Instrumental Neutron Activation Analysis……....40

2.3.3 Stable Isotope Analysis……..47
2.3.4 X-Ray Diffraction…….52
2.3.5 Cathodoluminescence……....52

CHAPTER THREE – RESULTS

3.1 Stratigraphy and Sedimentology……..54
3.1.1 The Commando Drift Dam Section……..54
3.1.2 The Wapadsberg Section……..56
3.2 Petrography……..56
3.3 Geochemistry……...67
3.3.1 Major Elements……..67
3.3.2 Trace Elements……...75
3.4 Stable Isotope Analysis……99
3.4.1 Carbon Isotopic Ratios……...99

CHAPTER FOUR – DISCUSSION AND CONCLUSION

4.1 Stratigraphy and Sedimentology……107
4.2 Petrography……111
4.3 Major and Trace Element Geochemistry……...111
4.3.1 The Commando Drift Dam Section…….112
4.3.2 The Wapadsberg Section…….113
4.3.3 Comparison of the Geochemical Data for Different Sections in the Karoo Basin…….....115
4.3.4 Palaeoclimatic Change Evaluated Using Geochemistry……..….117
4.4 Carbon Isotope Geochemistry……119
4.5 Evaluation of Previous Models of the Extinction Event……121
4.6 Conclusions……125

CHAPTER FIVE – REFERENCES

6. APPENDICES

Appendix 1: Commando Drift Dam Section: Geochemical Data

Appendix 2: Wapadsberg Section: Geochemical Data

Appendix 3: Conference Abstracts Related to the Project

LIST OF FIGURES

Figure 1: Summary of the temporal distribution of marine fauna through the Phanerozoic. The "Big Five" mass extinctions are denoted: A: Late Ordovician; B: Late Devonian; C: Late Permian; D: Late Triassic and E: Late Cretaceous (modified after: Hallam and Wignall, 1997)……..……2

Figure 2: Pangaea, at 251 Ma, showing the position of the Karoo Basin (grey) (modified after: de Wit et al., 2002)……..……...25

Figure 3: The Karoo Basin, South Africa, showing study sites of the Permian-Triassic Boundary (in white) (modified after: Catuneanu et al., 1998). Studies were undertaken by the following authors:
Senekal: Hancox et al., 2002; Maruoka et al., 2003; de Kock, 2003. Bethulie: Kirschvink and Ward, 1998; MacLeod et al., 2000; Ward et al., 2000, 2005; Smith and Ward, 2001; de Wit et al., 2002. Injusiti: Detailed studies still remain to be undertaken. Lootsberg: Smith, 1995; Kirschvink and Ward, 1998; Ward et al., 2000; Smith and Ward, 2001; de Wit et al., 2002; Retallack et al., 2003; Ward et al., 2005. Carlton Heights: Steiner et al., 2003; Ward et al., 2005. Wapadsberg: Ward et al., 2000, 2005; this study. Commando Drift Dam: de Kock, 2003; Ward et al., 2005; this study.....27

Figure 4: Stratigraphic cross-section from the southwest to the northeast of the Karoo Basin (modified after: Catuneanu et al., 1998).....28

Figure 5: Stratigraphic column of the Karoo Supergroup, showing the position of the P-Tr boundary (modified after: Catuneanu et al., 1998)…….....28

Figure 6: The palaeontological signature of the Karoo Basin, South Africa (from: Ward et al., 2005). P-Tr palaeontological boundary located at 0 m. The magnetostratigraphic results of De Kock (2003) are included (black indicates normal polarity, grey indicates unknown polarity and white indicates reversed polarity). The bold line at 0 m indicates the uppermost occurrence of *Dicynodon lacerticeps.* The second line at ~30 m indicates the base of the Katberg Formation, and the position of the fungal spike of Steiner et al. (2003)…....29

Figure 7: Potential placements of the P-Tr boundary in the Karoo Basin, South Africa……...……....32

Figure 8: The carbon isotopic signature from Bethulie (from: MacLeod et al., 2000)…….……...…35

Figure 9: Correlation between the carbon isotopic signatures in the marine realm (from: Krull et al., 2004) – Meishan (left; redrawn from Jin et al., 2000) and Heping (right; Krull et al., 2004). The following events are noted: (1) indicates the extinction event; (2) indicates a pronounced negative $\delta^{13}C_{carb}$ excursion; (3) indicates recovery (carb = carbonate)…….....35

Figure 10: Commando Drift Dam section, showing the position of the P-Tr boundary. The boundary is marked by the LAD *Dicynodon* and the first appearance of the red-brown and maroon mudstones of the Palingkloof Member. The Elandsberg Member is characterized by dark grey to greenish-grey mudstones. The Katberg Formation consists of a multistoried conglomeratic sandstone.....…….38

Figure 11: Correlation of XRF and INAA results: **a:** Commando Drift Dam samples: Fe (wt%); **b:** Commando Drift Dam samples: K (wt%); **c**: Wapadsberg: Na (wt%)…….....……..46

Figure 12: The lithological and palaeontological contact of the P-Tr boundary at the Commando Drift Dam section. The contact is sharp. The green-grey mudstones of the Elandsberg Member are overlain by the red-brown mudstones of the Palingkloof Member (chisel for scale ~20 cm long)…….……55

Figure 13: Commando Drift Dam Section: Stratigraphic column. Sample numbers (PCD) are shown on the left side of the column, with distances from the initial sample (at the bottom of the sequence) shown on the right side of the column. The P-Tr boundary (based on lithological as well as palaeontological data) and de Kock's (2003) palaeomagnetic boundary are also marked. Note that the section extends over 12.4 m on a 60^{o} layered slope (10.4 m in absolute height), but is represented vertically…….……...57

Figure 14: Wapadsberg Section: Stratigraphic column. Sample numbers (PW) are shown on the left side of the column, with distances from the initial sample (at the bottom of the sequence) shown on the right side of the column. The P-Tr boundary (based on lithological as well as palaeontological data) is indicated. Note that the section extends over 9.07 m on a 60^{o} layered slope (7.85 m in absolute height), but is represented vertically ……..…...59

Figure 15: **a:** The photomicrograph shows the green-grey mudstones (PCD 16; width of field of view: 600 μm; plane polarised light). **b:** The photomicrograph shows the red-brown mudstones (PCD 27; width of field of view: 600 μm; plane polarised light)……60

Figure 16: **a:** Photomicrograph showing the fine grained clastic component of the boundary mudstone (PCD 16; width of field of view: 1.4 mm; crossed polarised light). **b:** The photomicrograph shows the

homogeneity of the mudstones 14 cm above the boundary (PCD 29; width of field of view: 1.4 mm; plane polarised light)...…….64

Figure 17: Photomicrographs of a sample from a carbonate nodular horizon: widths of field of view: 1.4 mm. **a:** Plane polarized light. **b:** The application of cathodoluminescence only shows the presence of calcite, yellow-orange in colour. The texture of the carbonate nodular horizon indicates possible hydrothermal activity…….…65

Figure 18: **a:** The photomicrograph shows a typical quartz grain (ca. 10 µm in diameter) from a boundary sediment sample (PCD 16; width of field of view: 0.3 mm; crossed polarized light). **b:** The photomicrograph shows a quartz grain in rocks from the Vredefort impact structure, containing decorated planar deformation features (PDF's; plane polarised light, from: Leroux et al., 1994; in Gibson and Reimold, 2001). No such features were found in quartz grains from the P-Tr boundary..…….....66

Figure 19: Major element abundance patterns for the Commando Drift Dam section. All concentrations are in wt%. Red symbols indicate samples at the palaeomagnetic boundary…...…….……...69

Figure 20: Molecular weathering ratios for the Commando Drift Dam section……..……..70

Figure 21: Major element abundance patterns for the Wapadsberg section. All concentrations are in wt%.....72

Figure 22: Molecular weathering ratios for the Wapadsberg section…...…...74

Figure 23: Lithophile trace element abundance patterns (data in ppm) for the Commando Drift Dam section (compared to the SiO_2 pattern). Red symbols indicate the carbonate nodular horizons……..76

Figure 24: Siderophile trace element abundance patterns (data in ppm and ppb) for the Commando Drift Dam section (compared to the Fe_2O_3 pattern). Red symbols indicate the carbonate nodular horizons……...……...80

Figure 25: Chalcophile trace element abundance patterns (data in ppm) for the Commando Drift Dam section (compared to the S pattern). Red symbols indicate the carbonate nodular horizons……...…...…82

Figure 26: Rare earth element abundance patterns for selected samples from the Commando Drift Dam section (data normalized after Taylor and McLennan, 1985)……..……..85

Figure 27: La/Th ratios for the Commando Drift Dam section……...86

Figure 28: La_N/Yb_N and La/Lu ratios for the Commando Drift Dam section……..……..87

Figure 29: Lithophile trace element abundance patterns (data in ppm) for the Wapadsberg section (compared to the SiO_2 pattern). Red symbols indicate the carbonate nodular horizons……....90

Figure 30: Siderophile trace element abundance patterns (data in ppm) for the Wapadsberg section (compared to the Fe_2O_3 pattern). Red symbols indicate the carbonate nodular horizons……93

Figure 31: Chalcophile trace element abundance patterns (data in ppm) for the Wapadsberg section (compared to the S pattern). Red symbols indicate the carbonate nodular horizons……..……95

Figure 32: Rare earth element abundance patterns for selected samples from the Wapadsberg section (data normalized after Taylor and McLennan, 1985).....96

Figure 33: La/Th ratios for the Wapadsberg section……..……97

Figure 34: La_N/Yb_N and La/Lu ratios for the Wapadsberg section…….....98

Figure 35: Commando Drift Dam stratigraphic section: Initial results for bulk $\delta^{13}C$. Error bars shown represent 1σ standard deviations...…….104

Figure 36: Commando Drift Dam stratigraphic section: Full results for bulk $\delta^{13}C$. Error bars shown represent 1σ standard deviations..……..104

Figure 37: Commando Drift Dam stratigraphic section: Results for organic $\delta^{13}C$. Error bars shown represent 1σ standard deviations...…….105

Figure 38: Commando Drift Dam stratigraphic section: Apparent inorganic $\delta^{13}C$ variation, calculated as $\delta^{13}C_{bulk} - \delta^{13}C_{Org}$…….....……..106

Figure 39: Comparison of the stratigraphy of P-Tr sections in the southern Karoo Basin (modified after: Ward et al., 2005). Green indicates the green-grey mudstones; red indicates the red-brown mudstones. White indicates the sedimentological features of the sandstones and siltstones. Vertical scale in metres……109

Figure 40: Comparison of the carbon isotope signatures for **A** Lootsberg Pass (de Wit et al., 2002; the question marks represent the possible

positions of the P-Tr boundary, as hypothesized by these authors), and **B** Commando Drift Dam (this study)…….....…...122

LIST OF TABLES

Table 1: Critical assessment of the various hypotheses for the cause of the P-Tr mass extinction…….…….23

Table 2: Analytical precision for major element analysis by XRF (S. Turner, pers. comm., 2004)……...……..41

Table 3: Analytical precision for trace element analysis by XRF (S. Turner, pers. comm., 2004). LLD = Lower Limit of Detection…..…..….41

Table 4: Typical precision values for elements in the Vienna INAA Lab (C. Koeberl, pers. comm., 2004) (all elemental abundances in ppm, unless otherwise stated)…….....45

Table 5: Descriptions of the different lithologies in the Commando Drift Dam and Wapadsberg sections……..61

Table 6: Sulphur concentrations for both the Commando Drift Dam and the Wapadsberg sections, as determined by XRF. Data in wt%.....101

Table 7: Bulk carbon isotopic data for samples from the Commando Drift Dam section. Errors are 1σ. Data are given as $\delta^{13}C = \{(^{13}C/^{12}C$ sample)/($^{13}C/^{12}C$ standard) – 1} x 1000), expressed as per mil of the Vienna Pee Dee Belemnite standard (‰ PDB). Carbon concentrations in wt% are also shown, with standard deviations based on duplicate analyses ……...……...102

Table 8: Organic carbon isotopic data from the Commando Drift Dam section. Errors are 1σ. Data are given as $\delta^{13}C_{org}$, expressed as per mil of the Vienna Pee Dee Belemnite standard (‰ PDB). Carbon

concentrations in wt% are also shown, with standard deviations based on duplicate analyses…….103

Table 9: Summary of geochemical changes across the palaeontological and palaeomagentic boundaries for the Commando Drift Dam and the Wapadsberg sections……....116

CHAPTER ONE: INTRODUCTION

This project is aimed at characterisation of the geochemical and petrographic signature of the sequences across two continental Permian-Triassic (P-Tr) boundary sections in the southern Karoo Basin, South Africa. It represents an attempt to contribute to the ongoing debate about the cause of the P-Tr mass extinction.

1.1 Background

Sepkoski (1986) defined mass extinctions as "any substantial increase in the amount of extinction (that is, lineage termination) suffered by more than one geographically widespread higher taxon, during a relatively short interval of geological time, resulting in at least a temporal decline in their standing diversity". A number of such mass extinction events have been documented throughout geological history; the "Big Five" Phanerozoic marine mass extinctions (Raup and Sepkoski, 1982; Fig. 1) occurred during the: (1) Late Ordovician (Ordovician-Silurian); (2) Late Devonian (Devonian-Carboniferous); (3) Late Permian (Permian-Triassic); (4) Late Triassic (Triassic-Jurassic); and (5) Late Cretaceous (Cretaceous-Tertiary). The P-Tr mass extinction is the most severe of these events (Fig. 1) and has been termed the "mother of all mass extinctions" (Erwin, 1993), in that more than 90% of marine species, ~70% of terrestrial vertebrates, and ~90% of plant life were lost (Hallam and Wignall, 1997) over an extremely short interval of time – possibly 10^4 to 10^5 years (Bowring et al., 1998). The cause of this extinction event has been the subject of major debate (e.g., Renne et al., 1995; Erwin, 1996; Wignall and Twitchett, 1996; Isozaki, 1997; Retallack et al., 1998; Ward et al., 2000; Becker et al., 2001, 2004; Reichow et al., 2002; de Wit et al., 2002; Weidlich et al., 2003; Retallack et al., 2003; Maruoka et al., 2003; Petaev et al., 2004; Chapman, 2005). Correlation of the timing of the mass extinction in the marine and the non-marine realms has proved difficult, especially as well documented continental sections are rare. One P-Tr

boundary section in the continental realm that has been fairly well documented is that in the Karoo Basin of South Africa (e.g., Smith, 1995; Ward et al., 2000; Smith and Ward, 2001; Hancox et al., 2002; de Wit et al., 2002; Retallack et al., 2003; Maruoka et al., 2003; Ward et al., 2005).

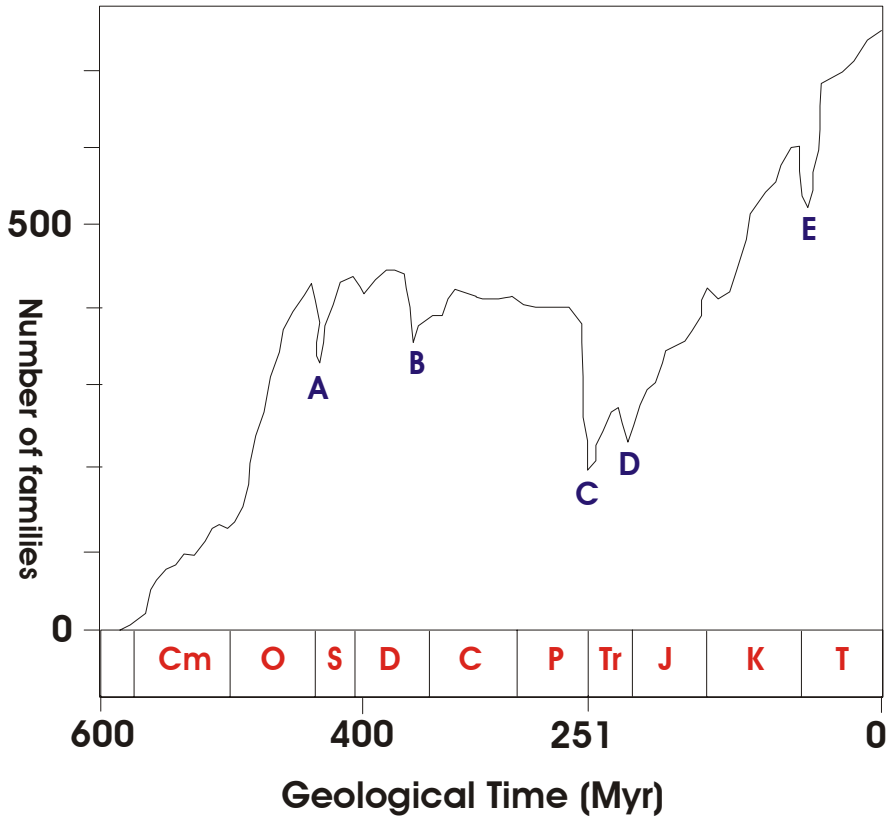


Figure 1: *Summary of the temporal distribution of marine fauna through the Phanerozoic. The "Big Five" mass extinctions are denoted: A: Late Ordovician; B: Late Devonian; C: Late Permian; D: Late Triassic and E: Late Cretaceous (modified after: Hallam and Wignall, 1997).*

1.1.1 The "Big Five" Phanerozoic Mass Extinctions

The study of mass extinctions was initiated by Georges Cuvier in the 1800s, who noted disappearances of certain species (in particular the mammoth and giant sloth) from the biological record (Hallam and Wignall, 1997). He argued for dramatic changes in fauna and, in effect, argued for catastrophic theory – that catastrophic events could radically change the distribution of fauna and flora. His theories were rejected by

many geologists at the time, who favoured gradualism and supported the view of Charles Darwin, who had stated that dramatic faunal changes reflected major stratigraphic hiatus (see Hallam and Wignall, 1997). Since this time much work has been undertaken on various aspects of the Phanerozoic extinction events, and the most recent of these are reviewed below.

1.1.1.1 The Late Ordovician Extinction Event

The Late Ordovician extinction event (443.7 ± 1.5 Ma; Gradstein et al., 2004) was the first major Phanerozoic extinction event, with 57% of genera and 25% of families becoming extinct (Hallam and Wignall, 1997). Marine organisms were particularly affected (Fig. 1). The extinction event has been hypothesized to be the product of climate and environmental changes related to periods of glaciation and deglaciation, and coincident relative sea-level changes (Brenchley and Marshall, 1999; Berry et al., 2002). Carbon isotope excursions have been recorded with cycles of sea-level change (Berry et al., 2002). Possible causes of the glaciation have been discussed (Brenchley and Marshall, 1999; Kump et al., 1999), but no consensus has been reached.

1.1.1.2 The Late Devonian Extinction Events

During the Late Devonian (359.2 ± 2.5 Ma; Gradstein et al., 2004), a number of sea-level changes and catastrophic events occured, at a number of different geological boundaries. The 18 sea-level changes that took place have been related to two mass extinction events (the Frasnian-Famennian mass extinction and the Devonian-Carboniferous mass extinction), one of which has been related to a meteorite impact (Sandberg et al., 2002). The Frasnian-Fammennian mass extinction took place at 374.5 ± 2.7 Ma (Gradstein et al., 2004). A number of species were affected by the extinction events, including brachiopods, bryozoa, corals and trilobites (Hallam and Wignall, 1997). These sea-level rises were proposed by Sandberg et al. (2002) to have been temporally coincident with a series of comet showers (the Alamo Impact in Nevada, and the

Amönau event in Germany). Sandberg et al. (2002) stated that there is the coincidence of impacts and comet showers with sea-level rises, but that the mass extinctions occurred during sea-level falls. A number of impact craters of relevant age have been documented [e.g., the Siljan (65-75 km diameter, 377 ± 2 Ma) and the Flynn Creek (3.6 km diameter, 360 Ma) impacts]. Reimold et al. (2005) presented new Ar-Ar laser spot and laser step heating ages (377 ± 2 Ma) for several melt breccias from the Siljan structure, which correlate with the age of the Frasnian-Famennian boundary. However, they query whether an impact causing an 80 km impact structure would be of a sufficient magnitude to cause global environmental catastrophe.

Global sea-level changes related to glaciation are the primary candidates as causes for the Late Devonian mass extinction, but the exact process that led to these changes is still under debate.

1.1.1.3 The Late Permian Extinction Event

Initial research, focused on the P-Tr extinction event, took place in the 1950s by Schindewolf (1954), who studied this mass extinction primarily from a palaeontological perspective. The P-Tr mass extinction (251.0 ± 0.4 Ma; Bowring et al., 1998) is universally acknowledged as the most consequential of the five "major" Phanerozoic mass extinctions (e.g., Erwin, 1993, 1994) and much study of this extinction event has been undertaken (Erwin et al., 2002, and references therein). There is some debate as to the timing of this event, and whether the marine and non-marine extinctions were contemporaneous (e.g., Steiner et al., 2003). More recently a date for the mass extinction of 252.6 ± 0.2 Ma has been proposed (Mundil et al., 2004), but the Bowring et al. (1998) date is generally accepted for the P-Tr boundary. Bowring et al. (1998) showed that the mass extinction in the marine realm occurred over a period of less than 500 000 years. This is confirmed by the appearance and disappearance of taxa around the P-Tr boundary (Jin et al., 2000). Marine sections crossing the P-Tr extinction event have been well documented in

terms of geochemistry, stratigraphy, palaeomagnetic and isotopic signatures, and a Global Stratotype Section and Point (GSSP) exists at Meishan, China (Yang et al., 1996; Jin et al., 2000; Erwin, 2000). A significant negative carbon isotope excursion has been documented at the marine section (Yin et al., 1996; Krull et al., 2000; Twitchett et al., 2001), and this has been used, together with magnetostratigraphy, to correlate marine P-Tr sections. Far less, however, is known about the pattern and duration of extinction among non-marine organisms (Benton et al., 2004). The event in non-marine sections is hypothesized to be relatively sudden, probably of a 50 000 year duration or less, and, hence, is considered a catastrophic one (Smith and Ward, 2001).

1.1.1.4 The Late Triassic Extinction Event

The Late Triassic extinction event occured at 199.6 ± 0.6 Ma ago (Gradstein et al., 2004) and was as profound as the Cretaceous-Tertiary (K-T) mass extinction. Tanner et al. (2004) questioned this extinction event as a mass extinction; they stated that many groups were already in decline throughout the Late Triassic. However, this extinction event is generally accepted as one of the "Big Five". Invertebrate fauna was most severely affected, and on land, non-dinosaurian tetrapods were largely replaced by the dinosaurs (Hallam and Wignall, 1997).

Negative carbon and nitrogen isotope excursions have been documented at the boundary (Sephton et al., 2002). This has been used to propose that the event was caused by multiple mechanisms, including the large-scale emission of carbon dioxide and the dissociation of methane clathrates, and change in nitrogen contents caused by a change in the nitrogen-fixing cyanobacteria populations (Sephton et al., 2002). In the many exposed rift basins of the Atlantic, the boundary is marked by abrupt floral and faunal changes, including a fern spike (Fowell et al., 1994; see Olsen et al., 2002).

There are also similarities with the Late Cretaceous mass extinction (the isotope excursions, coincident faunal spike), and many workers have looked for evidence of meteorite impact (e.g., Dietz, 1986; Olsen et al., 2002). A modest Iridium (Ir) anomaly has been found in the Newark Basin in North America (Olsen et al., 2002), which is associated with a fern spike. However, no shocked quartz has been found. Olsen et al. (2002) concluded that a non-impact cause for the mass extinction cannot be ruled out.

There is also the temporal coincidence of the Triassic-Jurassic (Tr-J) boundary and the Central Atlantic Magmatic Province, a large volcanic event. A problem with the volcanic hypothesis as the sole origin of the Tr-J mass extinction is that the flood basalts have been found to either post-date (Olsen et al., 2002) or pre-date (Olsen, 1999) the biological extinctions. This indicates that it is possible that at least a part of the Central Atlantic Magmatic Province could have been emplaced just before, or just after the extinction event. Pálfy et al. (2002) concluded that the isotope records and age of the event are compatible with volcanically-induced global environmental change, which could have been the initial cause of the extinction. The compilation of data suggests that the Late Triassic event coincided with the peak of the Central Atlantic Magmatic Province, and that terrestrial floral and faunal extinctions may have preceded the marine extinctions. Pálfy et al. (2002) suggested that a negative $\delta^{13}C$ anomaly could be attributed to the release of methane clathrates (induced by the flood basalt event), and that widespread oceanic anoxia would have followed.

The scarcity of and unconfirmed nature of impact evidence, together with the coincidence in timing of the Central Atlantic Magmatic Province, indicates that this extinction event was not caused by an impact event. It is possible that the extinction event was caused by disruption of the carbon cycle (possibly initiated by the volcanic event), but the exact mechanism still remains to be established.

In recent decades, the Jurassic-Cretaceous (J-K) extinction event has been suggested to be another of the "Big Five" Phanerozoic mass extinctions. The extinction event affected primarily marine genera and reptiles (Raup and Sepkoski, 1986; Rampino, 1999), but the timing and correlation of this extinction event remains relatively unknown, due to poor correlation of biostratigraphy (Hallam et al., 1991) and magnetostratigraphy (Ogg et al., 1991). The J-K period (146–141 Ma ago) records at least three impact events (Gosses Bluff, Mjølnir, and Morokweng) which may or may not have contributed to the extinction event. McDonald et al. (2005) examined platinum group element (PGE) signatures from rocks at the J-K boundary, and showed that there was no compelling evidence for an impact event. Additional research into this extinction event must be performed in order to contribute to the understanding of the cause of this event and to determine whether this extinction event should be listed as one of the great Phanerozoic mass extinctions.

1.1.1.5 The Late Cretaceous Extinction Event

The cause of the Cretaceous-Tertiary (K-T) boundary event at 65.5 ± 0.3 Ma (Gradstein et al., 2004) has been, and continues to be, studied extensively. Both marine and non-marine fauna were affected, and the extinction event remains famous for being the one that included the demise of the dinosaurs.

Initially, a number of workers suggested that the extinction event was related to the eruption of the Deccan Traps (e.g., Vogt, 1972; McLean, 1981; Courtillot and Besse, 1987); however; there is some contention as to the exact timing of the Deccan Traps with respect to the mass extinction (Courtillot et al., 1986; Courtillot et al., 2000).

Alvarez et al. (1980) were the first to suggest that the K-T mass extinction event could have been caused by a bolide impact evidenced by the enrichment in siderophile elements (in particular iridium) at the stratigraphic level of the K-T boundary. Boundary sample concentrations

of iridium were four orders of magnitude higher than the concentrations in the rocks below and above the boundary. These results were also independently reached by Jan Smit, who found high concentrations of siderophile elements, of extraterrestrial origin, together with a global turnover of microfossils, and interpreted this pattern as the result of an impact event (Smit, 1981; Smit, 1990). Hildebrand et al. (1991) suggested that the Chicxulub Crater, located on the Yucatán Peninsula, Mexico was the impact crater resulting from the bolide impact at the K-T boundary. This buried crater, ca. 180 km in diameter, was located through magnetic and gravity surveys, as well as a number of oil wells drilled inside and near the crater. The size of the crater corresponds to the hypothesized size of the bolide. The crater has been extensively studied through a number of drill cores including a recent International Continental Scientific Drilling Program (ICDP) project (e.g., see *Meteoritics and Planetary Science* ***39***). The bolide impact could have produced dramatic greenhouse warming by the shock production of carbon dioxide (CO_2) from the carbonate component of the target, as well as sulphur dioxide (SO_2) from anhydrite (O'Keefe and Ahrens, 1989).

Bhandari et al. (1996) recorded iridium and osmium enrichment in a layer in the Deccan Traps and concluded that the volcanic event had preceded the K-T boundary. Courtillot et al. (2000) used a combination of palaeontology, argon dating and mineralogy to support their view that volcanism was sporadic before and after the extinction event.

Keller et al. (2004) have recently suggested that the Chicxulub crater was not connected to the mass extinction. These workers claimed to find Cretaceous foraminifera above the impactites of the crater fill in the ICDP drill core from Yaxcopoil-1, indicating that the Chicxulub impact event predated the boundary by ca. 300,000 years. Keller et al. (2004) examined borehole core and suggested that, based on the sedimentology, stratigraphy, stable isotope data and iridium concentrations, the Chicxulub crater was not connected to the K-T mass extinction, and that there was

another impact event at the boundary, in addition to the volcanic event of the Deccan Traps. However, this work has been refuted on a number of different bases. Firstly, Goto et al. (2004) and Arz et al. (2004) suggested that the foraminifera were reworked by ocean water invasion, and that the cited evidence did not prove that the mass extinction and the impact event were not linked, and that there is no evidence to suggest that the Chicxulub crater pre-dates the mass extinction event. This was further supported by Smit et al. (2004), who re-examined the biostratigraphy, geochemistry, and petrology of the Yaxcopoil-1 borehole core, and stated that these parameters could not be used to argue against the synchroneity of the K-T mass extinction and the crater, and that the Chicxulub crater is in fact connected to the mass extinction.

Various causal mechanisms have therefore been proposed for the Phanerozoic mass extinctions, and knowledge of the different causes and accompanying mechanisms for the various Phanerozoic mass extinctions has guided researchers of the P-Tr mass extinction. In particular, similarities in the characteristics of the Late Triassic and Late Cretaceous mass extinction horizons, and the Late Permian mass extinction have been widely considered and tested.

1.2 Proposed Causes of the P-Tr Mass Extinction Event

Although the P-Tr boundary, and the cause of the associated extinction event, has been the subject of extensive debate, the cause of the mass extinction is, as yet, unresolved. Several possible exogenic and endogenic causes have been proposed, including: (1) asteroid/comet impact (e.g., Retallack et al., 1998; Becker et al., 2001, 2004; Petaev et al., 2004); (2) oceanic anoxia or overturn (e.g., Wignall and Twitchett, 1996; Isozaki, 1997; Weidlich et al., 2003); (3) volcanism (e.g., Renne et al., 1995; Reichow et al., 2002); (4) methane clathrate dissociation events (e.g., de Wit et al., 2002; Retallack et al., 2003), and (5) synergistic combinations

of these possible causes (e.g., Erwin, 1996; Ward et al., 2000; Maruoka et al., 2003).

1.2.1 Asteroid/Comet Impact

Since the conclusion that the K-T mass extinction was caused by a large meteorite impact, represented by the Chicxulub crater (Alvarez et al., 1980; Hildebrand et al., 1991), many scientists have leant towards an impact scenario for the P-Tr mass extinction (e.g., Retallack et al., 1998; Rampino, 1992; Kaiho et al., 2001; Becker et al., 2001, 2004; Petaev et al., 2004; Chapman, 2005).

Occurrences of planar deformation features (PDFs) in quartz in Australian and Antarctic sections (Graphite Peak) have been reported (e.g., Retallack et al., 1998; Shukolyukov et al., 2004; Petaev et al., 2004) but have not been confirmed (W.U. Reimold, pers. comm.), and they are not accepted by the impact community.

Part of the evidence that has been used to support extinction by asteroid impact at the K-T boundary is the presence of a consistent enrichment in Iridium, an element that is concentrated in meteorites, but not in terrestrial crustal rocks. Iridium concentrations at the P-Tr boundary are either below the detection limit, or show slight enrichment (e.g., Hancox et al., 2002). There is no conclusive evidence for a consistent iridium anomaly. An inconsistent iridium anomaly has also been observed in marine sections across the boundary by Jin et al. (2000). These workers have also shown that a negative $\delta^{13}C$ excursion is seen at the same level as the inconsistent iridium anomaly.

Becker et al. (2001) presented evidence that they claimed supported impact in the form of “extraterrestrial” noble gases (helium and argon), trapped in the cage structure of fullerenes (C_{60}) in sections from Japan and China. Fullerenes are large molecules of carbon atoms, which can be either purely terrestrial in origin (Heymann et al., 1996) or can form in

association with meteorite impact events. The samples were said to contain specific ratios of $^{3}He/^{36}Ar$ and $^{40}Ar/^{36}Ar$, which Becker et al. (2001) argued were extraterrestrial, thus supporting meteorite impact at the P-Tr boundary. This has, however, been solidly refuted by Farley and Mukhopadhyay (2001) and Isozaki (2001). Farley and Mukhopadhyay (2001) analysed samples from the same sites studied by Becker et al. (2001) using the same analytical procedures, and could not replicate the results by Becker et al. (2001). Isozaki (2001) stated that the P-Tr boundary is not in evidence in the Japanese section, and that Becker et al.'s samples came from below the boundary.

Kaiho et al. (2001) used a correlation of sulphur and strontium isotopic data and the presence of strange metallic iron-silica-nickel (Fe-Si-Ni) grains to suggest the event was caused by an impact-triggered release of mantle-derived sulphur and strontium. This was rejected by Koeberl et al. (2002) based on a number of different arguments. Firstly, Koeberl et al. (2002) disagreed with the interpretation that the Fe-Si-Ni-rich grains were impact generated, which was not supported by any data. Geochemical variations in nickel, aluminium, manganese and copper did not indicate an extraterrestrial source. Secondly, Kaiho et al.'s (2001) boundary horizon enriched in supposed "extraterrestrial" nickel was rejected on the basis that it is not supported by analytical data, nor is the nickel conclusively extraterrestrial in origin – it may have been concentrated by other means. A lack of shocked quartz was interpreted by Kaiho et al. (2001) to represent an oceanic impact event. This is inconclusive, as shocked quartz could be present at an impact event in a shallow marine environment as well (e.g., the K-T Boundary). Kaiho et al.'s (2001) assumptions used in calculating crater diameter ratios were also discarded by Koeberl et al. (2002) as unfounded. The range of sulphur isotopic ratios that are quoted and used to calculate the crater volume can be explained by fractionation via bacterial sulphate reduction, and oxidation of H_2S, together with the isotopic signature of Late Permian seawater. The values did not support an extraterrestrial cause for the extinction event.

Kaiho et al. (2001) speculated on the role of impact-induced volcanism and/or excavation of mantle material. A number of other authors have argued that it is possible that a meteorite impact could have triggered the Siberian Flood Basalts (Rampino, 1987; Jones et al., 2002). However, such a link (flood basalts resulting from a meteorite impact) has never been observed anywhere in the world (Ivanov and Melosh, 2003). Ivanov and Melosh (2003) made a strong case – based on numerical modeling - that flood basalts could not result from an asteroid/comet strike. They performed simulations using an asteroid with a diameter of 20 km striking at 15 $km \cdot s^{-1}$ and found that an impact crater 250 - 300 km in diameter would be formed. However, the crater would then collapse and pressures would return to lithostatic ones, and thus would not induce decompression melting of the underlying rocks.

Erwin (2003) evaluated the impact hypothesis for the P-Tr boundary extinction event in detail and noted that considerable evidence that could be regarded as consistent with, but not diagnostic of (e.g., the coincident carbon shift at the P-Tr boundary, the apparent correlation between terrestrial and marine extinctions) the impact scenario, has been found at the P-Tr boundary. Also, the rapidity of the extinction of vertebrates in the Karoo Basin, South Africa (Smith and Ward, 2001) indicated a possible extinction by bolide impact. However, the coincidence between the Siberian Traps (section 1.2.3) and the complex nature of the carbon isotopic signature are in clear conflict with the impact hypothesis (Erwin, 2003). At the K-T boundary, only one large, broad carbon isotope excursion is seen, indicating a single event, whereas a number of other isotopic excursions are thought to represent multiple events (Erwin, 2003).

Some workers have proposed potential impact craters for the P-Tr event, but on the whole these ideas remain contentious in terms of age constraints and crater size problems. Initially a circular structure off the coast of Cameroon was suggested as an impact site, on the basis that it was related to the break-up of Pangaea (Brown, 2002). This idea has, however, been

questioned due to a lack of conclusive geochronological evidence, and the existence of such an impact structure has remained speculative. Mory et al. (2000) suggested a buried impact structure at Woodleigh in Western Australia as being of P-Tr boundary age. Evidence for the impact-nature of the structure included a central core of uplifted basement rocks, which displayed shock-induced features (e.g., planar deformation features in quartz, diaplectic feldspar). The structure was defined using magnetic and gravity surveys, and its age was said to coincide with the P-Tr boundary (on the basis of apatite fission-track ages, and overlying Jurassic strata). Questions concerning the quality of the data, particularly the dating of this cratering event, were raised by Reimold and Koeberl (2000). Uysal et al. (2001) performed K-Ar dating and concluded that the Woodleigh impact structure was, in fact, Late Devonian in age. Renne et al. (2002) concluded that the data of Uysal et al. (2001) did not objectively constrain the age of the impact event, and did not establish a link to the Late Devonian extinction event.

Recently, the Bedout structure in the Canning Basin, offshore north-west Australia, was proposed by Becker et al. (2004) as a possible impact structure for the P-Tr boundary, but this has been strongly refuted by a number of groups on the basis of a lack of bona fide impact evidence and poor geophysical and chronological constraints (e.g., Glikson, 2004; Kerr, 2004; Renne et al., 2004). There is one piece of evidence presented by Becker et al. (2004) that has not been refuted (yet?): the alleged presence of diaplectic feldspar glass (maskelynite) around and within plagioclase within the drill cores taken from the Bedout Structure (Basu et al., 2004). Basu et al. (2004) performed laser Raman spectroscopic analysis of allegedly isotropic plagioclase from the Bedout structure. They concluded that the presence of maskelynite was confirmed and that this had to be a shock induced feature, and that it followed that the Bedout structure was an impact crater. Further work by a number of groups is in progress. The debate continues.

Reliable evidence for an impact event at the P-Tr boundary (in the form of a coeval impact site, shocked quartz, other impact debris, or a consistent iridium anomaly) has therefore not been found to date.

1.2.2 Oceanic Anoxia or Overturn

Oceanic anoxia is the process of changing the chemistry of the oceans such that they become oxygen-depleted rather than oxygen-rich. This process is a viable option for the extinctions in the marine realm, but is unable to explain the extinctions in the terrestrial realm. Evidence for oceanic anoxia has been found in the shallow marine realm, but this may have been a consequence of either a volcanic event or an impact event. (Knoll et al., 1996). Oceanic overturn is the process of producing oceanic anoxia by bottom waters moving towards the surface of the oceans, and the accompanying change in chemistry.

Knoll et al. (1996) provided evidence that there was preferential extinction of oxygen-dependant organisms suggesting that oceanic anoxia produced elevated levels of CO_2. This effect could also have been a secondary effect of volcanism.

Weidlich et al. (2003) studied the distribution and biological composition of coral reefs and found that their ecological traits coincide with a modeled decline of atmospheric oxygen throughout the Permian Period. These authors used this to support extinction by oceanic anoxia, together with carbon cycle reorganization. Selective extinction and recovery patterns are similar to those observed in modern benthic communities approaching oxygen minimum zones. Carbon cycle reorganization is caused by short-term perturbations of the carbon cycle, leading to changes in the reservoirs of carbon and oxygen. They proposed that the gradual decline in atmospheric oxygen left reef communities vulnerable to abrupt environmental changes.

Ward (2004) hypothesized that a lowering of atmospheric oxygen could have taken place as a result of dropping ocean levels, which expose anoxic materials to the atmosphere. The ocean has a constant volume, and changes are controlled by temperature (and either adding or subtracting water from that volume) and by changes in the size of mid-ocean ridges, controlled by plate tectonics (see also Kearey and Vine, 1996). A lowering of the sea level usually takes place under conditions of decreasing temperature (and the consequential build-up of ice-caps). However, Ward (2004) believed that the Permian was hot and that the change in sea level was controlled by the internal heat flow produced by plate tectonics. When the heat flow increases, mid-ocean ridges spread apart and seawater is displaced, elevating the sea level. If the heat flow then decreases, the spreading centres would become reduced in size, leading to a decrease of the sea level. Anoxic organic materials would then be exposed to the surface, and would have become oxidized, creating red beds. However, this idea is contentious, as the red beds that have been observed at the boundary could also be the results of post-depositional diagenesis.

1.2.3 Volcanism

The Siberian Flood Basalts (the Siberian Traps), a volcanic province covering some 1.6 million km^2 in eastern Russia (Siberia) with a thickness of 400 – 3000 m, have been dated to the same time as the P-Tr event (Fig. 2; Kamo et al., 2003). Kamo et al. (2003) dated the Siberian Flood Basalts at 251.7 ± 0.4 Ma for the lowermost unit, and 251.1 ± 0.3 Ma for the uppermost unit by U-Pb perovskite and zircon dating. This is synchronous with the P-Tr mass extinction as discussed by Erwin (2000) and dated by Mundil et al. (2004). It has been widely accepted that the volcanic event is coincident with the extinction event. These ages also suggest the extrusion took place over less than 1 million years (Kamo et al., 2003). Emplacement of the Norilsk'-Talnakh ore-bearing intrusions also took place at this time (Kamo et al., 2003). Thus, there appears to be a temporal relationship between the mass extinction event and massive volcanic eruption.

The volcanic event would have resulted in a number of environmental effects, including global warming caused by the greenhouse gases carbon dioxide, sulphur dioxide and methane (Retallack et al., 2003). Evidence for anomalously high carbon dioxide levels have been documented (de Wit et al., 2002). Kamo et al. (2003) discussed that 2 x 10^6 km^3 of basalt would produce 4 x 10^{19} g of CO_2 and more than 10^{19}g of SO_2, based on estimates from Kilauea volcano (McCartney et al., 1990; Gerlach and Graeber, 1985). The volcanic input would cause a negative shift, by 4 ‰, in the carbon isotopic composition ($\delta^{13}C$) to a lower value. The observed shift in the isotope values of carbon would be from +2 to -2. The observed negative excursion in the carbon isotope ratio measured at the P-Tr boundary (e.g., MacLeod et al., 2000; de Wit et al., 2002; Retallack et al., 2003) is far larger and the amount of volcanogenic CO_2 that would have been released from the Siberian Traps only contributes a fifth of this considerable carbon isotope excursion.

Grard et al. (2005) believe that two concurrent events took place at the P-Tr boundary. First, the eruption of the Siberian Traps would have produced large amounts of ^{13}C depleted CO_2 degassed from the mantle. This would have been added to the ocean through silicate weathering, and would have changed the carbon isotopic signature of the oceans. Then, in the second stage, a rapid collapse in productivity would have induced a strong decrease in the global organic carbon burial, further enhancing the initial change in the carbon isotopic ratios. Grard et al. (2005) suggested that these effects explain the low values of $\delta^{13}C$ across the P-Tr boundary.

The coincidence of the Siberian Traps with the P-Tr boundary (at ca. 251 Ma) indicates that it is extremely likely that the volcanic event contributed to the P-Tr mass extinction, but carbon isotopic data indicate that it could not have been the sole cause of the mass extinction (see also White and Saunders, 2005). It may have been a trigger mechanism to the global warming that took place, but would not have been exclusively responsible for the extinction event.

1.2.4 Methane Clathrate Dissociation Events

Methane clathrates are a form of water ice that contains a large methane (CH_4) component within its crystal structure (Kvenvolden, 1998). Large deposits of methane clathrates are found under the ocean floor, and occur as outcrops on the ocean floor and in deep sea sedimentary structures (Kvenvolden, 1998). They are believed to form by the migration of gas along geological structures, followed by precipitation or crystallization when a change of temperature is encountered (i.e., when hot gas meets cold sea water). As the deep oceans have conditions of low temperature and elevated pressure, the clathrates are very stable. Sudden release of these methane clathrates is hypothesized to be able to cause dramatic climate changes, as methane is a strong greenhouse gas (Matsumato, 1995).

Retallack et al. (2003) presented evidence from the southern Karoo Basin, South Africa, using carbon isotopes, as well as stratigraphic, palaeontological and sedimentological evidence, to suggest oceanic anoxia and a severe greenhouse effect occurred as a result of degassing from shallow marine and permafrost clathrates. Palaeoclimatic changes were not as dramatic as expected and included a changeover from arid and seasonal (Permian) to semi-arid and less seasonal (Triassic). A warmer and wetter palaeoclimate for the Early Triassic is evidenced by increased chemical weathering. Retallack et al. (2003) noted the characteristics of carbonate nodular horizons – firstly, the spread of the carbonate nodular horizons which indicates climatic seasonality, and secondly the depth of nodules which is related to the mean annual precipitation. A change from diffuse and shallow calcareous nodules in the Permian to deep and well-focused calcic horizons in the Triassic was observed (Retallack et al., 2003). These nodular characteristics indicated a distinct change of environmental conditions. The authors concluded that the change in the environmental conditions was not solely responsible for the extinction event. Based on a series of negative carbon isotope excursions (measured from therapsid tusks, pedogenic carbonate nodules and organic matter),

Retallack et al. (2003) concluded that a greenhouse effect caused by the degassing of methane took place. The values of the $\delta^{13}C$ excursion measured by Retallack et al. (2003) corresponded to a lowering in the carbon isotope ratio by the addition of organic matter (-22 to -24‰). The isotopic composition of volcanic matter (which would have been produced from emissions from the Siberian Traps) is only -7 to -15‰ and would not have caused the low excursions observed. Furthermore, the volcanic event would not have produced sufficient quantities of carbon dioxide, sulphur dioxide and water vapour rapidly enough to cause such a large extinction event over such a short time interval. Retallack et al. (2003) believed the voluminous release of methane would have caused a greenhouse condition leading to extinction. They rejected "pure" oceanic anoxia, as this would have been unlikely to affect land animals, and does not allow the isotopic depletion in carbon isotope values.

This conclusion is also supported by the work of de Wit et al. (2002), who examined and carried out carbon isotope analysis across several terrestrial, palaeontologically and/or palynologically defined P-Tr boundary sections, including sections in the Karoo Basin, South Africa, the Morondava Basin, Madagascar, and the Son, Mahandi, Damodar and Pranhita-Godavari coal-bearing basins of India. These authors found a number of large, negative ^{13}C excursions before and after the P-Tr transition. These excursions complement similar smaller excursions seen in marine sections. The coincidence between faunal change and the $\delta^{13}C$ excursion at the boundary at different sections around the world (de Wit et al., 2002) was interpreted to indicate that palaeoenvironmental and biological change were temporally coincident with the P-Tr boundary in other regions and environments (MacLeod et al, 2000; de Wit et al., 2002).

De Wit et al. (2002) stated that the number of excursions argue against a single disruption at the boundary, rather proposing that a number of changes took place to disturb ecosystem stability. De Wit et al. (2002) believed the catalyst to the event(s) at the P-Tr extinction could have been

the movement of Gondwana's continental shelf to lower latitudes, together with the disintegration of the northern marine platform, which would have destabilized methane clathrates along the margins of the southern Tethys. A gradual negative trend in the carbon isotope ratio from ~270 Ma to the Late Permian was noted (de Wit et al., 2002; compare Fig. 40). Following this, a series of rapid, large, negative excursions of the carbon isotope ratio (that occurred before and after the P-Tr boundary) were observed. The episodic release of methane, from clathrates into the atmosphere or into the oceans, would have accounted for the gradual decrease in values before the boundary. These processes would have increased the concentration of carbon dioxide in the atmosphere, and would have aided global warming. De Wit et al. (2002) did not speculate on the specifics of the event(s) at the boundary, but believed that the initial effect of methane clathrate dissociation would have played a large role in the extinction event.

Dissociation of extensive reservoirs of methane clathrates is well supported by the carbon isotope data of MacLeod et al. (2000), de Wit et al., (2002) and Retallack et al. (2003), and provides an attractive hypothesis for the cause of the P-Tr mass extinction. The catalyst to this dissociation event still needs to be conclusively established.

1.2.5 Synergistic Mechanisms

A combination of several of these possible causes seems to some the most likely scenario (Maruoka et al., 2003; Benton and Twitchett, 2003; Erwin, 2000; MacLeod et al., 2000). The eruption of the Siberian Traps would have introduced large volumes of sulphates (Maruoka et al., 2003) into the atmosphere, which could have triggered extensive acid rain. The associated climatic warming could have been sufficient to warm the ocean, to then release 1200 gigatons of methane-bound carbon, which could have triggered oceanic anoxia (Erwin, 2000).

Sulphur isotope compositions, together with concentrations of sulphur and carbon, across a P-Tr section in the northern Karoo Basin were determined by Maruoka et al. (2003). These authors found elevated concentrations of sulphide (hypothesized to have been produced by sulphate-reducing bacteria) below and at the proposed P-Tr boundary. Organic carbon to sulphide ratios were calculated for the sedimentary rocks containing high concentrations of sulphide and found to be similar to values found in marine environments (Berner and Berner, 1996). This indicated that the enhanced accumulation of sulphide is the result of enrichment of sulphate in water. Sulphide concentrations were found to be independent of factors such as temperature and carbon dioxide. This indicates that the sulphate may have been supplied by an event such as a meteorite impact or a volcanic event that would have produced large quantities of acid rain, in which the sulphate would have been directly supplied to freshwater. Maruoka et al. (2003) favored a volcanic cause, as there is a lack of direct evidence for an impact event (see section 1.2.1).

The observed $\delta^{13}C$ excursions could have been caused by the rapid release of methane or carbon dioxide from strongly ^{13}C depleted reservoirs, such as organic carbon in the deep ocean, or methane stored in gas clathrates (MacLeod et al, 2000). The rapid release of these gases, as well as sulphur, to the atmosphere, could have had strong palaeoclimatic effects.

Benton and Twitchett (2003) also speculated as to what combination of environmental changes could have caused the mass extinction, and the characteristics of it. They came to a number of conclusions that have been widely accepted: Firstly, the P-Tr boundary has been dated to 251 Ma. Secondly, there is a coincidence with the timing of the Siberian Flood Basalt event. Third, extensive studies of both marine and non-marine sections across the boundary have yielded similar results in many cases (suggesting a synchroneity of cause), and lastly, stable isotopes have shown an increase in temperature and that anoxic conditions existed after

the extinction event. These authors used these points to link the marine and non-marine events.

Benton and Twitchett (2003) initially examined the oxygen isotope record, which showed that a global temperature rise of 6 °C took place across the boundary. This increase in temperature could have caused a reduction in oceanic circulation, which would have created benthic anoxia (Hotinski et al., 2001). This is supported by marine palaeontological studies (lack of burrows and fossils of marine benthic invertebrates), as well as sedimentological changes (sedimentary rocks are dark-coloured and pyrite-rich in the Early Triassic), which indicate widespread benthic anoxia (Wignall and Twitchett, 2002) in the marine rocks following the P-Tr event.

As recounted in sections 1.2.3 and 1.2.4, a number of negative carbon isotopic excursions are seen across the boundary. Part of these excursions can be accounted for by light carbon (^{12}C) injected into the atmosphere from the Siberian Flood Basalts, but this was insufficient to account for the entire shift observed. However, the coincident timing of the volcanic event may indicate that it was part of the reason for the mass extinction, but not the sole cause. The occurrence and size of the negative carbon excursions agree with the proposed methane-clathrate source (Wignall, 2001; Erwin et al., 2002; White, 2002; de Wit et al., 2002; Retallack et al., 2003). In addition to this, Benton and Twitchett (2003) proposed a positive-feedback loop, called the ‘runaway greenhouse’ model, which involves a trigger mechanism, and then environmental conditions to continue the atmospheric changes. Due to the suddenness of the extinction (Bowring et al., 1998), Benton and Twitchett (2003) proposed that there must have been a dramatic cause to the event, such as a meteorite impact or volcanism. As impact evidence had largely been rejected (section 1.2.1), they proposed that the dramatic event was volcanism, which triggered the breakdown in environmental mechanisms.

Destabilization of methane clathrates due to oceanic warming, caused by a volcanically triggered greenhouse effect, could produce the observed values of $\delta^{13}C$ (Hallam and Wignall, 1997; Wignall, 2001; Erwin et al., 2002; Wignall and Twitchett, 2002; de Wit et al., 2002) at the P-Tr Boundary. These would have, in turn, produced oceanic anoxia, and would have triggered excessive global warming. This is a potential mechanism for the cause of the P-Tr mass extinction, but it needs to be verified by additional data.

White and Saunders (2005) suggested that the kill mechanisms associated with either flood basalts or impacts alone do not appear to be sufficiently powerful to have caused global environmental change leading to a mass extinction event. Rather, they favour that both catastrophic events took place for the largest mass extinctions (e.g., Late Permian, Late Triassic and Late Cretaceous), and were in fact pre-requisites to these large extinction events.

Table 1 gives a summary of the arguments for and against the various possible causes of the P-Tr mass extinction.

1.3 Non-marine P-Tr Sections

A number of potentially complete continental sections across the P-Tr boundary have been identified around the world (Karoo Basin, South Africa; Tunguska Basin, Asia; others in South America, East Africa, Antarctica and Australia).

Sedimentary successions across the continental P-Tr boundary are difficult to interpret because of episodes of non-deposition and erosion, and because terrestrial fossils are rare compared to the marine fossils (e.g., Alvarez and O'Connor, 1999, 2002; Hancox et al., 2002).

Table 1: *Critical assessment of the various hypotheses for the cause of the P-Tr mass extinction.*

Hypothesis:	Arguments for:	Arguments against:
Asteroid/ Comet Impact	Extinction event was sudden, as shown by the palaeontological record in both marine and non-marine sections, especially the rapidity of the vertebrate extinctions. The coincident carbon isotopic shift.	Direct evidence for an impact event at the P-Tr boundary (in the form of a coeval impact site, shocked quartz, other impact debris, or a consistent iridium anomaly) has not been found. The complex nature of the carbon isotope excursions suggests multiple events, not a single impact.
Oceanic anoxia	Evidence has been found for this in the shallow marine sedimentological record.	Can not be solely responsible for the mass extinction, as it does not explain the terrestrial extinctions. Most likely a secondary mechanism.
Volcanism	Coincidence of the Siberian Flood Basalt event; negative carbon isotope excursions, indicating input from a source rich in CO_2.	The documented carbon isotope excursion is too large to have been caused by the volcanic event alone. Another mechanism must have been involved in order to produce the size of the excursion seen.
Methane Clathrate Dissociation	This mechanism accounts for the size of the negative carbon isotope excursion.	An initial trigger that all workers agree upon has yet to be found. It is unknown how this mechanism would be self-sustaining.
Synergistic mechanisms	A number of effects would be able to explain all the characteristics of the mass extinction and boundary layer.	

The main contenders for the non-marine P-Tr boundary Global Stratotype Section and Point (GSSP) are sections from the Karoo Basin, South Africa (Fig. 2) and from the Tunguska Basin, Siberia (Lozovsky, 1998). The Karoo Basin preserves a largely uninterrupted 100 million year palaeontological record, which has aided in the biostratigraphic subdivision of the sequence (Rubidge, 1995; Rubidge and Hancox, 1999; MacRae, 1999).

A number of sections that may typify the P-Tr extinction in the continental realm have already been studied in the southern Karoo Basin of South Africa (e.g., Smith, 1995; Ward et al., 2000; Smith and Ward, 2001; De Wit et al., 2002; Retallack et al., 2003; Steiner et al., 2003), as well as in the northern part of the basin (e.g., Hancox et al., 2002; Maruoka et al., 2003). There is a distinct lack of stratigraphically constrained geochemical data in the southern Karoo Basin, particularly regarding trace element variations. Apart from work performed in the northern Karoo Basin (Hancox et al., 2002), there has been no detailed search for shocked quartz or iridium enrichment in the southern Karoo Basin, and this is therefore a major focus of this project.

1.3.1 The Karoo Basin

The Karoo Basin is a large retro-arc foreland basin, which was situated in southwestern Gondwana, from the Late Carboniferous (300 Ma) through to the Early Jurassic (180 Ma) (Catuneanu et al., 1998). At this time Africa was linked to Antarctica, South America and Australia (Fig. 2). The region was bound by upland areas to the north and east, and in the south there was a large mountain chain, the Gondwanide mountains (of which the Cape Fold Belt is a component). The sedimentary rocks of the Karoo Supergroup reflect the changing palaeoclimates, caused predominantly by the movement of the Gondwanan landmass northwards, in relation to the palaeo-south pole. The rocks of the Karoo Supergroup are several thousand metres thick (Johnson, 1991) and cover two thirds of the surface area of South Africa (Fig. 3).The basin is highly asymmetrical in nature

(Fig. 4), being thickest in the south and thinning to the north (Catuneanu et al., 1998). The fill of the Karoo Basin is divided into a number of groups (Figs. 3 and 5).

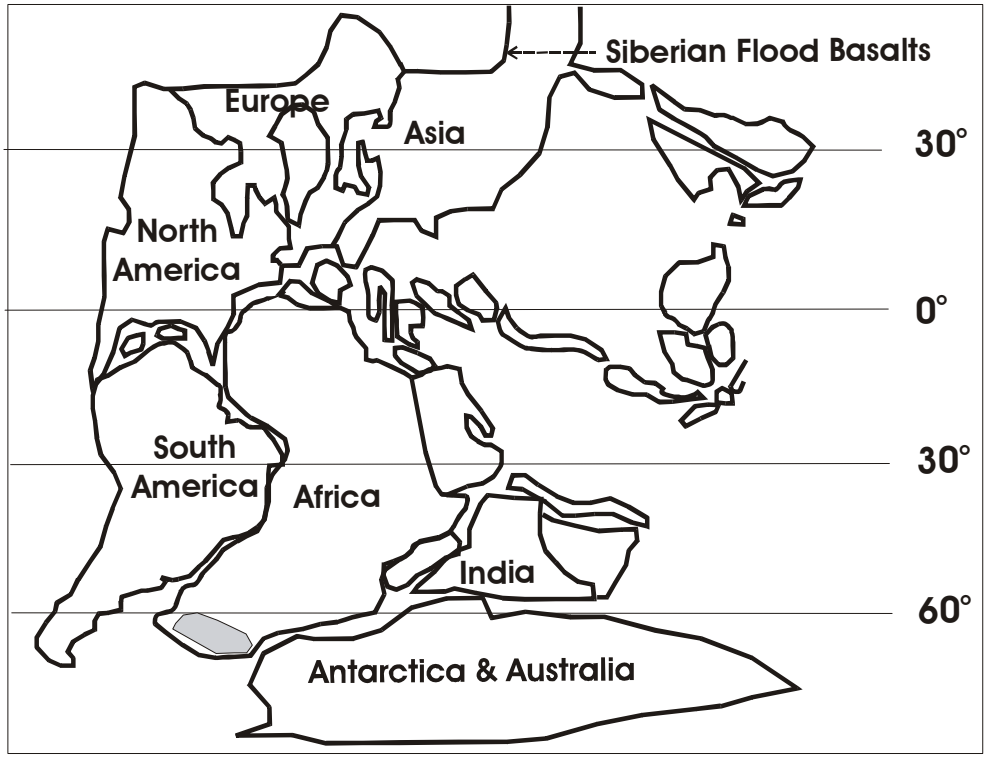


Figure 2: *Pangaea, at 251 Ma, showing the position of the Karoo Basin (grey) (modified after: de Wit et al., 2002).*

It has been shown that, from the Middle Permian, deposition in the Karoo Basin was purely non-marine (Hancox, 2000). The Beaufort Group is divided into the Adelaide and Tarkastad subgroups, the former of which contains the rock interval of the P-Tr extinction (Fig. 5; Rubidge and Hancox, 1999). The Beaufort Group reflects the drying-out and infilling of the inland sea (MacRae, 1999); consequently the deposits of the Late Permian are non-marine. The Adelaide Subgroup is divided into the Koonap, Middleton and Balfour formations, and the overlying Tarkastad Subgroup is divided into the Katberg and Burgersdorp formations. In the southern Karoo, the P-Tr boundary occurs at, or a few metres above, the base of the Palingkloof Member at the top of the Balfour Formation in the Adelaide Subgroup (Fig. 5). The Balfour Formation is dominated by

floodplain siltstones and has a transitional contact with the overlying arenaceous Katberg Formation. The P-Tr boundary sequence occurs within this transitional zone. The latest Permian strata have a rich diversity and abundance of vertebrate taxa dominated by therapsids, the earliest Triassic faunas on the other hand are of low diversity yet still abundant. At the actual boundary Smith (1995) records a thin, barren laminated mudstone bed which he interprets as the results of de-vegetation with increased mean annual temperatures and seasonality of rainfall.

Unlike earlier authors who favoured a unitary subsiding basin, Catuneanu et al. (1998) proposed a reciprocal basin development model for the Karoo Basin, which states that in a unitary basin without dynamic subsidence, flexurally induced subsidence will be out of phase in the proximal and distal sectors. As such temporally complete sequences can only be created at different times in the two sectors – essentially when a temporally complete sequence exists in the proximal sector, then the distal sector will have an incomplete sequence, and vice versa. It has been shown that in the distal sector (in the northern Karoo Basin), the P-Tr boundary is likely characterized by an unconformity surface (Hancox et al., 2002). Thus, the southern Karoo Basin (proximal sector) is expected to be temporally (more) complete, and it is for this reason that sites in the southern Karoo Basin were chosen for this project (Fig. 3). The Commando Drift Dam section (Fig. 3) is the most proximal site to the original orogen, and should be stratigraphically the most continuous one.

1.3.2 Placement of the P-Tr Boundary in the Karoo Basin

The Karoo Basin has a well constrained record of the P-Tr vertebrate extinction with only 6 of 44 reptilian genera recovered from the Late Permian *Dicynodon* Assemblage Zone also found in the Triassic sequence of the *Lystrosaurus* Assemblage Zone (Rubidge, 1995; Fig. 6). The first placement of the P-Tr boundary in the Karoo Basin was coincident with the lithostratigraphic contact of the Balfour and Katberg formations (see Johnson, 1994; SACS, 1980).

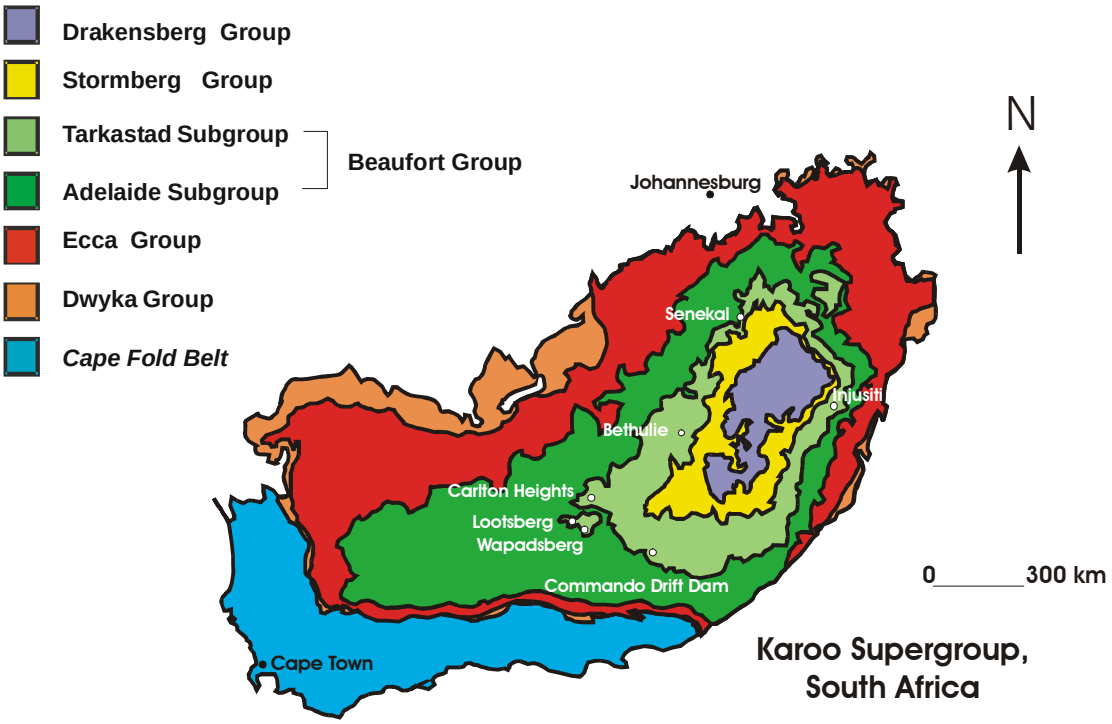


Figure 3: *The Karoo Basin, South Africa, showing study sites of the Permian-Triassic Boundary (in white) (modified after: Catuneanu et al., 1998). Studies were undertaken by the following authors:*

Senekal: Hancox et al., 2002; Maruoka et al., 2003; de Kock, 2003.

Bethulie: Kirschvink and Ward, 1998; MacLeod et al., 2000; Ward et al., 2000, 2005; Smith and Ward, 2001; de Wit et al., 2002.

Injusiti: Detailed studies still remain to be undertaken.

Lootsberg: Smith, 1995; Kirschvink and Ward, 1998; Ward et al., 2000; Smith and Ward, 2001; de Wit et al., 2002; Retallack et al., 2003; Ward et al., 2005.

Carlton Heights: Steiner et al., 2003; Ward et al., 2005.

Wapadsberg: Ward et al., 2000, 2005; this study.

Commando Drift Dam: de Kock, 2003; Ward et al., 2005; this study.

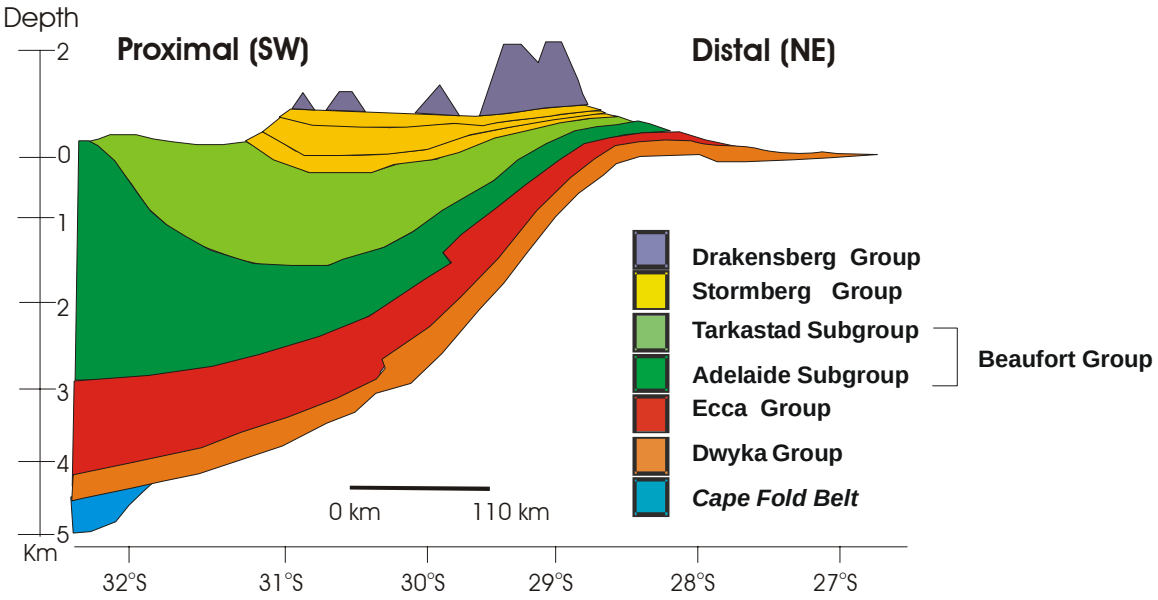


Figure 4: *Stratigraphic cross-section from the southwest to the northeast of the Karoo Basin (modified after: Catuneanu et al., 1998).*

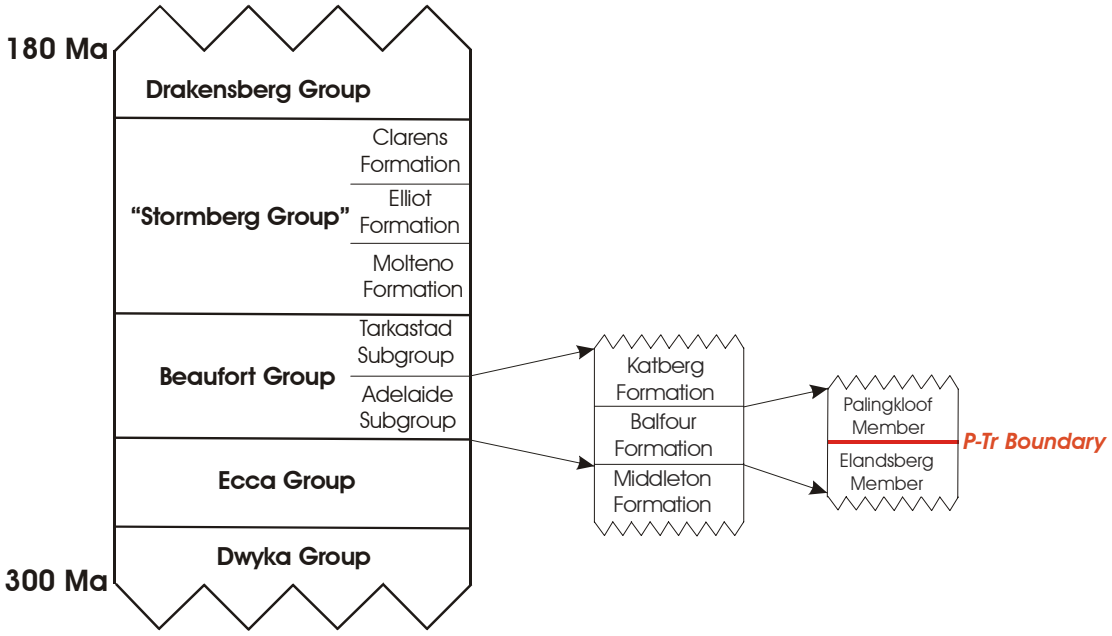


Figure 5: *Stratigraphic column of the Karoo Supergroup, showing the position of the P-Tr boundary (modified after: Catuneanu et al., 1998).*

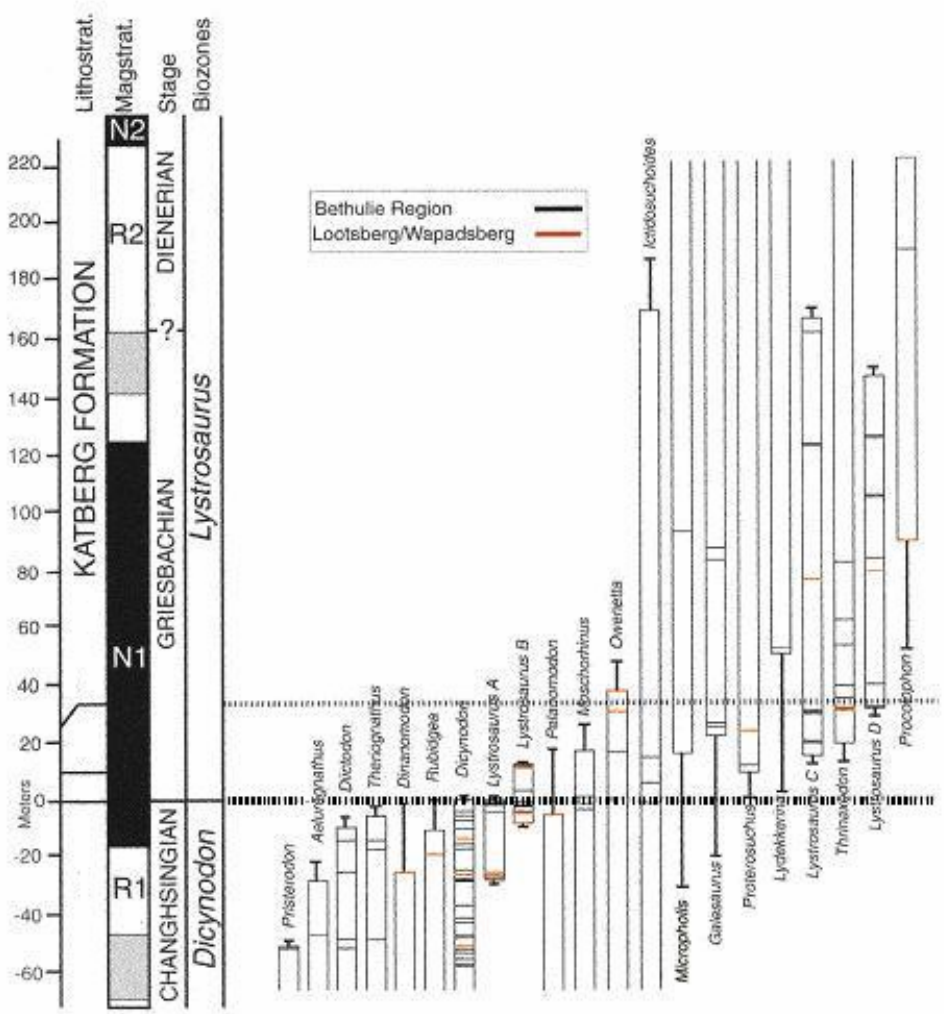


Figure 6: *The palaeontological signature of the Karoo Basin, South Africa (from: Ward et al., 2005). P-Tr palaeontological boundary located at 0 m. The magnetostratigraphic results of De Kock (2003) are included (black indicates normal polarity, grey indicates unknown polarity and white indicates reversed polarity). The bold line at 0 m indicates the uppermost occurrence of Dicynodon lacerticeps. The second line at ~30 m indicates the base of the Katberg Formation, and the position of the fungal spike of Steiner et al. (2003).*

After intensive fossil collection, the P-Tr boundary was placed biostratigraphically at the contact between the *Dicynodon* and *Lystrosaurus* Assemblage Zones (King, 1990; Rubidge, 1995); however, Smith (1995), and Smith and Ward (2001) have shown that the boundary is better placed at the Last Appearance Datum (LAD) of *Dicynodon lacerticeps* (Figs. 6 and 7). This is because the First Appearance Datum (FAD) of *Lystrosaurus* actually occurs in the Permian (Cheng, 1993; Smith, 1993; Fig. 6) and the LAD of *Dicynodon* records the vertebrate extinction, whereas *Lystrosaurus* was one of the few vertebrates to survive the mass extinction event. This has been widely accepted by other workers (e.g., Hancox et al., 2002; Retallack et al., 2003).

Botha and Smith (2004) recently examined the various species of *Lystrosaurus* and found that *Lystrosaurus curvatus*, *L. maccaigi* and *L. murrayi* are present in Late Permian strata in South Africa. *Lystrosaurus murrayi* is found in the Katberg Formation, but not in as great abundance as in the Permian strata, and *L. curvatus* is only found in the Palingkloof Member of the Balfour Formation (and is not found in the Katberg sandstones). *L. maccagi* is not found in the Triassic (i.e., it becomes extinct at the boundary). Once these results have been verified, this may provide further constraints on the position of the P-Tr boundary in the Karoo Basin.

The Commando Drift Dam section (Fig. 3) of this study has also been the subject of a palaeomagnetic study (de Kock, 2003; Fig. 7). It was initially expected that a magnetic reversal would coincide with the palaeontological boundary. In fact, two reversed magnetic chrons separated by an interval normal polarity were found, giving a R/N/R (Reversed/Normal/Reversed) pattern (Fig. 6). The change from reversed to normal signatures is found 5.3 m above the palaeontologically defined boundary [hence the palaeontological boundary after Smith (1995) and Smith and Ward (2001) falls within the normal polarity interval].

Results from the marine realm (Heller et al., 1995; Steiner et al., 1989) indicate that the marine extinction occurred near, or at the end of, an interval of reversed magnetic polarity, and was associated with an inorganic $\delta^{13}C$ spike. The normal chron within the Karoo Basin might correlate with the known Triassic normal polarity found in marine sections, should the magnetic signature be recorded instantaneously. Even though the palaeontological boundary falls within normal polarity, de Kock (2003) hypothesizes that the P-Tr extinction may have taken place at a time of reversed polarity due to the delayed acquisition of magnetic remanence, which would then be consistent with the marine extinction being contemporaneous with the terrestrial one. De Kock (2003) concluded that the marine and terrestrial events most likely coincided.

Steiner et al. (2003) have documented a 1-m-thick interval where fossil pollen is virtually absent and fungal spores dominate the samples (termed the "fungal spike"), at the Carlton Heights section (Fig. 3) in the southern Karoo Basin. This spike occurs simultaneously with the LAD of typically Late Permian gymnosperm pollen, and lies 50 cm below the Katberg Formation, being some 30 m above the LAD of *Dicynodon lacerticeps* (Fig. 7). A number of other fungal spikes are seen at other levels below the boundary in the Late Permian, but these are substantially smaller and do not correspond to the major disappearance of Late Permian pollen.

The spike is hypothesized to represent the widespread loss of arboreous vegetation and accumulation of organic debris (Poort et al., 1997). In marine sections, the fungal proliferation event occurs in a brief interval close to the extinction of marine species and the change in carbon isotopic ratio (Visscher et al., 1996; Twitchett et al., 2001). A sharp, negative shift in the carbon isotopic ratio also occurs at the time of reduction of gymnosperms (Looy et al., 2000). Steiner et al. (2003) suggested that the extinction of mammal-like reptiles may have preceded the land-plant and fungal extinction by less than 100 000 years, based on estimated sedimentation rates. This, however, contradicts itself: if the vertebrates

died from a lack of food, caused by palaeoclimatic changes, the extinctions would be synchronous. Steiner et al. (2003) suggested that the latest Permian flood of fungal remains might serve as a marker bed of brief duration for marine and terrestrial deposits. However, in the Karoo Basin, the fungal spike post-dates the vertebrate extinction, which may suggest that the marine extinction is a separate event from the non-marine extinction.

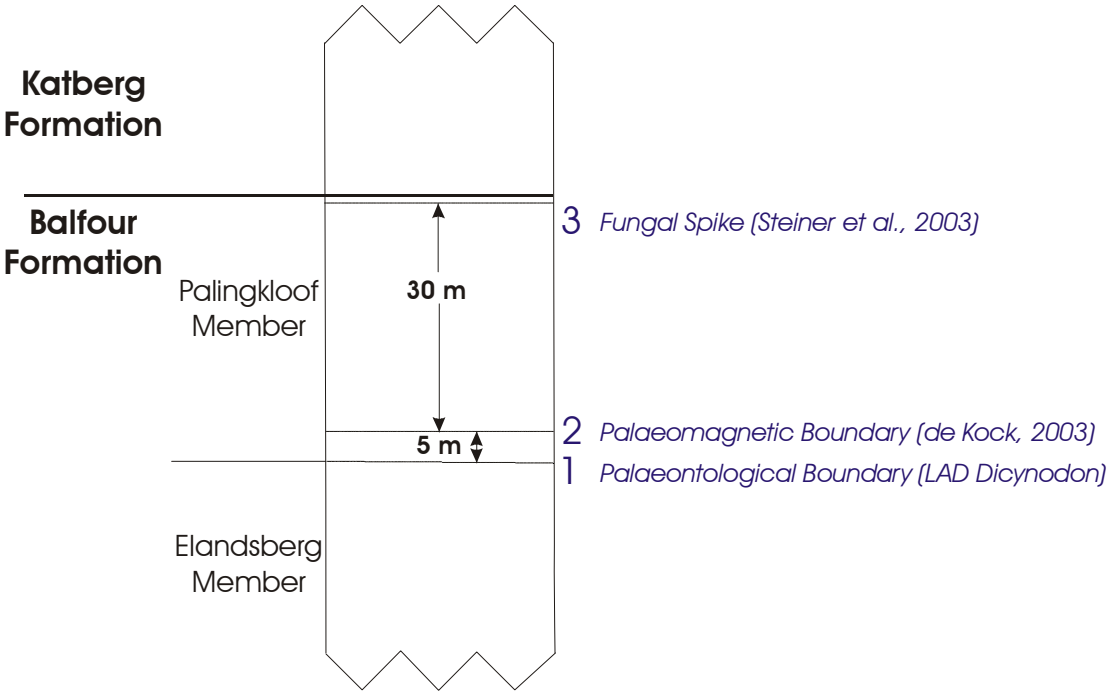


Figure 7: *Potential placements of the P-Tr boundary in the Karoo Basin, South Africa.*

Palynological studies in the Karoo Basin remain contentious due to diagenetic alteration (de Wit et al., 2002). De Wit et al. (2002) noted that pollen was poorly preserved in the southern Karoo due to the effects of secondary alteration, and thus palynofloral change could not be evaluated, unlike in other continental sections worldwide (e.g., Damodar Basin, India; de Wit et al., 2002). Additionally, there are several fungal spikes at and above the boundary (Steiner et al., 2003; Retallack et al., 2003), making it difficult to determine an exact placement of the P-Tr boundary

using fungal remains. This study therefore rejects the placement of the boundary at the layer of the fungal spike (Steiner et al., 2003; Fig. 7) and places it to coincide with the vertebrate extinction, and possibly within the palaeomagnetic constraints. This agrees with previous studies performed both in the southern and northern Karoo Basin (Smith, 1995; Smith and Ward, 2001; Hancox et al., 2002; de Wit et al., 2002; Retallack et al., 2003).

1.3.3 Previous Work on the P-Tr Boundary in the Karoo Basin

Initial work on the P-Tr boundary in the Karoo Basin was focused on establishing the palaeontological constraints on the boundary (see section 1.3.2; Kitching, 1977; King, 1990; Rubidge, 1995; Smith, 1995; Smith and Ward, 2001). Thackeray et al. (1990) and Faure et al. (1995) performed carbon isotopic measurements on a number of sites and both found a negative trend of ~10‰ from stable lower Permian background values, leading up to the palaeontological boundary.

Smith (1995) was the first to document a change in fluvial style across the P-Tr boundary, from high sinuosity and meandering to low sinuosity and braided river systems. This change in fluvial environment was interpreted as a general drying of the floodplain and re-distribution of the vegetation. Smith (1995) hypothesized that this was caused by a pulse of thrusting.

Kirschvink and Ward (1998) performed some of the first magnetostratigraphic studies of the P-Tr boundary in the Karoo Basin. Samples taken from Lootsberg, Bethulie and Doornplaats (located close to Lootsberg) (Fig. 3) were measured, and results suggested that a change from normal to reversed magnetic signatures was seen across the P-Tr boundary.

MacLeod et al. (2000) also measured carbon isotopic ratios (Figs. 8 and 9) for sections from different sites, and found conflicting results to those of Thackeray et al. (1990) and Faure et al. (1995). At Doornplaats and

Lootsberg, no discernable excursion was detected at the stratigraphic level of the palaeontological boundary, together with a lack of change in the carbon isotope ratio below and at the palaeontological boundary (MacLeod et al., 2000). This was attributed to diagenetic alteration (MacLeod et al., 2000), but alternatively could be attributed to later stage fluid activity within the basin (de Wit et al., 2002). At the Bethulie section, however, MacLeod et al. (2000) found a negative carbon isotopic excursion at the level of the palaeontologically defined boundary (Fig. 8).

Ward et al. (2000) confirmed the findings of Smith (1995) with regard to the change in fluvial style. The change in facies from high to low sinuosity occurs over 30 m or less and could have been caused by a number of mechanisms. Tectonically, if slopes were made steeper, a change in fluvial style would be seen. Ward et al. (2000) accepted that a tectonic pulse may have caused this change in slope, however they proposed that the observed change in fluvial style was more likely caused by a loss of bank strength following widespread plant die-off. This would have produced an increased sediment load, which would have caused a change in the fluvial style. The authors favoured the change by major plant die-off, i.e., a catastrophic and global event, rather than a gradual one due to tectonic activity, as there was no evidence for this mechanism.

Smith and Ward (2001) examined the pattern of vertebrate extinctions and suggested that the extinction in the non-marine realm was not gradual but sudden. They documented the existence of an event bed (also documented by Ward et al., 2000; Fig. 6), located at the level of the P-Tr boundary. The event bed is located within the succession, documenting the change in fluvial style, and consists of 3 to 5 m of distinctively laminated maroon mudrock. Smith and Ward (2001) agreed with the interpretations of Smith (1995) and proposed a palaeoclimatic change by drying across the alluvial plain.

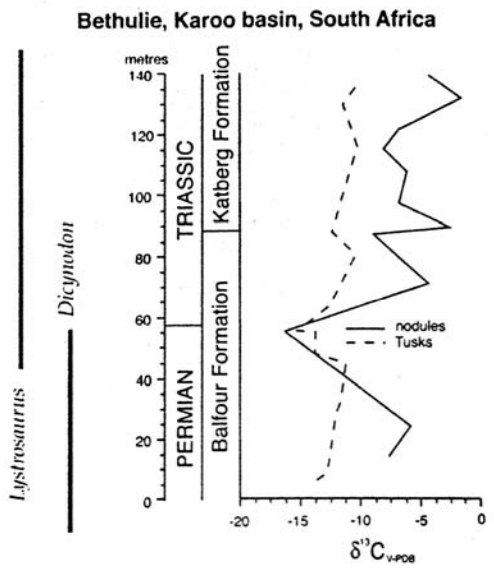


Figure 8: *The carbon isotopic signature from Bethulie (from: MacLeod et al., 2000).*

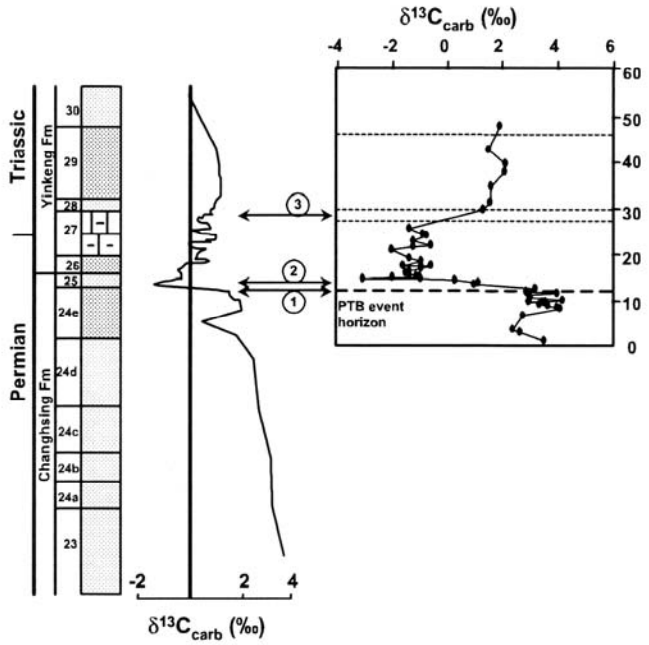


Figure 9: *Correlation between the carbon isotopic signatures in the marine realm (from: Krull et al., 2004) – Meishan (left; redrawn from Jin et al., 2000) and Heping (right; Krull et al., 2004). The following events are noted: (1) indicates the extinction event; (2) indicates a pronounced negative* $\delta^{13}C_{carb}$ *excursion; (3) indicates recovery (carb = carbonate).*

Hancox et al. (2002) examined two sections in the northern Karoo Basin, using geochemical and petrographic techniques, and conducted the first search for evidence of meteorite impact in the Karoo Basin (section 1.2.1). Hancox et al. (2002) found modest levels of iridium (up to 320 ppt over a background of 100-200 ppt) around the presumed boundary, but significant enrichment of iridium, together with impact deformation (for example, in the form of planar deformation features in quartz), was not seen. Hancox et al. (2002) concluded that the boundary may not be complete in the northern Karoo Basin, agreeing with the work of Catuneanu et al. (1998). They concluded that this iridium enrichment was not significant with respect to a possible impact event at P-Tr boundary times.

Ward et al. (2005) presented results incorporating palaeomagnetic and carbon isotope data to suggest that the vertebrate extinction was gradual in the Late Permian, but that it is punctuated by a large extinction pulse at the P-Tr boundary. This is coincident with negative carbon isotopic anomalies. Additionally, these authors suggested that factors other than the extinction of taxa stimulated the appearance of new species in the Karoo Basin in the Triassic. Ward et al. (2005) believed that there was a long-term deterioration of the ecosystem, followed by an extinction and subsequent origination pulse at the P-Tr boundary.

1.4 Objectives of this Study

Two sections from the southern Karoo Basin were chosen for this project. The first, Commando Drift Dam (Fig. 3), is constrained both palaeontologically and palaeomagnetically. The GPS coordinates of this site are 32°10.173'S and 26° 03.199'E. It is located near the town of Cradock, in the Eastern Cape, on a secondary road near Tarkastad, on the farm Hartebeeslaagte. The second study site, Wapadsberg (Fig. 3), has been constrained palaeontologically (by R.M.H. Smith), and occurs near

the well-studied Lootsberg Pass section (Fig. 3). It is located at GPS coordinates 31°52.474'S and 24°54.882'W.

A number of different techniques have been employed to test the various hypotheses regarding the cause of the P-Tr extinction. The primary objective was to produce detailed geochemical and petrographic data across the palaeontologically and at the palaeomagnetically defined boundaries, and to ascertain if any contribution towards the cause of the P-Tr mass extinction event could be made.

Major and trace element geochemistry by X-ray fluorescence spectrometry (XRF) and instrumental neutron activation analysis (INAA) were carried out. The main focus of the INAA was to detect iridium, as, if present in anomalous amounts, this would indicate a potential impact origin for the P-Tr mass extinction in the Karoo Basin. To complement the geochemistry, petrographic analysis of all minerals in thin section took place. Quartz grains were examined specifically, from thin sections of samples from below, at and above the palaeontologically-defined boundary for planar deformation features, an unequivocal indicator of meteorite impact. Planar deformation features are shock metamorphic features which are considered diagnostic of impact origin, as only a meteorite impact could produce sufficient pressures (~8 to 30 GPa) to form such features in upper crustal rocks (e.g., Stöffler and Langenhorst, 1994; Grieve et al., 1996).

In order to test the hypothesis that extinction was caused as a result of volcanism or by methane clathrate dissociation, samples were collected for carbon isotope analysis at Commando Drift Dam. Measuring the ratio of the stable isotopes ^{13}C and ^{12}C in carbon-rich material provides a palaeoclimatic indicator. The amount of any difference between the carbon isotope ratio of the sample and a standard indicates a change in the biological productivity or an input of carbon (e.g., by volcanic means) into the atmosphere (see for e.g., Benton and Twitchett, 2003).

CHAPTER TWO: METHODOLOGY

Two sections from the southern Karoo (Wapadsberg and Commando Drift Dam, see Fig. 3) were sampled. The P-Tr boundary was identified, for both Commando Drift Dam and Wapadsberg, using sedimentological and palaeontological constraints (LAD *Dicynodon*, J. Hancox, pers. comm., 2003). Additionally, the section from Commando Drift Dam was already palaeomagnetically constrained, through the palaeomagnetic results of de Kock (2003).

The palaeontologically-defined P-Tr boundary is located at the contact of the Palingkloof Member and the Elandsberg Member, within the Balfour Formation (Fig. 10). In places, a laminated mudstone layer, only a few centimetres thick, can be seen to separate the Palingkloof and Elandsberg Members. The first occurrence of the red-brown mudstones is commonly, but not always, coincident with the LAD *Dicynodon.*

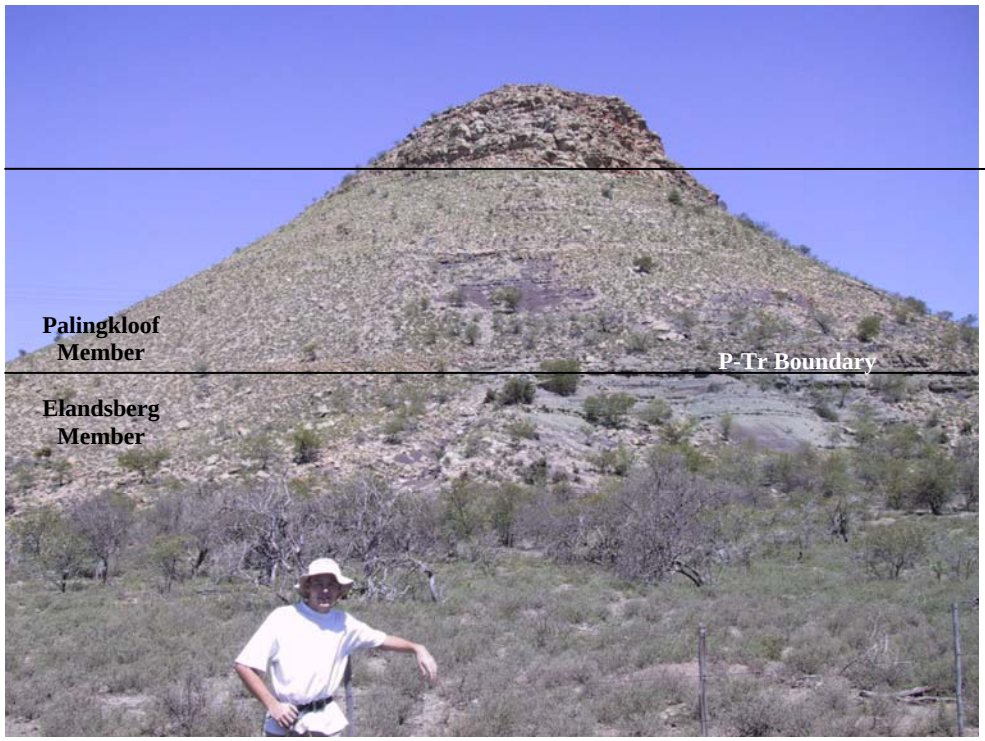


Figure 10: *Commando Drift Dam section, showing the position of the P-Tr boundary. The boundary is marked by the* LAD *Dicynodon and the first appearance of the red-brown and maroon mudstones of the Palingkloof*

Member. The Elandsberg Member is characterized by dark grey to greenish-grey mudstones. The Katberg Formation consists of a multistoried conglomeratic sandstone.

2.1 Sample Collection

Samples were collected at the two localities using both a rock drill and a hammer and chisel, dependent on the nature of the rock. In general, the drill was used to collect sandstone and carbonate samples, as these were harder than the siltstones and mudstones. Samples were collected from both below and above the palaeontological boundary, and up to, and above the palaeomagnetic boundary for the Commando Drift Dam section. Sample spacing was initially every 50 to 100 cm, but close to the boundary this was decreased to a smaller spacing (± 2 cm), in order to obtain the best resolution for geochemical analysis. For the Commando Drift Dam section, samples were collected from 6.5 m of the uppermost Elandsberg Member and 5.9 m of the lowermost part of the Palingkloof Member. For the Wapadsberg section, 6.97 m of the uppermost Elandsberg Member and 2.1 m of the lowermost part of the Palingkloof Member were sampled.

2.2 Thin Section Preparation

Polished thin sections were prepared in the School of Geosciences (University of the Witwatersrand) in order to examine petrographic changes across the palaeontological and palaeomagnetically defined P-Tr boundaries, as well as to examine quartz grains for PDFs. Samples representative of all the different lithologies were chosen.

2.3 Geochemical Analyses

A number of mineralogical and geochemical methods were used in the analysis of the samples, including X-ray fluorescence spectrometry,

instrumental neutron activation analysis, stable isotope analysis, X-ray diffraction (XRD) and cathodoluminescence (CL).

2.3.1 X-Ray Fluorescence Spectrometry

X-ray fluorescence spectrometry is used to determine both major and trace element compositions of a sample. The samples were first crushed and milled to talcum-powder fineness (after pre-contamination of crushing instruments by sample for each sample). Samples were milled in tungsten metal carbide swing mills. Pressed powder pellets (used for trace element analysis) were prepared from the sample powder; the powder was combined with glue (Mowiol) and placed into aluminium cups. Fusion discs (used for major element analysis) were made using 1.28 g of sample with 1.5 g flux (a mixture of lithium tetraborate, lithium carbonate and lanthanum oxide) and sodium nitrate (an oxidising agent). A PW 1400 XRF machine was used at the School of Geosciences, University of the Witwatersrand. A Rhodium x-ray tube was used, run at 50 KV and 50 mA.

Standards used for major element analysis were NIM G (granite), and NIM N (norite), and standards used for trace element analysis were SGR-1 (Green River shale), STM-1 (syenite), NIM G (granite) and GS-N (granite).

For the major elements, analytical precision is listed in Table 2 (S. Turner, pers. comm., 2004). Trace element analytical precisions are given in Table 3 (S. Turner, pers. comm., 2004).

2.3.2 Instrumental Neutron Activation Analysis

Instrumental neutron activation analysis (INAA) is a method that is used for the simultaneous determination of about 25-40 major, minor and trace elements in small geological samples (Koeberl, 1993, 1994). This method allows selective determination of elements in the ppm or ppb range without chemical treatment. It is based on the “activation” of powdered rock samples with neutrons.

Table 2: *Analytical precision for major element analysis by XRF (S. Turner, pers. comm., 2004).*

Element	Standard Deviation	Absolute % Error	Relative Error %	Standard Range (wt%)
Fe_2O_3	0.09	-0.03	-3.7	0.09-26.65
MnO	0.01	-0.009	4.8	0.01-0.35
TiO_2	0.07	-0.04	13.7	0.00-2.69
CaO	0.04	0.003	0.2	0.11-16.03
K_2O	0.07	0.005	-5.6	0.01-15.40
P_2O_5	0.02	-0.02	14.2	0.01-1.40
SiO_2	0.36	0.06	-0.09	34.40-76.31
Al_2O_3	0.07	0.07	1.3	0.30-30.04
MgO	0.18	-0.05	-6.1	0.03-43.18
Na_2O	0.13	-0.05	-6.8	0.04-6.57
LOI	0.26	-0.21	7.1	
Total	0.58	-0.18	0.2	

Table 3: *Analytical precision for trace element analysis by XRF (S. Turner, pers. comm., 2004). LLD = Lower Limit of Detection.*

Element	Standard Deviation	Absolute Error - ppm	Relative Error - %	LLD - ppm
Rb	2	1.0	-1.9	3
Sr	2	1.3	0.4	3
Y	2	-0.7	-3.7	3
Zr	3	4.3	1.2	8
Nb	1	-2.4	-8.5	3
V	9	-3.8	-12.7	12
Cr	7	0.7	5.2	12
Co	2	0.7	-10.7	6
Ni	2	0.6	-9.3	6
Cu	5	1.9	-0.3	6
Zn	2	2.8	-6.2	6
Ba	7	12.0	3.1	20
Pb	2	3.1		10
As	2	4.7		15

During the irradiation with neutrons, the naturally occurring stable isotopes of the constituent elements are transformed into higher-mass unstable isotopes by neutron capture reactions. Prompt gamma radiation is also produced, and this can be used as the analytical signal if measured during irradiation (prompt-gamma instrumental neutron activation analysis); this is not to be confused with the analytical signal in standard INAA (as used here). After irradiation, the activated nuclei decay, usually emitting beta and gamma rays, the latter with one or more characteristic energies (in the range between 60–2000 keV). The amount of the radioactive nuclide is then determined by measuring the intensity of these decays, using a gamma-ray detector. As irradiated geological samples contain radionuclides of different half-lives, the gamma spectra change with time, and thus three counting cycles are recorded over a period of two weeks in order to detect all the isotopes present in the sample.

A nuclear reactor is used as the source of neutrons for the irradiation of samples. Neutrons emitted during the fission of ^{235}U (the most commonly used element for nuclear reactors) are too energetic (too fast) to be used for neutron activation analysis (or to sustain a chain reaction). They are therefore slowed down (or moderated, usually by water), which leads to a loss in kinetic energy and to a different energy spectrum. This process of moderation is essential to keep the chain reaction in the reactor fuel going. There are three groups of neutrons (based on energy) produced, and INAA makes use of thermal neutrons, which have energies in the range of 0.001-0.5 eV. In a standard research reactor, these neutrons have the highest neutron flux, which is essential for the interaction between the reactor neutrons and the target nuclei (the probability of which is known as the neutron capture cross-section). The larger the cross-section of an isotope, the more neutron capture reactions occur, and the “easier” the isotope can be determined by neutron activation analysis (Koeberl, 1994).

The instrumentation for INAA consists of three main parts: the gamma ray detector, the electronic signal processing and amplification part, and a

multi-channel analyser (for storage of all measured signals). A computer system is used for evaluation (and acts as the multichannel analyzer as well).

Aliquots of powders (100–250 mg) were weighed into polyethylene vials. The vials were then heat sealed, together with geological standards [AC-E, a granite standard from France (Govindaraju, 1989); ALL, the Allende meteorite sample (Jarosewich et al., 1987); G2, a granite from the USGS (Govindaraju, 1989), and WMG1, a PGE reference material (CANMET, 1994)]. The samples were packed into aluminium foil, and then packed into a larger irradiation vial and irradiated at the Atomic Institute of the University of Vienna in a TRIGA Mark II type reactor for ~8 hours at a flux of 2.10×10^{12} $ncm^{-2}s^{-1}$. After a cooling period of one day, the samples were transferred to the INAA laboratory at the Department of Geological Sciences (Geochemistry) at the University of Vienna. After decontamination (washing with HCl, NaOH and distilled H_2O), the samples were counted repeatably using HpGe (high-purity germanium) detectors. The first counting period (to detect short-lived isotopes; e.g., Na, K, Ga, As, Br, Mo, Sb, W, Au) is done 1-3 days after irradiation, and takes 45 minutes per sample. The second counting period (to detect medium-lived isotopes; e.g., Cr, Fe, Rb, Sb, Zr, Ba, rare earth elements) takes 2-4 hours per sample and takes place 3-7 days after irradition. A third counting cycle (for the long-lived isotopes; e.g., Sc, Co, Ni, Z, Se, Sr, Ir) takes place 2-3 weeks after the end of the second one, and involves 12-24 hour counting.

Data evaluation takes place after all three measurement cycles have been completed. This involves calibration of the spectra and correction for errors using the computer software, and then calculations of the concentrations of the elements using comparison with standard data, whilst correcting for peak interference.

Precision and accuracy of this method can be very good, if procedures and analysis are followed correctly. Factors affecting precision are (1) weighing errors, (2) geometry errors during counting, (3) flux variation during irradiation, (4) poor counting statistics in the peak area determination, and (5) sampling errors. On the whole, these errors should not create much of a problem, as the first 3 errors can be taken into account and corrected for using the computer software, and sampling errors can be avoided using standard techniques. The fourth error (which is generally affected by small sample quantities) was avoided here, as enough sample material had been collected, and counting times were adjusted in order to ensure that these were correct. Some samples were duplicated to check for precision. For most elements there is ~5% relative precision in the INAA data (Table 4), although in some cases it can reach 10 or 15 relative percent.

Accuracy is affected by (1) interfering nuclear reactions yielding the same product nuclide, (2) spectral interferences from overlapping gamma peaks, (3) self-shielding in the samples due to the presence of high cross-section elements, (4) dead-time errors (the detector and electronic system processing one pulse and missing another), and (5) problems with standards. These factors can be quantified and corrected for; thus, this method of analysis is very accurate. Accuracy was checked by treating standard reference materials with known compositions the same way as unknown samples.

Detection limits for INAA are difficult to estimate because there are many factors involved, including matrix composition, counting times and geometry, detector characteristics, sample size, etc. Typical detection limits range from 10^{-3} to 10^{-10} g/g for different elements (Koeberl, 1994).

Table 4: *Typical precision values for elements in the Vienna INAA Lab (C. Koeberl, pers. comm., 2004) (all elemental abundances in ppm, unless otherwise stated).*

Element	Precision (relative %)	Element	Precision (relative %)
Na (wt %)	2	La	2
K (wt %)	5	Ce	3
Sc	2	Nd	5
Cr	3	Sm	2
Fe (wt %)	4	Eu	2
Co	2	Gd	5
Ni	15	Tb	2
Zn	3	Tm	5
As	10	Yb	2
Se	10	Lu	2
Br	10	Hf	2
Rb	2	Ta	2
Sr	5	W	10
Zr	10	Ir (ppb)	Dependent on detection limit
Sn	2	Au (ppb)	15
Sb	5	Th	2
Cs	2	U	10
Ba	10		

INAA confirmed the accuracy of the XRF results for several elements that were measured using both methods. For Fe, K and Na, a straight line is produced when the element concentrations from both methods are plotted against one another (Fig. 11), and these regression lines are all approximately at 45^{o} slopes.

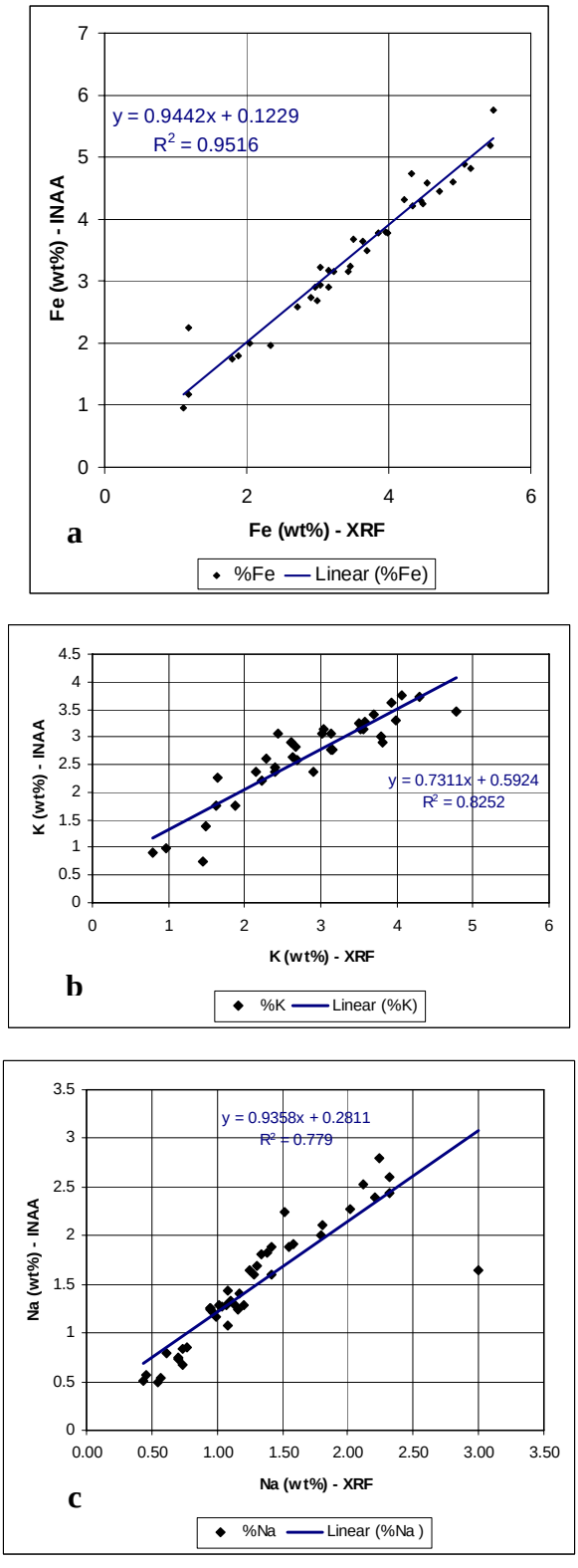


Figure 11: *Correlation of XRF and INAA results:* **a:** *Commando Drift Dam samples: Fe (wt%);* **b:** *Commando Drift Dam samples: K (wt%);* **c**: *Wapadsberg: Na (wt%).*

2.3.3 Stable Isotope Analysis

Samples chosen for stable isotope analysis were from the Commando Drift Dam section, as this section is constrained both palaeontologically and palaeomagnetically. Initially, the samples were analysed to determine whether there was enough sulphur and/or carbon present for isotopic analysis. Samples were analysed for sulphur and carbon concentrations at both the School of Geosciences, University of the Witwatersrand (by XRF) and at the Department of Geological Sciences (Geochemistry) at the University of Vienna, Austria (by XRF), and the isotope measurements were made at the University of Vienna. The technique of Isotope Ratio Mass Spectrometry, which is commonly used for the determination of stable isotope ratios, was employed (Gill, 1997). Mass spectrometry is based on the principle that the motion of a charged particle (ion) is affected by the mass to charge ratio (m/z) (Gill, 1997).

For stable isotope analysis, the difference in the ratio between the abundances of two stable isotopes of a sample and a standard is measured. The present day ratio is known, and standards exist for each of the different isotopic systems. The ratio of the stable isotopes in a sample is measured, and any difference between this ratio and that of the standard indicates palaeoclimatic changes from the present day climate, or alteration, diagenesis, fractionation and other chemical effects, and may indicate what has caused that change (see Benton and Twitchett, 2003).

2.3.3.1 Carbon Isotopic Analysis

For carbon isotope analysis, the ratio $^{13}C/^{12}C$ is measured. In nature, ^{12}C is the dominant isotope (98.9%), with much smaller amounts (1.1%) of ^{13}C (Gill, 1997). The ratios of these two stable isotopes vary within different substances, e.g., rainwater vs. seawater. Plants will preferentially take up ^{12}C during photosynthesis to produce organic matter, and should this organic matter be buried, then the carbon

isotope ratio (expressed as $\delta^{13}C = \{(^{13}C/^{12}C \text{ sample})/(^{13}C/^{12}C \text{ standard}) - 1\} \times 1000$) will shift in favour of the heavier isotope (see Benton and Twitchett, 2003). During periods of high productivity, large amounts of organic matter become fixed in the surface waters of the oceans and become enriched in ^{13}C; thus, any carbonates that are precipitated from these surface waters will record a positive shift in $\delta^{13}C$ (see Benton and Twitchett, 2003).

A Carla Erba NC 2500 elemental analyser, connected to a Micromass Optima mass spectrometer was used for these analyses. For bulk carbon measurements, each powdered sample was weighed into a 12 x 5 mm tin capsule with a mixture of V_2O_5 and SiO_2 to promote full combustion (Yanagisawa and Sakai, 1983). For each sample, duplicates were processed. A continuous flow system was utilised in order to introduce the samples to the mass spectrometer. The samples were placed into an auto-sampler carousel. The samples were then dropped into the combustion reactor (the elemental analyser Carla Erba NC 2500) – a vertical quartz tube maintained at 1020^{o}C, which was filled with silvered cobaltous cobaltic oxide, overlain by chromium oxide. The cobaltous cobaltic oxide and the chromium oxide function as oxidising agents. The reduction reactor, a second quartz tube, was filled with pure copper (a reducing agent) and was maintained at 650^{o}C. Once the sample was dropped into the reactor, the helium stream was enriched with pure O_2 and both sample and tin capsule were oxidised in a flash combustion reaction at ~1800^{o}C. The temperature is so high that all carbon forms (high- and low-temperature carbon: probably present as hydrocarbons, condensed carbonaceous film, graphite, carbonates, CO_2 and organic carbon) are used for concentration and isotopic analyses.

After the gas mixtures pass through the reduction reactor, they are dehydrated using a water trap filled with $Mg(ClO_4)_2$. They then enter a chromatography column (maintained at 50^{o}C), in which the mixture is

separated into its individual gaseous products (N_2, CO_2 and SO_2). The CO_2 is separated (using a He carrier gas) into a split interface and is then measured by the mass spectrometer for both the concentration and isotopic ratio of carbon.

The Micromass Optima mass spectrometer is a magnetic isotope ratio mass spectrometer and consists of (1) an ion optics system, (2) an ion source, (3) an ion collector, (4) a sample inlet system, and (5) a data processing unit (B. Bodiselitsch, University of Vienna, pers. comm., 2004).

The ion optics system must fulfil the following requirements: (1) the optical transmission must be high, stable and independent of mass, and (2) mass dispersion must be large enough in order for three or more ion collectors (Faraday cups) to be used. For CO_2 analyses, the accelerating voltage must be higher (3.5 kV) than for SO_2 analyses (2.5 kV) in order to ensure good resolution and sensitivity.

The ion source must have high sensitivity, high stability and a low energy dispersion ion beam. Average currents larger than 10^{-10} A should be produced for highest precision. The ion source for the Micromass Optima mass spectrometer produces electrons by thermal extraction from a rhenium wire filament. The electrons collide with gas molecules and combine to produce charged ions, and the majority of these are collected in an electron trap to provide a constant flow of electrons through the source.

After the charged ions have been produced and after separation of two (or more) ion currents (with different isotopic ratios), the different beams enter the ion collectors (Faraday cups). The collected ions are converted into an electric current, which is fed into an amplifier. The Faraday cups are metal cups which are grounded with a resistor. Three Faraday cups are utilized with the Micromass Optima mass

spectrometer. The Micromass Optima mass spectrometer is kept at a constant, high vacuum (about 10^{-8} Torr within the mass spectrometer). For organic carbon measurements, ~0.3 mg of the sample was treated with 10% HCl for 24 hours to eliminate carbonate content. After centrifuging, the samples were washed with distilled water, and then dried in a 70^{o}C oven for three days. The samples were then measured in the same way as described above.

The reference gas for isotopic calibration is supplied from a CO_2 bottle injected into the carrier gas between the elemental analyzer and the split interface. The standard for carbon is the Vienna Pee Dee Belemnite (a Cretaceous marine fossil, *Belemnitella americana*, from the Pee Dee Formation in South Carolina) which has an absolute ratio of $^{13}C/^{12}C$ of 0.0112372 (Coplen, 1996). The measured precision for the isotopic measurements (1σ) is ± 0.3 ‰. Detection limits for the carbon concentrations are ~10 ppm.

2.3.3.2 Sulphur Isotope Analysis

For sulphur isotopic analysis, the ratio of the ^{34}S (4.2% natural abundance) to ^{32}S (95%) is measured (Gill, 1997). In groundwater, sulphur isotopes are useful for determining the source of dissolved sulphate and/or determining the geochemical processes that affected the sulphate concentration in the groundwater.

The elemental analyser (Carla Erba NC 2500) connected to the Micromass Optima mass spectrometer was also used for this analysis, where the ratio $^{34}S/^{32}S$ was measured. A combination of both a continuous flow inlet system and a dual inlet system was used. SO_2 is separated from the other combustion gases by gas chromatography, and the SO_2 gas enters the mass spectrometer through the split interface for the measurement of the isotopic ratios.

Differences to the technique for carbon analyses include (1) oxidation and reduction in a single quartz tube, instead of two, and (2) a dual inlet system is used instead of a continuous flow system. Initially, powdered samples were weighed into a 12 x 5 mm tin capsule with a 1:2 mixture of V_2O_5 and SiO_2. For each sample, duplicates were processed. The samples were placed into an auto-sampler carousel. The samples were then dropped into a vertical quartz tube maintained at 1020^{o}C. The reactor was filled with pure copper overlying a mixture of WO_3 and Al_2O_3. Once the sample was dropped into the reactor, the helium stream was temporarily enriched with pure O_2, and both sample and tin capsule were oxidised in a flash combustion reaction at ~1800^{o}C.

After the gas mixtures pass through the reduction reactor, they are dehydrated using a water trap filled with $Mg(ClO_4)_2$ and the gas mixtures then enter a chromatography column (maintained at 80^{o}C), in which individual gas products are separated (N_2, CO_2 and SO_2). The SO_2 is introduced with He carrier gas into a split interface and is then measured by the mass spectrometer for both the concentration and isotopic ratio of sulphur.

The reference gas for isotopic calibration was supplied by a dual-inlet system filled with SO_2 gas, which is injected into the carrier gas between the elemental analyzer and the mass spectrometer. The reference material is the hypothetical Canyon Diablo Troilite (combined standards IAEA-S 1, 2, 3; Govindaraju, 1989), and the measured precision for the isotopic measurements (1σ) is ± 0.4 ‰. The detection limit for the sulphur concentration is ~30 ppm.

Sulphur contents were measured using XRF after grinding and milling of the samples. The concentration of sulphur was, however, below the detection limit of ~30 ppm, and thus the samples could not be analysed for sulphur content, as part of this project.

2.3.4 X-Ray Diffraction

X-ray diffraction was used in order to qualitatively determine the mineral phases in the rock samples. The samples were powdered to talcum-powder fineness using an agate mortar and pestle (after initial crushing and milling as described in section 2.3.1). They were then pressed into chromium frames that are mounted in the machine. The samples were scanned through 70 degrees. Measurements of various angles can be used to determine the inter-planar spacings that are characteristic of the diffracting crystal, and thus to determine the identity of the minerals in the sample.

A PW 1830 machine was used at the School of Geosciences, University of the Witwatersrand. The X-ray tube is made of copper and was run at 50 KV and 50 mA. A Si standard was used to calibrate the instrument (S. Turner, pers. comm., 2004).

2.3.5 Cathodoluminescence

Cathodoluminescence (CL) is the emission of photons of UV to IR wavelengths, produced by bombarding a material with an electron beam (Hayward, 1998). Electrons are excited in a material, and as they decay, photons are released. Emissions are caused by the presence of various defects in the crystal structure. The technique is particularly useful in analysing carbonate samples. It is a rapid and simply applied technique for gathering information on fine-grained samples, which cannot be fully assessed by optical microscopy. Here, fine-grained samples were analysed in order to determine the carbonate phases. Calcite ($CaCO_3$) luminesced with an orange colour, as Ca^{2+} was excited by Mn^{2+}. Dolomite ($CaMg(CO_3)_2$) is also activated by Mn^{2+}, but as it excites both Ca^{2+} and Mg^{2+} sites, it luminesced with a redder colour.

A CITL Mk.3a cold cathode optical CL system was used, together with an Olympus BH-2 petrographic microscope. The samples (polished thin sections) were analysed at the School of Geosciences, University of the Witwatersrand. A Leica DC 100 CCD camera was used with Leica DC

100 software version 2.31 to record CL effects. For cold-cathode optical CL, a vacuum chamber and a cold-cathode electron gun are mounted on the stage of a petrographic microscope. The beam voltage used was 15-20 kV at currents of 250-300 μA.

CHAPTER THREE: RESULTS

3.1 Stratigraphy and Sedimentology

The P-Tr boundary in the Karoo Basin of South Africa occurs at the contact of the Palingkloof and Elandsberg members, within the Balfour Group (Figs. 5 and 7). The sharp contact between these groups is marked in places by the appearance of a thin laminated mudstone layer (Smith and Ward, 2001; this work). The Palingkloof Member is characterised by red-brown and maroon mudstones as opposed to the dark grey to greenish-grey mudstones of the underlying strata of the Elandsberg Member (Fig. 12). This is seen for both the sections at Commando Drift Dam and Wapadsberg as well as for other sections in the southern Karoo Basin (e.g., Ward et al., 2000; Smith and Ward, 2001; Retallack et al., 2003). Palaeontologically, the boundary is marked by the Last Appearance Datumn (LAD) *Dicynodon* (Fig. 6), as determined by P.J. Hancox (pers. comm., 2004).

3.1.1 The Commando Drift Dam Section

The sampled section extends over 12.4 m on a 60^{o} layered slope (10.4 m in actual height) (Fig. 13), due to the fact that the section was sampled in an erosion gulley. This is exactly the same site where de Kock sampled for his palaeomagnetic work (de Kock, 2003). Approximately 6.5 m of the uppermost Elandsberg Member and 5.9 m of the lower part of the Palingkloof Member (Balfour Formation) were sampled. The P-Tr Boundary was taken at the lithological contact of the Elandsberg and Palingkloof members. This layer occurs 5.3 m below the level of the palaeomagnetic reversal as established by de Kock (2003), and 6.5 m above the first sample taken in the rocks of the Permian.

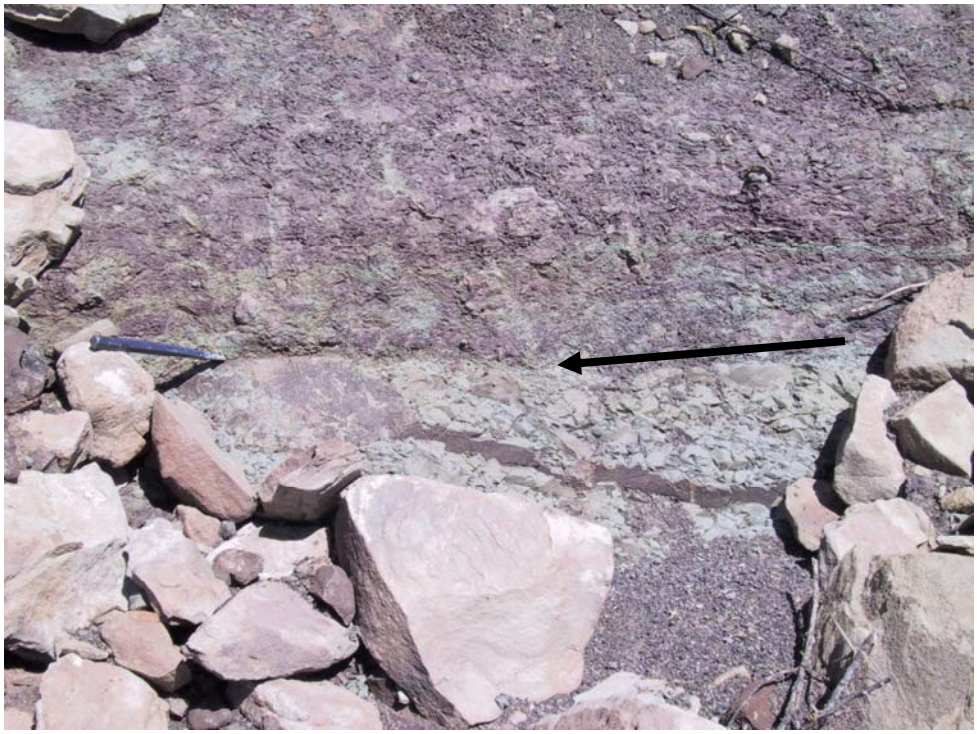


Figure 12: *The lithological and palaeontological contact of the P-Tr boundary at the Commando Drift Dam section. The contact is sharp. The green-grey mudstones of the Elandsberg Member are overlain by the red-brown mudstones of the Palingkloof Member (chisel for scale ~20 cm long).*

At the Commando Drift Dam section (Fig. 13), the lower part of the sequence contains a number of siltstones and lenticular sandstone bodies, in addition to the green-grey mudstones. The section is interrupted by four smooth-surfaced carbonate nodular horizons. The end of the Permian is marked by paleosol development and a laminated mudstone layer, referred to as an "event bed" by Smith and Ward (2001). The event bed is red-brown in colour. The lower Elandsberg Member is dominated by fines, and is also fining-upward in nature. This is interpreted to have been caused by low energy, high sinuosity meandering rivers (Smith and Ward, 2001). Above the event horizon, the siltstones and mudstones become

redder in colour (red-brown). A continuous sequence of these red-brown mudstones is observed for 2.1 m before the first irregularly surfaced carbonate nodular horizon occurs. Cross-stratified sandstones with gutter cast erosional bases, which are laterally more continuous, occur above this nodular horizon, constituting a coarsening-upward sequence to the base of the arenaceous Katberg Formation (Fig. 5). This indicates a higher energy environment, and the presence of rivers which were more braided than meandering in character (Smith and Ward, 2001).

3.1.2 The Wapadsberg Section

The entire stratigraphic sequence sampled at Wapadsberg covers 9.07 m on a 60^{o} slope (7.85 m in actual height), and is predominantly composed of mudstones (69%) (Fig.14). Approximately 6.9 m of the Elandsberg Member and 2.1 m of the Palingkloof Member were sampled. The same lithological and palaeontological observations as made along the Commando Drift Dam section (contact of Elandsberg Member and Palingkloof Member; change in colour from green-grey to red-brown sedimentary rocks; LAD *Dicynodon*) were used to define the P-Tr boundary, which was taken at the event bed of Smith and Ward (2001), 6.97 m from the first sampling location.

.

At the Wapadsberg section (Fig. 14), the stratigraphy and sedimentology are very similar to those of the Commando Drift Dam section. However, there are only two distinct carbonate nodular horizons, and these occur immediately below the boundary layer. The succession below the boundary consists of an alternating sequence of sandstones and siltstones, capped by the green-grey mudstones. Once again, there is paleosol development and a laminated mudstone layer at the boundary. Thereafter follows a succession of red-brown mudstones. Irregularly based channel sandstones and siltstones cap the section.

Fig.13

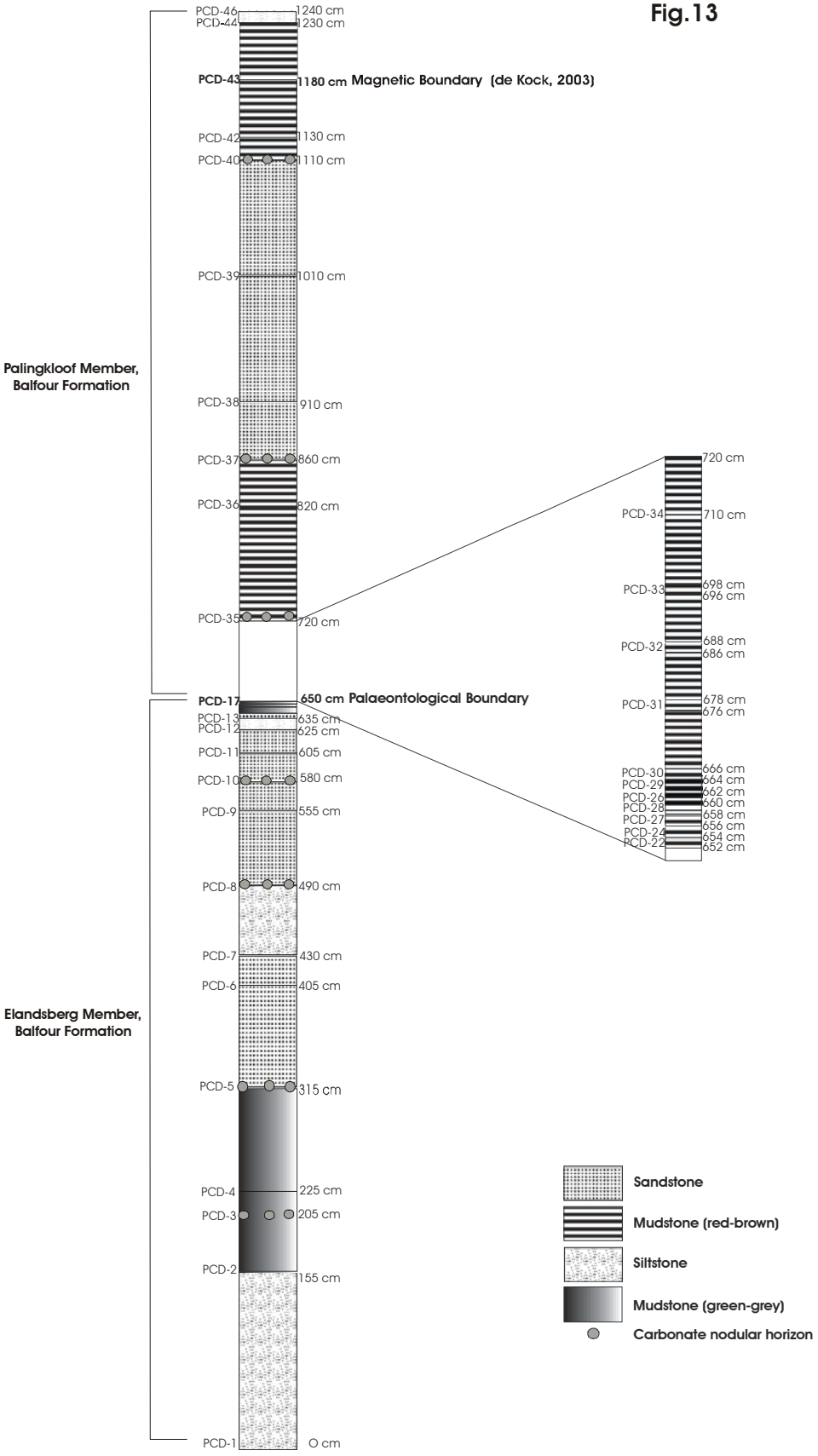

PCD-46 1240 cm
PCD-44 1230 cm
PCD-43 1180 cm Magnetic Boundary (de Kock, 2003)
PCD-42 1130 cm
PCD-40 1110 cm
PCD-39 1010 cm
PCD-38 910 cm
PCD-37 860 cm
PCD-36 820 cm
PCD-35 720 cm
PCD-17 650 cm Palaeontological Boundary
PCD-13 635 cm
PCD-12 625 cm
PCD-11 605 cm
PCD-10 580 cm
PCD-9 555 cm
PCD-8 490 cm
PCD-7 430 cm
PCD-6 405 cm
PCD-5 315 cm
PCD-4 225 cm
PCD-3 205 cm
PCD-2 155 cm
PCD-1 O cm
720 cm
PCD-34 710 cm
PCD-33 698 cm
696 cm
PCD-32 688 cm
686 cm
PCD-31 678 cm
676 cm
PCD-30 666 cm
PCD-29 664 cm
PCD-26 662 cm
PCD-26 660 cm
PCD-26 658 cm
PCD-27 656 cm
PCD-24 654 cm
PCD-22 652 cm
Palingkloof Member, Balfour Formation
Elandsberg Member, Balfour Formation
Sandstone
Mudstone (red-brown)
Siltstone
Mudstone (green-grey)
Carbonate nodular horizon

Figure 13: *Commando Drift Dam Section: Stratigraphic column. Sample numbers (PCD) are shown on the left side of the column, with distances from the initial sample (at the bottom of the sequence) shown on the right side of the column. The P-Tr boundary (based on lithological as well as palaeontological data) and de Kock's (2003) palaeomagnetic boundary are also marked. Note that the section extends over 12.4 m on a 60^{o} layered slope (10.4 m in absolute height), but is represented vertically.*

A fining-upward sequence is found below the boundary, followed by a coarsening-upward sequence above the boundary, and the same gradual hange in fluvial style as documented in the Commando Drift Dam section is noted.

3.2 Petrography

Polished thin sections were made of all the samples for the interval of the palaeontologically defined boundary, those at the palaeomagnetically defined boundary (for the Commando Drift Dam section), and of selected samples characterizing the lithologies above and below the boundary (Table 5).

There are very few changes in the mineralogy of the various lithologies, as indicated in Table 5, and most changes are based on grain size and degree of iron staining. Iron staining increases in intensity in the mudstones up sequence, and is particularly noticeable when the changeover from green-grey to red-brown mudstones is encountered at the boundary (Fig. 15). No petrographic changes are seen across the palaeomagnetically defined boundary, and these samples have the characteristics of the red-brown mudstones (see Table 5).

Fig. 14

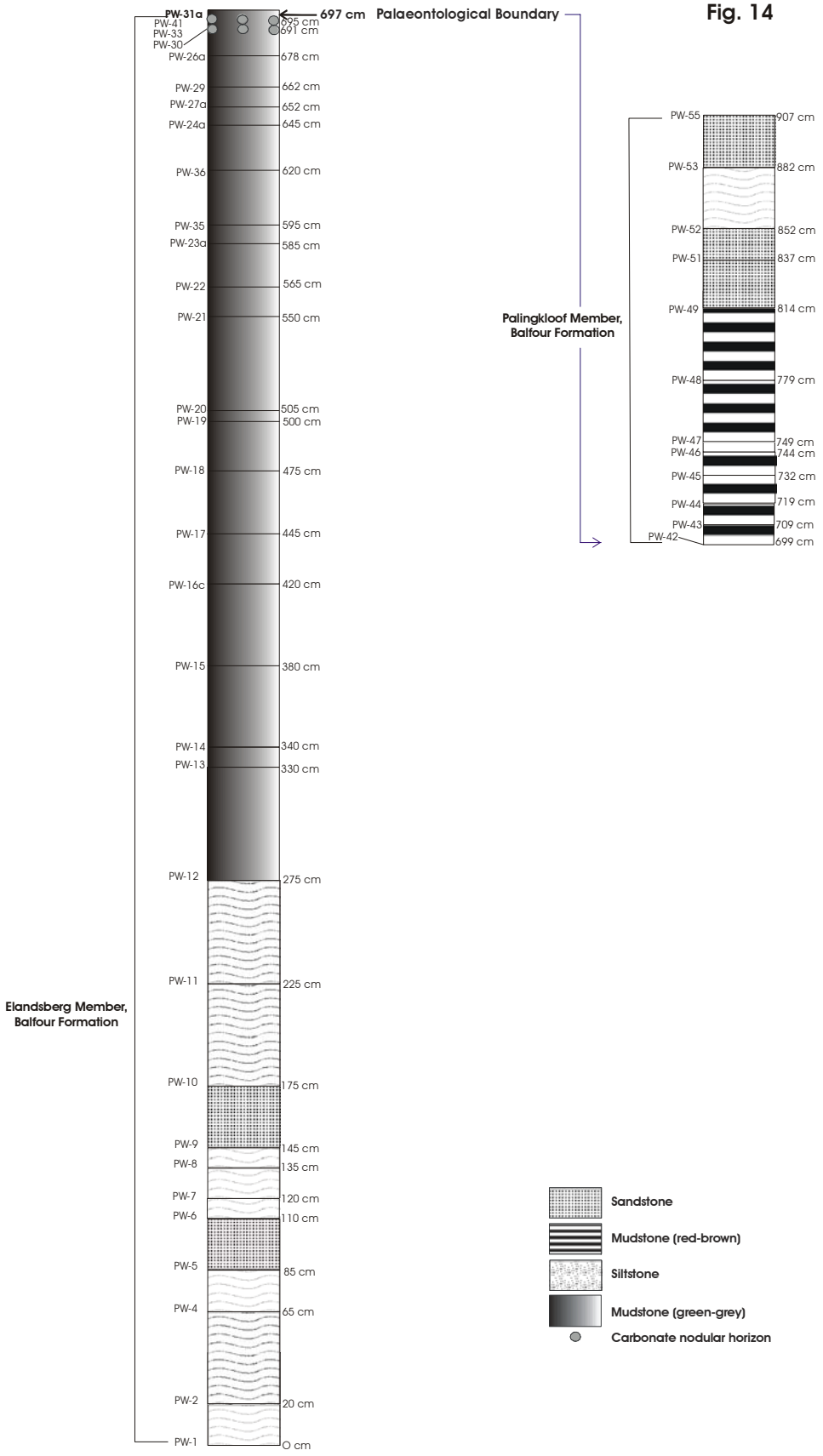

PW-31a
PW-41
PW-33
PW-30
697 cm
695 cm
691 cm
Palaeontological Boundary
PW-26a
678 cm
PW-29
662 cm
PW-27a
652 cm
PW-24a
645 cm
PW-36
620 cm
PW-35
595 cm
PW-23a
585 cm
PW-22
565 cm
PW-21
550 cm
PW-20
505 cm
PW-19
500 cm
PW-18
475 cm
PW-17
445 cm
PW-16c
420 cm
PW-15
380 cm
PW-14
340 cm
PW-13
330 cm
PW-12
275 cm
PW-11
225 cm
PW-10
175 cm
PW-9
145 cm
PW-8
135 cm
PW-7
120 cm
PW-6
110 cm
PW-5
85 cm
PW-4
65 cm
PW-2
20 cm
PW-1
0 cm
Elandsberg Member, Balfour Formation
Palingkloof Member, Balfour Formation
PW-55
907 cm
PW-53
882 cm
PW-52
852 cm
PW-51
837 cm
PW-49
814 cm
PW-48
779 cm
PW-47
749 cm
PW-46
744 cm
PW-45
732 cm
PW-44
719 cm
PW-43
709 cm
PW-42
699 cm
Sandstone
Mudstone (red-brown)
Siltstone
Mudstone (green-grey)
Carbonate nodular horizon

Figure 14: *Wapadsberg Section: Stratigraphic column. Sample numbers (PW) are shown on the left side of the column, with distances from the initial sample (at the bottom of the sequence) shown on the right side of the column. The P-Tr boundary (based on lithological as well as palaeontological data) is indicated. Note that the section extends over 9.07 m on a 60^{o} layered slope (7.85 m in absolute height), but is represented vertically.*

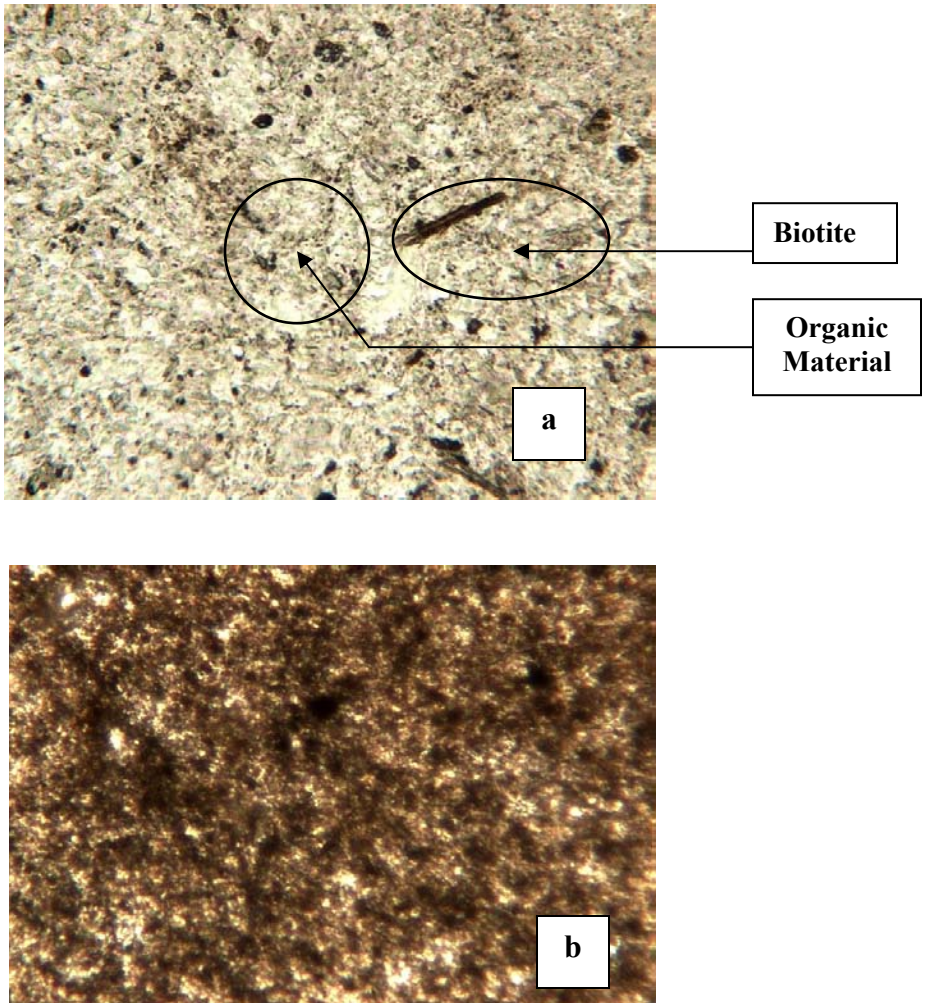


Figure 15: a: *The photomicrograph shows the green-grey mudstones (PCD 16; width of field of view: 600μm; plane polarised light).* **b:** *The photomicrograph shows the red-brown mudstones (PCD 27; width of field of view: 600 μm; plane polarised light).*

Table 5: *Descriptions of the different lithologies in the Commando Drift Dam and Wapadsberg sections.*

Lithology	Characteristics
Mudstone	The mudstones are very homogeneous in thin section, throughout the samples from both localities. The samples are very fine-grained, dominated by phyllosilicates (70-80 vol%), followed by quartz and feldspar (25-15 vol%), and ~5 vol% other detrital material. XRD was used to classify the type of phyllosilicates, and it is found that biotite is the dominant mineral, followed by montmorillonite and illite. Detrital minerals include quartz, orthoclase, biotite and chlorite, which are present in all the thin sections.
Green-grey mudstone specifics (Permian)	The mudstones in the lower part of the sequence consist of quartz, albite and anorthite, together with illite, montmorillonite and biotite which form the finer material. Towards the P-Tr boundary, the mudstones become redder in colour and show evidence of iron staining. This increases in intensity towards the P-Tr boundary.
Red-brown mudstone specifics (Triassic)	The Triassic mudstones have all been stained by iron and are redder in colour than those in the Permian. Textural changes are observed in the samples, in that some strata are coarser-grained than others. Mineralogically all these samples are similar. The samples just above the P-Tr boundary are brecciated (see Fig. 16). Sample PCD 33 was analysed by XRD, and its composition is very similar to that of the Permian mudstones in that quartz, anorthite, albite and biotite are found, in addition to chlorite.
Carbonate Nodular Horizons – Permian and Triassic	The carbonate nodular horizons are very homogeneous and fine grained. In thin section, a carbonate phase was identified, together with very fine-grained phases. Using both cathodoluminescence (CL) and X-Ray diffraction (XRD), it was shown that only calcite (orange under CL), and not dolomite (red under CL), is present as the carbonate phase (Fig. 17). The nodular horizons also have minor quartz, biotite and chlorite in the fine fraction. Figure 17 shows a photomicrograph of a typical sample from a nodular horizon.
Siltstone	The siltstones are the most homogeneous of all the lithologies in these

	profiles. The samples consist of small, angular grains. The small grain size makes it difficult to ascertain the different proportions of the minerals, but a fine fraction of phyllosilicates is present in large amounts, together with quartz and feldspar. Chlorite was detected in XRD analysis (PCD 1). Larger grains include quartz, mudflakes, and opaque minerals. The samples from the Permian part of the sequence show little iron staining, except for those close to the boundary, where this staining increases in intensity. All Triassic samples have been stained by iron. This is the major difference between the Permian and Triassic siltstones in the sequences.
Sandstone	The samples are all very similar in terms of mineralogy and grain size throughout the sequence. The sandstones have more clasts (~0.7 mm in diameter for the largest clasts) than matrix (approximately 40%). The samples are dominated by quartz and feldspars (K-feldspar – in particular microcline – and plagioclase, in similar proportions). The clast shapes are usually more angular than rounded. Some of the larger feldspar and quartz grains have been brecciated into smaller grains (Fig. 16), which can be identified due to original grain boundaries and common extinction angles. The rocks below the P-Tr boundary are green-grey in colour and there is very little iron staining, and little micaceous material (chlorite, biotite). Thin sections indicate that the amount of biotite is less in the Permian rocks than in the Triassic rocks. In thin section, grains of chlorite were not observed above the boundary, however XRD analysis revealed that chlorite is present both below and above the P-Tr boundary. Thus, chlorite may exist as a smaller fraction as part of the matrix, below and above the P-Tr boundary. The sandstones above the P-Tr boundary are red-brown in colour, and are extensively stained by iron. Mudflakes and an increase in the amount of quartz grains are observed in samples above the P-Tr boundary. Hematite is also part of the matrix material.
The Event Bed	The samples showing the event bed comprise a combination of a fine grained red-brown mudstone together with a little carbonate (calcite). The samples are somewhat brecciated, on a fine scale (Fig. 16a), and consist of subrounded to angular fragments of quartz and feldspar. The fragments are up to 0.2 mm in diameter.

Quartz grains were examined at high optical magnification for deformation features, and in particular for planar deformation features (Fig. 18). The samples from both sections are very homogeneous and fine grained, making it difficult to identify individual quartz grains, as these are all on the order of 10-50 μm in size (Fig. 16b). A number of the larger quartz grains have been brecciated into smaller fragments, which also increases the difficulty of identifying planar deformation features (Fig. 16a). However, several hundred relatively larger quartz grains that could be examined were investigated. Neither planar deformation features nor planar fracturing were found. The grains were subrounded to subangular and only contained rare fluid inclusion trails.

Apart from the change in colour (green-grey below the boundary to red-brown above the boundary), the mudstones above the boundary are less homogeneous, and are brecciated (Fig. 16). Brecciation has only been observed in two boundary samples of the Commando Drift Dam section. There was a smaller degree of brecciation observed in the boundary samples of the Wapadsberg section. This brecciation has been observed at other P-Tr boundary sites as well (Retallack, 1999; Retallack et al., 1998). Retallack et al. (1998) interpreted the claystone breccias seen in sections in Antarctica and Australia as redeposited soil (pedoliths), as many of the claystone clasts contained microfabrics typical of soils. Retallack et al. (1998) suggested that these breccias may represent soil erosion following deforestation at the P-Tr boundary. No evidence was found in the studies of Retallack et al. (1998) and in this study of impact-generated features associated with the breccias. These breccias may provide a possible correlative tool for non-marine P-Tr boundary sections.

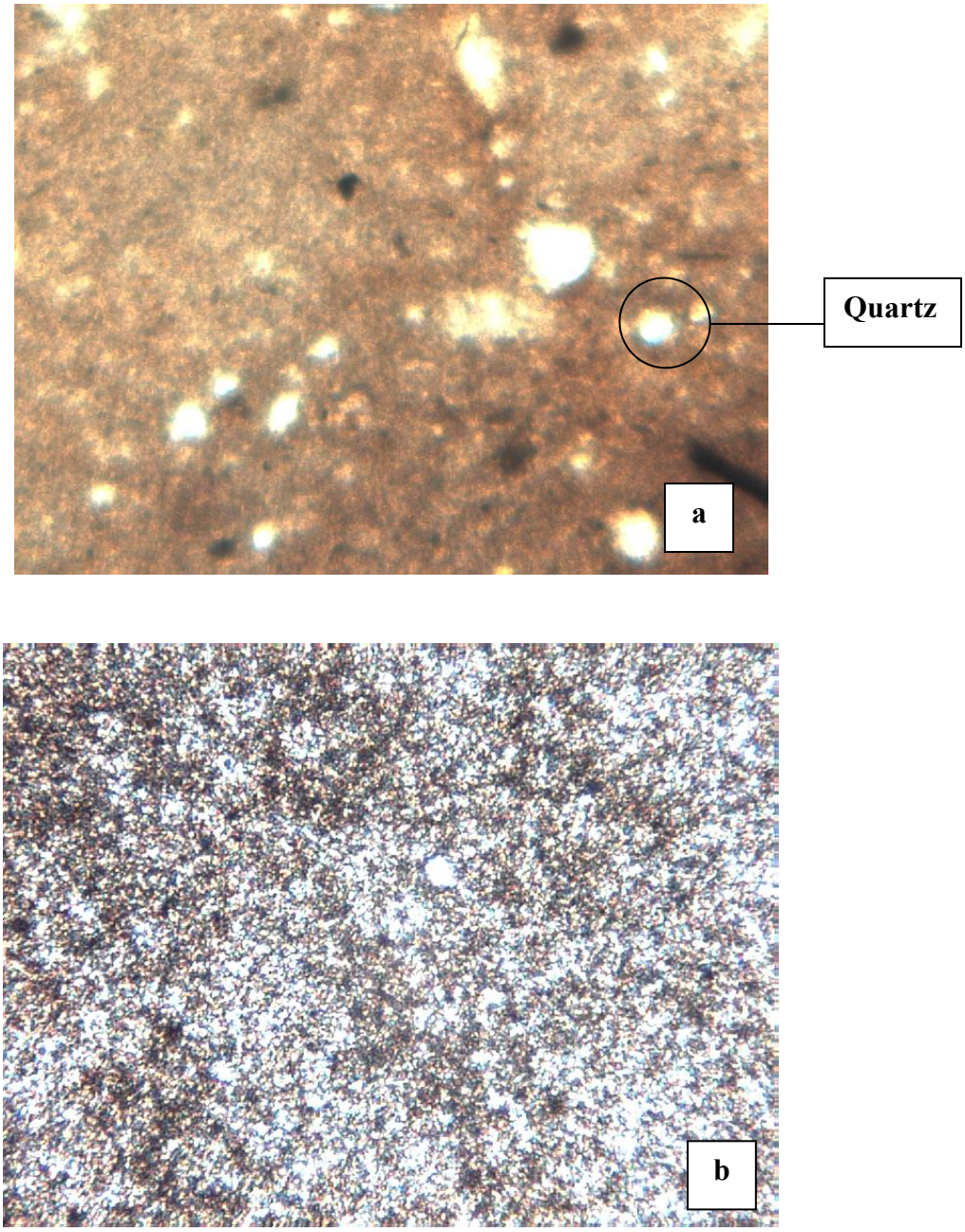


Figure 16: ***a:*** *Photomicrograph showing the fine-grained clastic component of the boundary mudstone (PCD 16; width of field of view: 1.4 mm; cross polarised light).* ***b:*** *The photomicrograph shows the homogeneity of the mudstones 14 cm above the boundary (PCD 29; width of field of view: 1.4 mm; plane polarised light).*

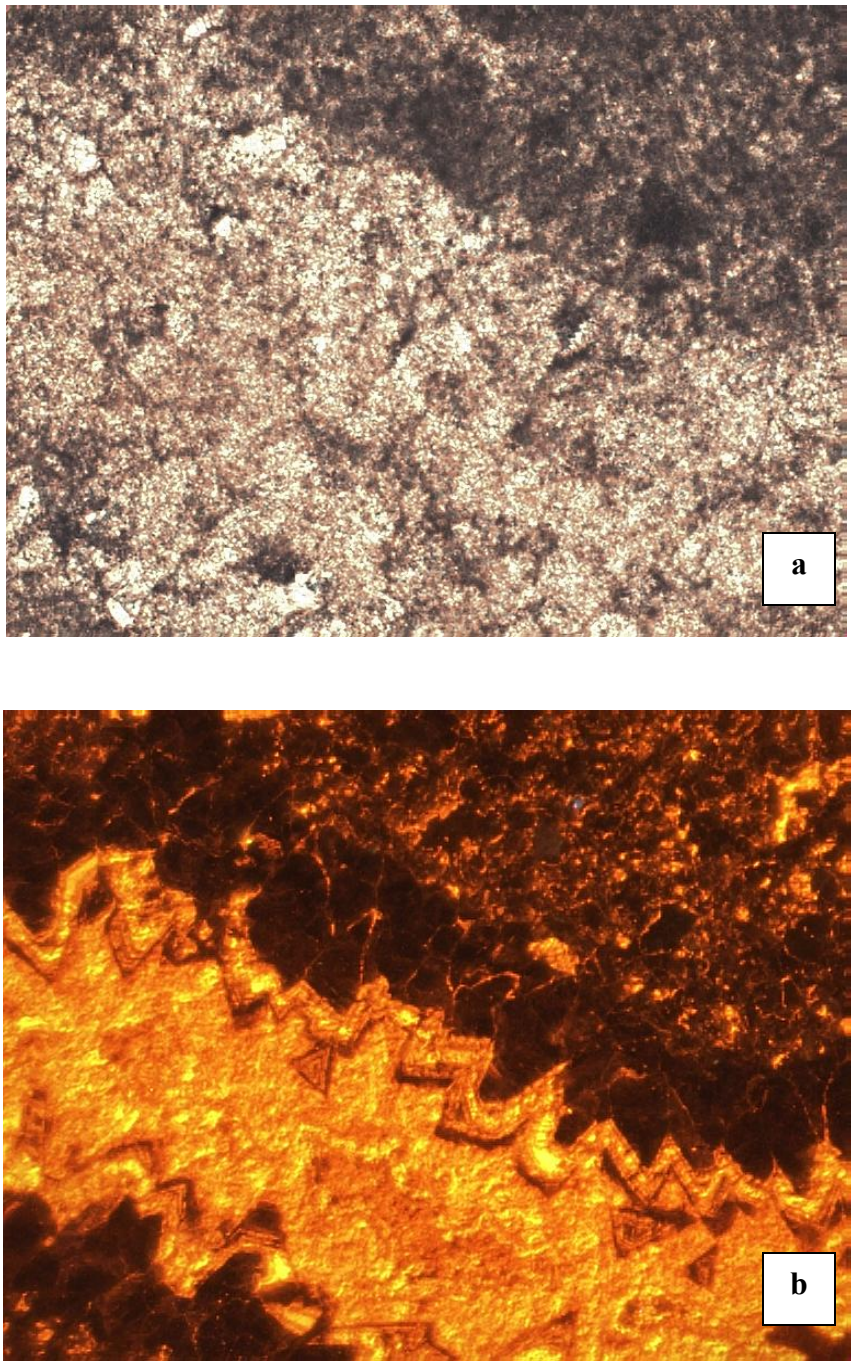


Figure 17: *Photomicrographs of a sample from a carbonate nodular horizon: widths of field of view: 1.4 mm.* ***a:*** *Plane polarised light.* ***b:*** *The application of cathodoluminescence only shows the presence of calcite, yellow-orange in colour. The texture of the carbonate nodular horizon indicates possible hydrothermal activity.*

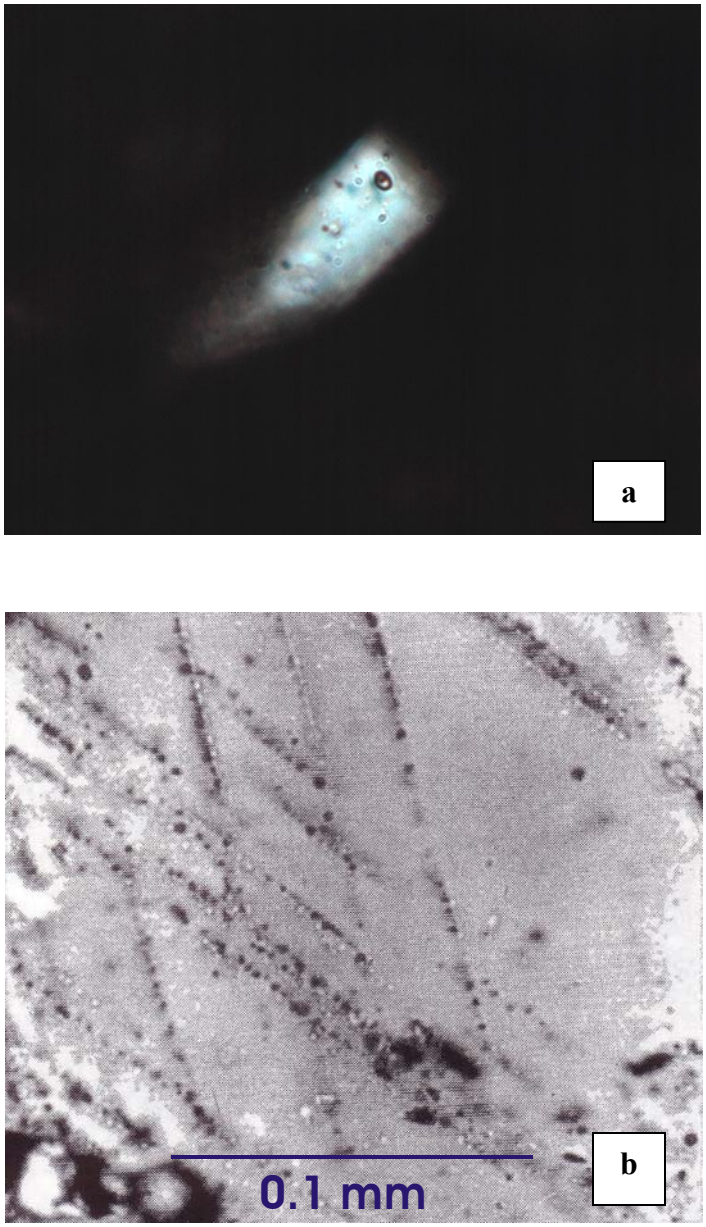


Figure 18: a: *The photomicrograph shows a typical quartz grain (ca. 10 µm in diameter) from a boundary sediment sample (PCD 17; width of field of view: 0.1 mm; cross polarised light)* **b:** *The photomicrograph shows a quartz grain in rocks from the Vredefort impact structure, containing decorated planar deformation features (PDF's; plane polarised light, from: Leroux et al., 1994; in Gibson and Reimold, 2001). No such features were found in the quartz grains from the P-Tr boundary.*

3.3 Geochemistry

Geochemical analysis was performed in order to ascertain if any major chemical changes characterize the P-Tr boundary in these continental sections. The geochemical data for the Commando Drift Dam section are contained in Appendix 1, and for the Wapadsberg section in Appendix 2.

3.3.1. Major Elements

Both sections are dominated by silicate-rich rocks, with several carbonate nodular horizons. SiO_2 contents are ~70 wt% for all rocks, except for the carbonate nodular horizons. This concentration increases by a few percent up sequence for both sections, indicating either an increase in chemical weathering (Johnson, 1991) or a change in the sediment provenance area. The next most abundant element is Al_2O_3 – with ~15 wt% in most samples. Iron (as Fe_2O_3) follows with a range in concentrations from ~4 wt% to 6.5 wt%. The carbonate nodular horizons are characterized by high CaO and low SiO_2 and Al_2O_3 contents, relative to the siliceous strata.

3.3.1.1 The Commando Drift Dam Section

The variation in major element composition (Fig. 19) is dominated by the presence of the carbonate nodular horizons. In these horizons, sharp decreases in the contents of SiO_2, Al_2O_3, Fe_2O_3, Na_2O, K_2O, MgO and TiO_2 are observed, together with strong increases in the CaO, MnO and P_2O_5 contents.

The MnO contents show consistent sharp increases from ca. 0.1 wt% to 0.4 wt% at the carbonate nodular horizons. Fe_2O_3 concentrations and MnO contents usually show similar geochemical patterns; here, however, the MnO contents form a broad peak over the second-last carbonate horizon, which extends over 3.1 m, whilst the Fe_2O_3 abundances (and MgO contents) form a wide trough at the same level. This coincides with a

sandstone layer, indicating that there must be some lithological control on the MnO and Fe_2O_3 contents at this level. This may have been caused by a post-depositional process, or possibly by a change in sedimentary provenance.

Fe_2O_3 abundance shows the most variation amongst the major elements. Iron content increases across the palaeontologically defined boundary (coincident with the colour change from green-grey to red-brown) and also attains a maximum at the palaeomagnetically defined boundary. This pattern is also shown by the variation in the MgO contents.

Molecular weathering ratios are ratios of major elements, which represent the different processes that take place during soil formation (Retallack, 2003). In the Commando Drift Dam section, the molecular weathering ratios are largely constant (Fig. 20) and indicate only changes as a result of the presence of carbonate nodular horizons. For the ratios Al_2O_3/SiO_2 and $Al_2O_3/(CaO+MgO+Na_2O+K_2O)$, a broad decrease in values is observed below the palaeomagnetically defined boundary (between 8.20 and 11.3 m above the initial sample). This decrease in the ratios Al_2O_3/SiO_2 and $Al_2O_3/(CaO+MgO+Na_2O+K_2O)$ coincides with the broad increase in MnO concentrations and decrease in Fe_2O_3 concentrations (see above), and this indicates that the cause of these two features (change in Fe_2O_3 and MnO contents and molecular weathering ratios) may be the same. It is likely that this change represents a post-depositional process (such as an input of hydrothermal fluids), which affected the chemical content of the sandstone.

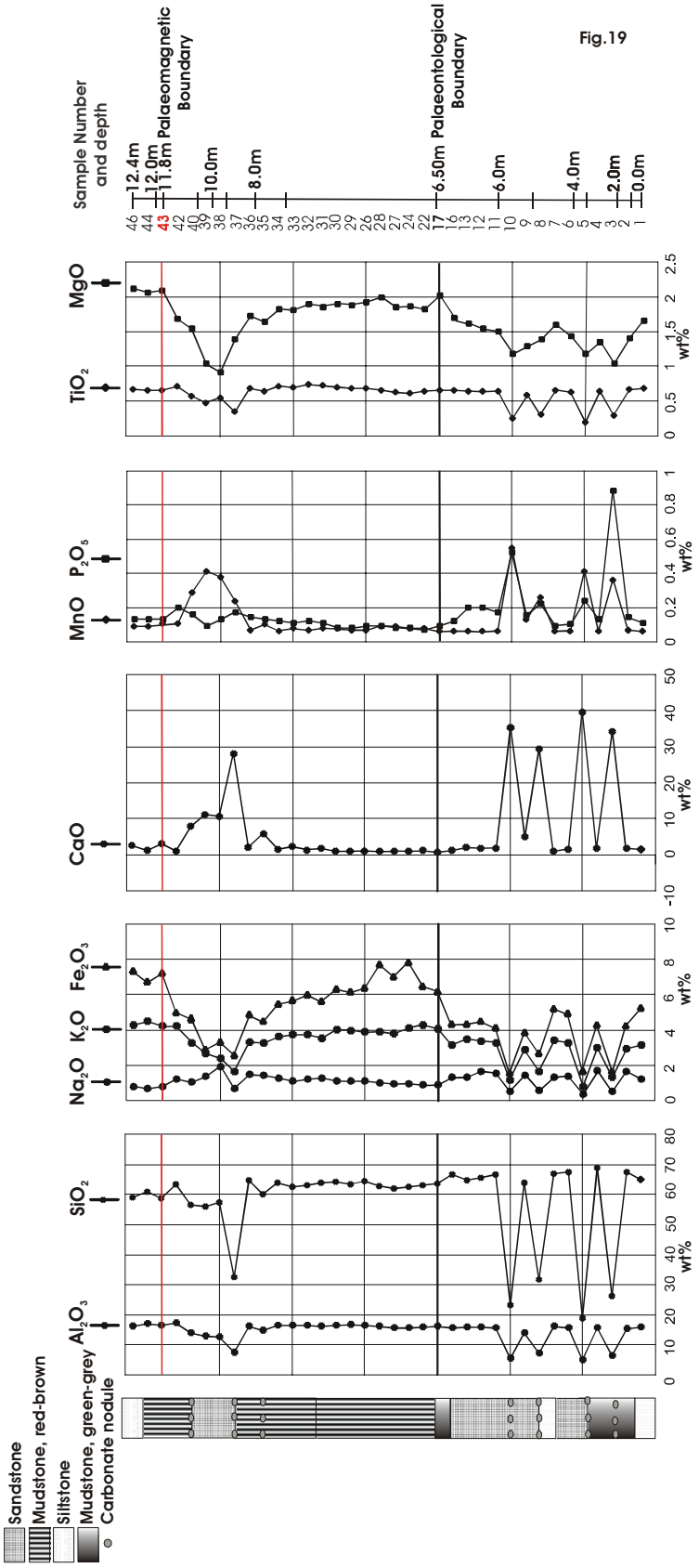

Sandstone
Mudstone, red-brown
Siltstone
Mudstone, green-grey
Carbonate nodule
Al2O3
SiO2
Na2O
K2O
Fe2O3
CaO
MnO
P2O5
TiO2
MgO
wt%
Sample Number and depth
12.4m
12.0m
11.8m Palaeomagnetic Boundary
10.0m
8.0m
6.50m Palaeontological Boundary
6.0m
4.0m
2.0m
0.0m
Fig.19

Figure 19: *Major element abundance patterns for the Commando Drift Dam section. All concentrations are in wt%. Red symbols indicate samples at the palaeomagnetic boundary.*

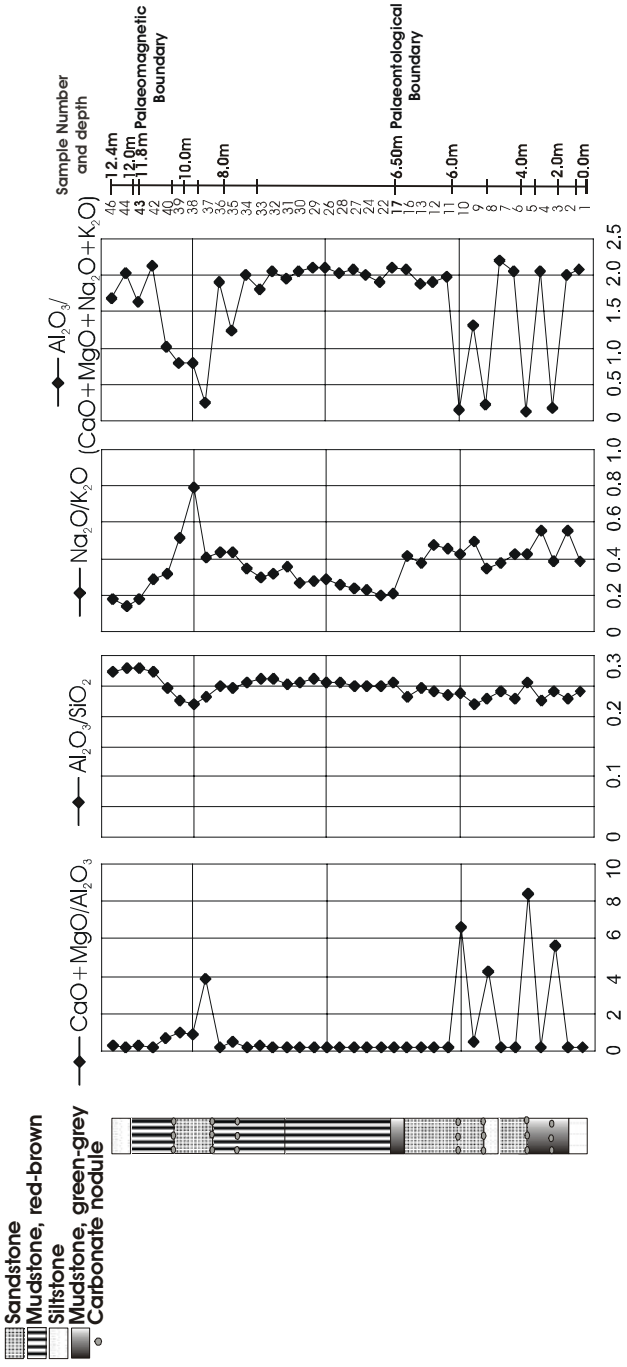


Figure 20: *Molecular weathering ratios for the Commando Drift Dam section.*

3.3.1.2 The Wapadsberg Section

The major element signature of the Wapadsberg section (Fig. 21) is very similar to that of the Commando Drift Dam section. It is dominated by the anomalies related to the presence of carbonate nodular horizons. Only two carbonate nodular horizons are seen, both below the P-Tr boundary. They are clearly indicated by the CaO contents, which increase from an average of 1.2 wt% to 29 wt% and 31 wt%, respectively.

SiO_2, Al_2O_3, Na_2O, K_2O and P_2O_5 contents decrease at the carbonate nodular horizons. Al_2O_3 abundances vary between 13 and 16 wt%. SiO_2 and Al_2O_3 concentrations are lower in the sandstones than in the siltstones. MnO contents increase within the carbonate nodular horizons (from ca. 0.05 wt% to 1.6 wt% and 2.3 wt%, respectively). The difference in the MnO contents between the two carbonate nodular horizons corresponds to the increase in concentration of CaO from the first to the second carbonate nodular horizon. No $MnCO_3$ was detected in the XRD analysis.

MgO and the K_2O contents increase above the palaeontologically defined boundary, and their patterns are similar to that of Fe_2O_3 contents. The increase in Fe_2O_3 contents is not as pronounced as in the Commando Drift Dam section.

There is a more pronounced lithological control, at Wapadsberg, on the major element concentrations between the sandstones, siltstones and mudstones than for the Commando Drift Dam section. This is particularly apparent in the lower part of the sequence. MgO contents are higher and more variable in the siltstones (1.2-1.7 wt%) than in the sandstones (0.9 wt %). The MgO concentrations are fairly constant within the mudstones (ca. 1.7 wt%). These contents decrease to 1.41 wt% at the carbonate nodular horizons.

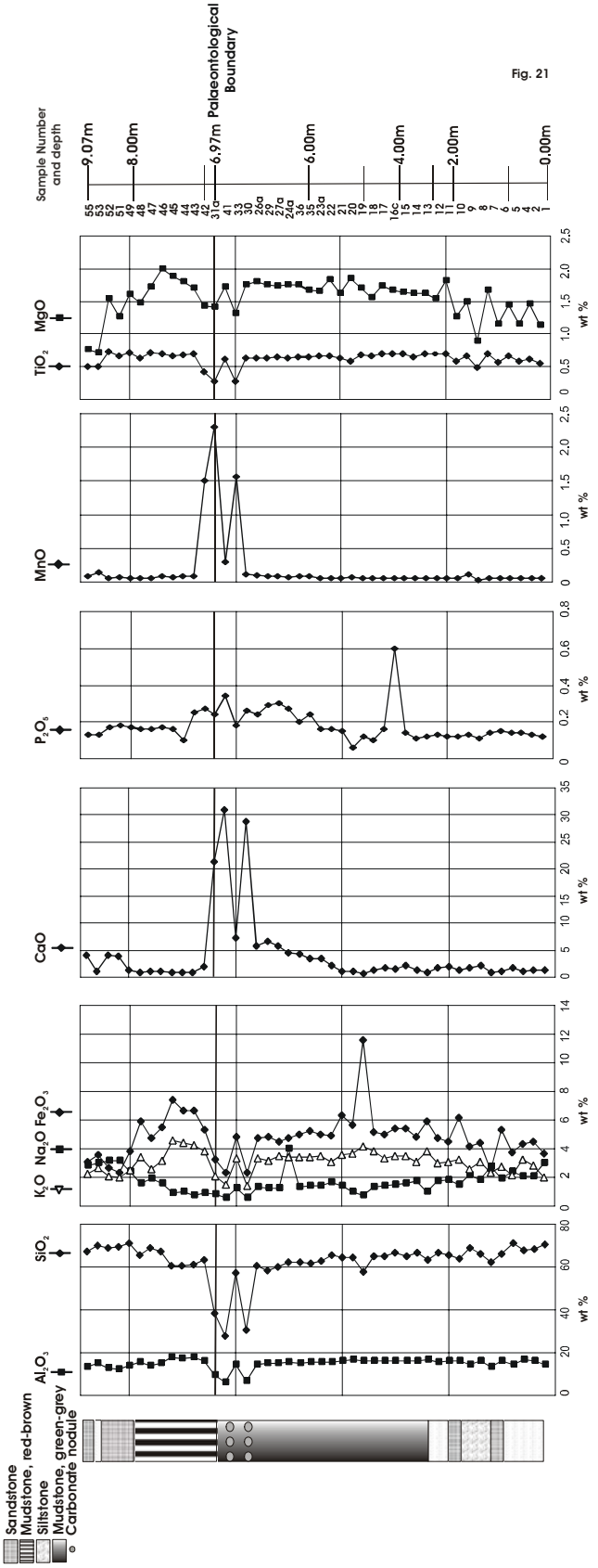

Fig. 21
Sample Number and depth
9.07m
8.00m
6.97m Palaeontological Boundary
6.00m
4.00m
2.00m
0.00m
55 53 52 51 49 48 47 46 45 44 43 42 31a 41 33 30 26a 29 27a 24a 34 35 23a 22 21 20 19 18 17 16c 15 14 13 12 11 10 9 8 7 6 5 4 2 1
TiO2 MgO
MnO
P2O5
CaO
K2O Na2O Fe2O3
SiO2
Al2O3
wt %
Sandstone
Mudstone, red-brown
Siltstone
Mudstone, green-grey
Carbonate nodule

Figure 21: *Major element abundance patterns for the Wapadsberg section. All concentrations are in wt%.*

The P_2O_5 contents are higher within the mudstones than in the sandstones, siltstones and carbonate nodular horizons.

The TiO_2 concentrations show some variation in the lower part of the sequence, and the concentrations are generally significantly higher in the sandstones (0.7 wt%) than in the siltstones (0.5-0.6 wt%). There is more variation in the TiO_2 abundances of the Wapadsberg section than in those of the Commando Drift Dam section.

Molecular weathering ratios (Fig. 22) for the Wapadsberg section show some differences to those for the Commando Drift Dam section, but generally have similar trends to those calculated for the Commando Drift Dam section. The presence of the two carbonate nodular horizons is clearly indicated by differences in the ratios, particularly those containing CaO. The Na_2O/K_2O ratio shows much variation, and this ratio is lowest in the mudstones, and highest in the sandstones. The ratio Al_2O_3/SiO_2 increases above the palaeontologically defined boundary, and this coincides with an increase in the $Al_2O_3/(CaO+MgO+Na_2O+K_2O)$ ratio. Below the palaeontologically defined boundary (at 5.50 m from the initial sample) the ratio $Al_2O_3/(CaO+MgO+Na_2O+K_2O)$ decreases gradually from average values of ca. 2.0 to 1.4. The carbonate nodular horizons have ratios of ca. 0.2. A sharp increase to average levels is seen in the sample immediately above the boundary (PW 42). This pattern has not been previously observed in the Karoo Basin (e.g., Retallack et al., 2003). As with the Commando Drift Dam, this feature could be post-depositional in origin.

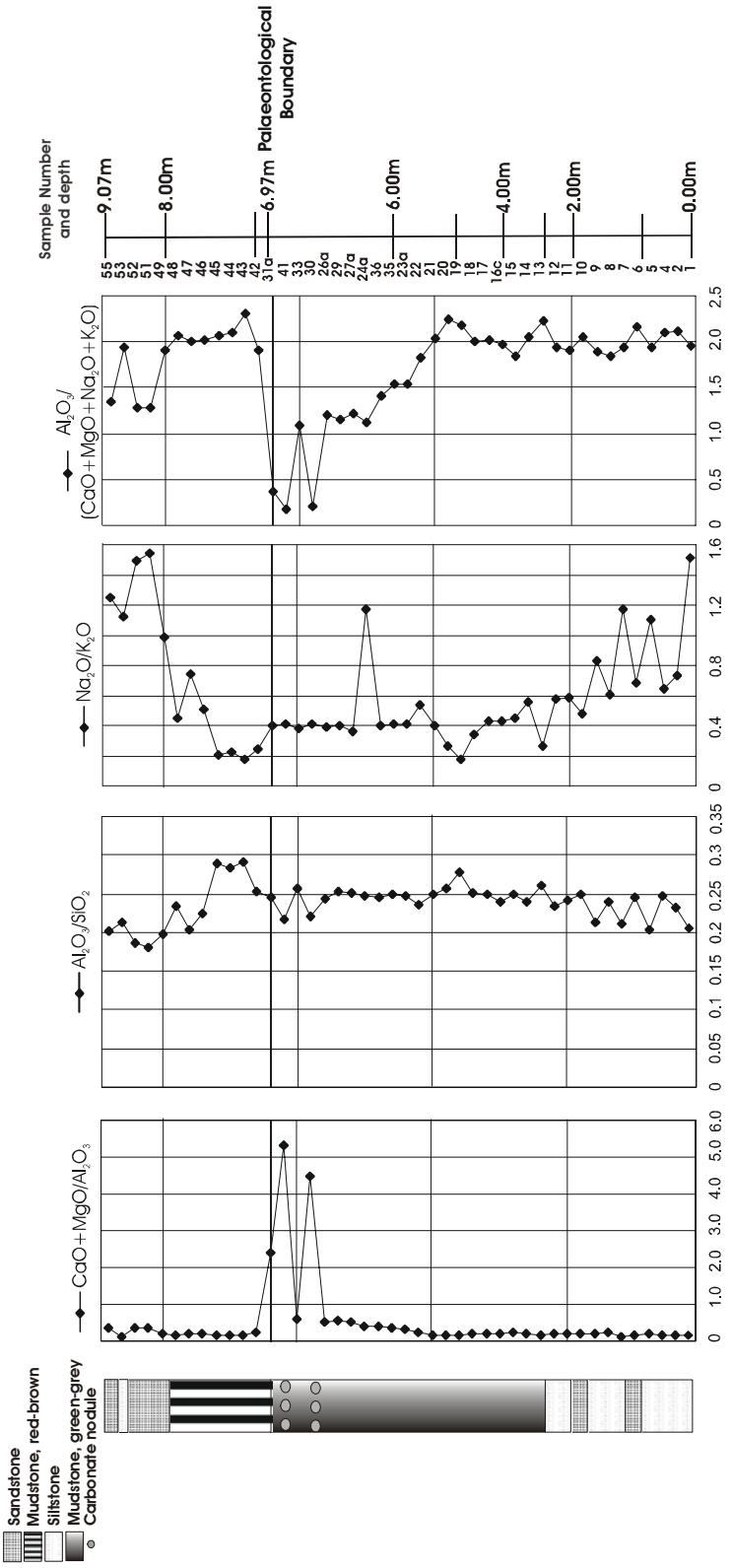


Figure 22: *Molecular weathering ratios for the Wapadsberg section.*

3.3.2 Trace Elements

3.3.2.1 The Commando Drift Dam Section

As expected, a number of the trace elements show associations with the major elements, as these trace elements would substitute into various lattice positions in the place of major elements within a mineral.

3.3.2.1.1 Lithophile Elements

The lithophile elements are associated with silica, and thus generally show patterns similar to silica (Farndon, 1994). However, some differences are seen, related to other chemical associations, such as an association with the siderophile and chalcophile elements. The lithophile element concentration variations are shown in Figure 23.

The concentrations of rubidium (Rb), zirconium (Zr), niobium (Nb), chromium (Cr), hafnium (Hf), scandium (Sc), cesium (Cs) and tantalum (Ta) all follow the pattern for silica (Fig. 23), decreasing at the carbonate nodular horizons. Uranium (U) is the only lithophile element that shows concentration increase at these horizons. Thorium (Th) and tantalum (Ta) concentrations show little change from average values for the entire section. Both strontium (Sr) and yttrium (Y) concentrations are inconsistent in that the concentrations increase at some of the carbonate nodular horizons but decrease at others. This indicates that both of these elements are relatively mobile, probably during weathering (Taylor and McLennan, 1985), or that the elements are present only in scattered, and thus randomly sampled, minerals.

Hafnium and zirconium have lower concentrations in the red-brown mudstones than in the other lithologies, except within the carbonate nodular horizons, reflecting their strong partitioning into relatively few, rare minerals such as zircon and monazite.

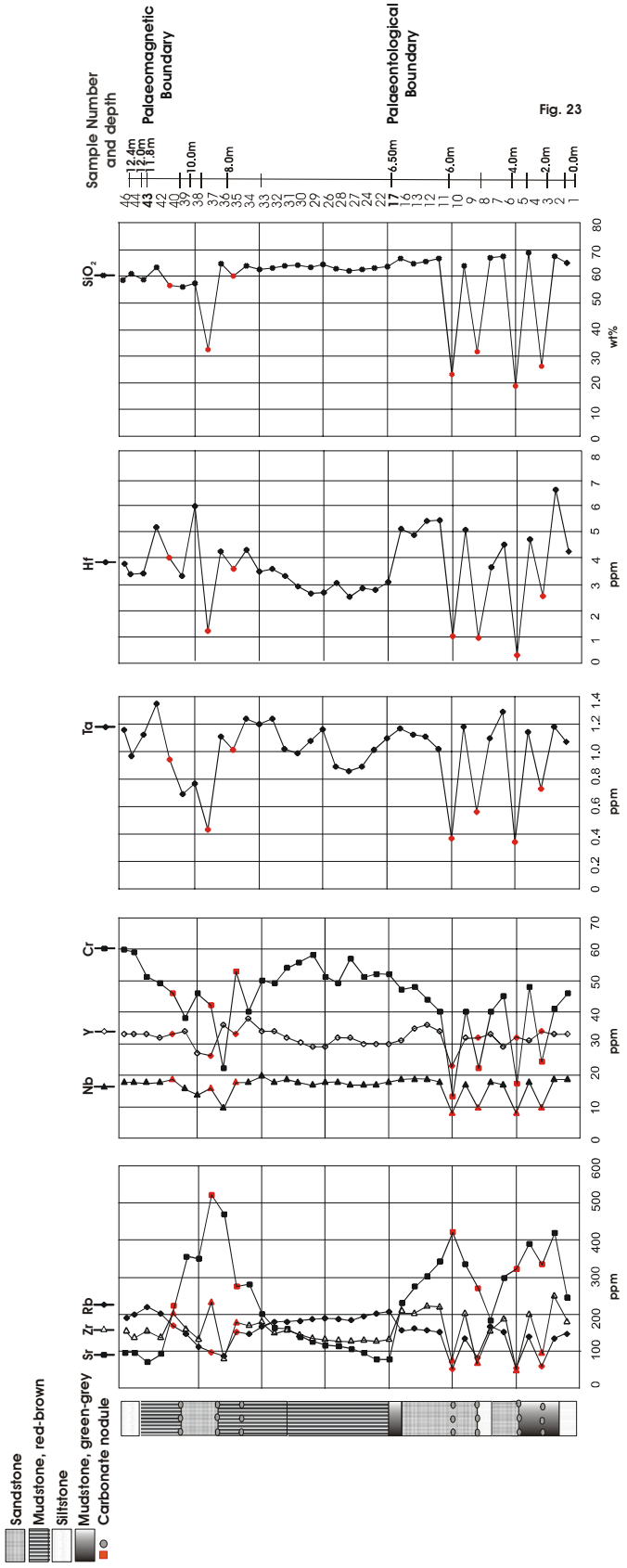

Sandstone
Mudstone, red-brown
Siltstone
Mudstone, green-grey
Carbonate nodule
Sr
Zr
Y
Rb
ppm
Nb
Y
Cr
ppm
Ta
ppm
Hf
ppm
SiO2
wt%
Sample Number and depth
Palaeomagnetic Boundary
Palaeontological Boundary
12.4m
11.8m
10.0m
8.0m
6.50m
6.0m
4.0m
2.0m
0.0m

Fig. 23

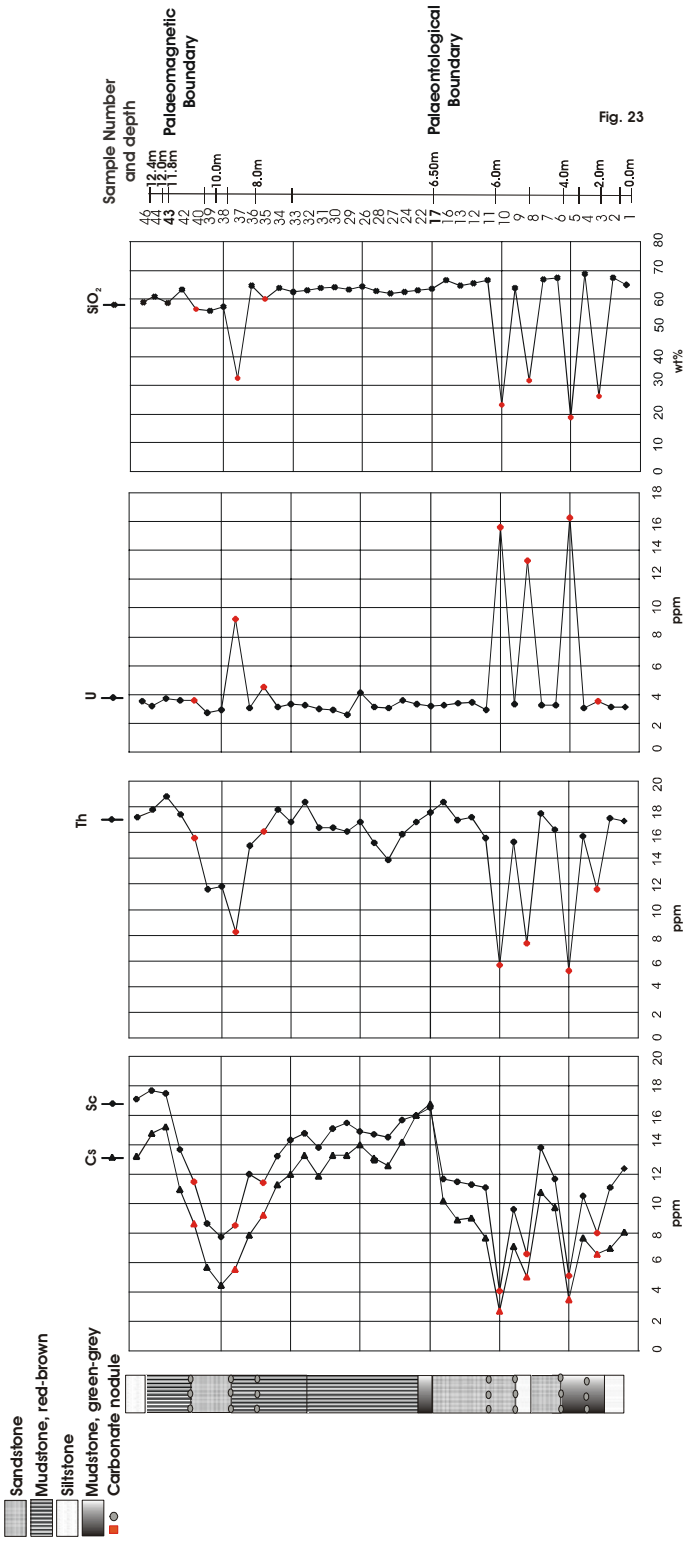


Figure 23: *Lithophile trace element abundance patterns (data in ppm) for the Commando Drift Dam section (compared to the SiO_2 pattern). Red symbols indicate the carbonate nodular horizons.*

Niobium and chromium contents do not vary within the particular lithologies (i.e. sandstone, mudstone, or siltstone), except at the carbonate nodular horizons. The abundances of both elements are, however, close to the respective detection limits.

Chromium contents also correlate with the Fe_2O_3 concentrations, as the concentrations increase slightly at the palaeontologically defined boundary level (reaching a maximum value of 56.7 ppm at PCD 27), around the changeover from green-grey to red-brown mudstones. Rubidium concentrations also increase where the red-brown mudstones are encountered (to a maximum of 219 ppm from an average of 138-163 ppm). Above this value, the concentrations then steadily decrease up the sequence towards the appearance of the 5^{th} carbonate nodular horizon at ~7 m from the beginning of the traverse. For the carbonate nodular horizons, Rb concentrations are around 50-60 ppm.

Scandium and Cesium have very similar geochemical signatures: they both decrease at the carbonate horizons and have higher concentrations in the sandstones than in the siltstones. They also have their maximum concentrations in the mudstones, showing that these elements experience a strong lithological control, probably by concentration in the fines. A general decrease in concentrations up sequence is seen in the red-brown mudstones.

Uranium concentrations increase at the carbonate nodular horizons from an average level of ca. 3 ppm to 15 ppm. Uranium contents do not change from average levels at the palaeontologically defined and the palaeomagnetically defined boundaries.

Strontium content shows much variation. In general, Sr decreases at the carbonate nodular horizons, but a couple of samples show increases

instead (e.g., PCD 10). The changes in concentration of Sr are more gradual than the changes seen for SiO_2. The concentration decreases within the mudstones, with minimum values at the palaeontologically and palaeomagnetically defined boundaries. In general, Sr is as much concentrated in the siltstones as in the carbonate samples. Yttrium does not show consistent increases or decreases at the carbonate nodular horizons, and all values are in the range of 30 to 36 ppm. No distinctive changes can be seen at either boundary level.

3.3.2.1.2 Siderophile Elements

A number of elements, including nickel (Ni), cobalt (Co), vanadium (V), iridium (Ir) and gold (Au), are generally associated with Fe_2O_3, and these are termed siderophile elements (Farndon, 1994). With the exception of Au, they show similar stratigraphic variation in the study sections to that of Fe_2O_3 (Fig. 24). They all show increases at the changeover from green-grey to red-brown mudstones, except for Ir and Au which are generally below the detection limit.

Almost all iridium concentrations are below the detection limit. The lowest limit of detection for this sample suite, for iridium, is ~2 ppb for carbonate poor samples, with ~0.5 ppb for carbonate rich samples. Samples with measurable iridium content show concentrations less than 1.2 ppb (see Appendix 1).

Nickel, cobalt and vanadium all show decreases at the carbonate nodular horizons. Nickel values decrease to 8 ppm at the carbonate nodular horizons, from a section average of 15-19 ppm in the siliceous strata. Nickel attains a maximum value of 34 ppm just above the palaeomagnetically defined boundary. Cobalt contents vary between 7 and 14 ppm in the siliceous strata and decrease to 4 ppm at the carbonate nodular horizons.

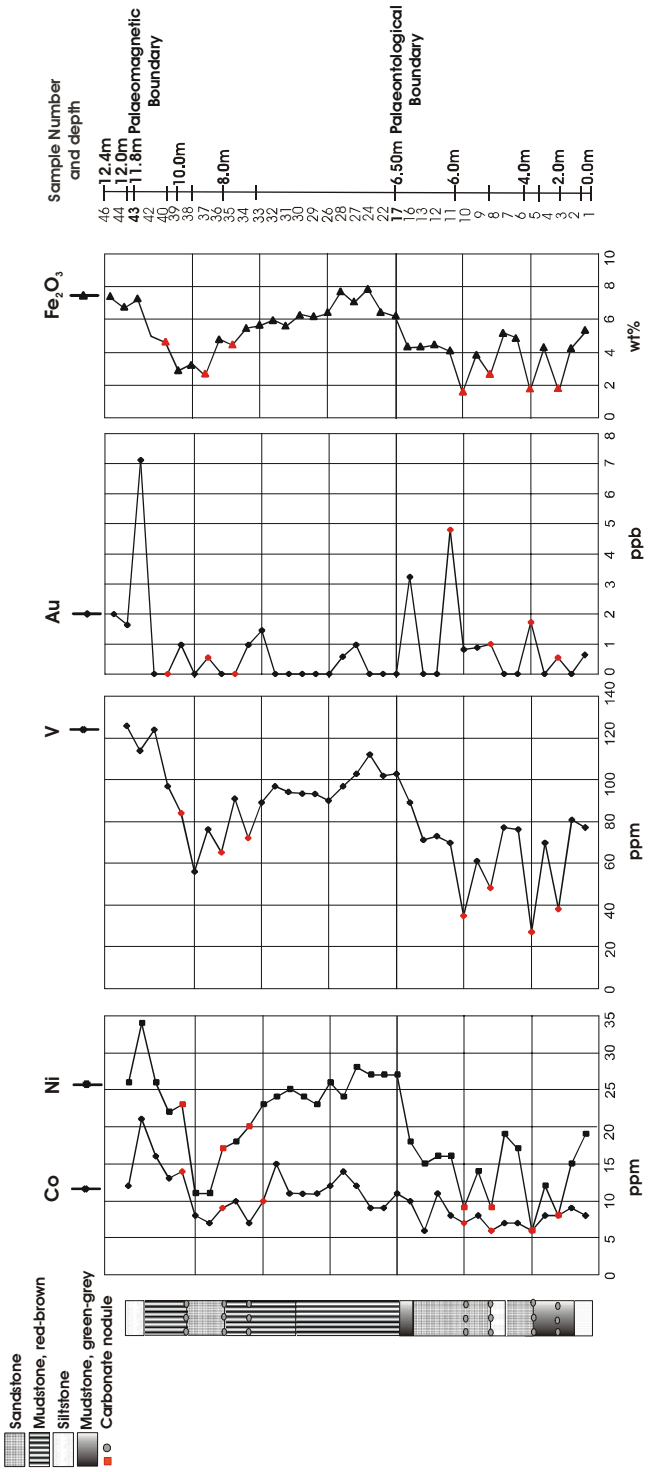


Figure 24: *Siderophile trace element abundance patterns (data in ppm and ppb) for the Commando Drift Dam section (compared to the Fe_2O_3 pattern). Red symbols indicate the carbonate nodular horizons.*

Vanadium concentrations show much variation, with decreases from 70-81 ppm (in the siltstones and sandstones) to 27–56 ppm at the carbonate nodular horizons. Concentrations in the red-brown mudstones are generally about 100 ppm, with a maximum concentration of 126 ppm just above the palaeomagnetically defined boundary.

Most of the samples have gold concentrations that are below the detection limit (between 0.2 ppb and 2 ppb depending on sample type), and the concentrations that are above the detection limit show no correlation with lithology, or change across either the palaeontologically defined or palaeomagnetically defined boundaries.

3.3.2.1.3 Chalcophile Elements

The chalcophile elements (Fig. 25) are associated with sulphur (Farndon, 1994). Sulphur concentrations measured by XRF (Table 6) are also plotted. Sulphur concentration varies with lithology. Higher concentrations are seen for the carbonate nodular horizons than for the rest of the sequence. There is an increase in the Triassic sandstones above the boundary from generally lower values in the mudstones. There are no distinctive changes above and below the palaeontologically and palaeomagnetically defined boundaries other than lithological changes.

Both zinc (Zn) and copper (Cu) concentrations decrease at the carbonate nodular horizons. The decreases are sharp for the first four carbonate nodular horizons (from 75–115 ppm in the siliceous strata to values of 39-45 ppm in the carbonate horizons), but are less apparent for the top three carbonate nodular horizons (above the palaeontologically defined boundary). Copper concentrations decrease at the carbonate horizons from an average of 16-25 ppm (silicates) to 6-12 ppm. Zinc concentrations show no consistent lithological association other than those for the carbonate nodular horizons.

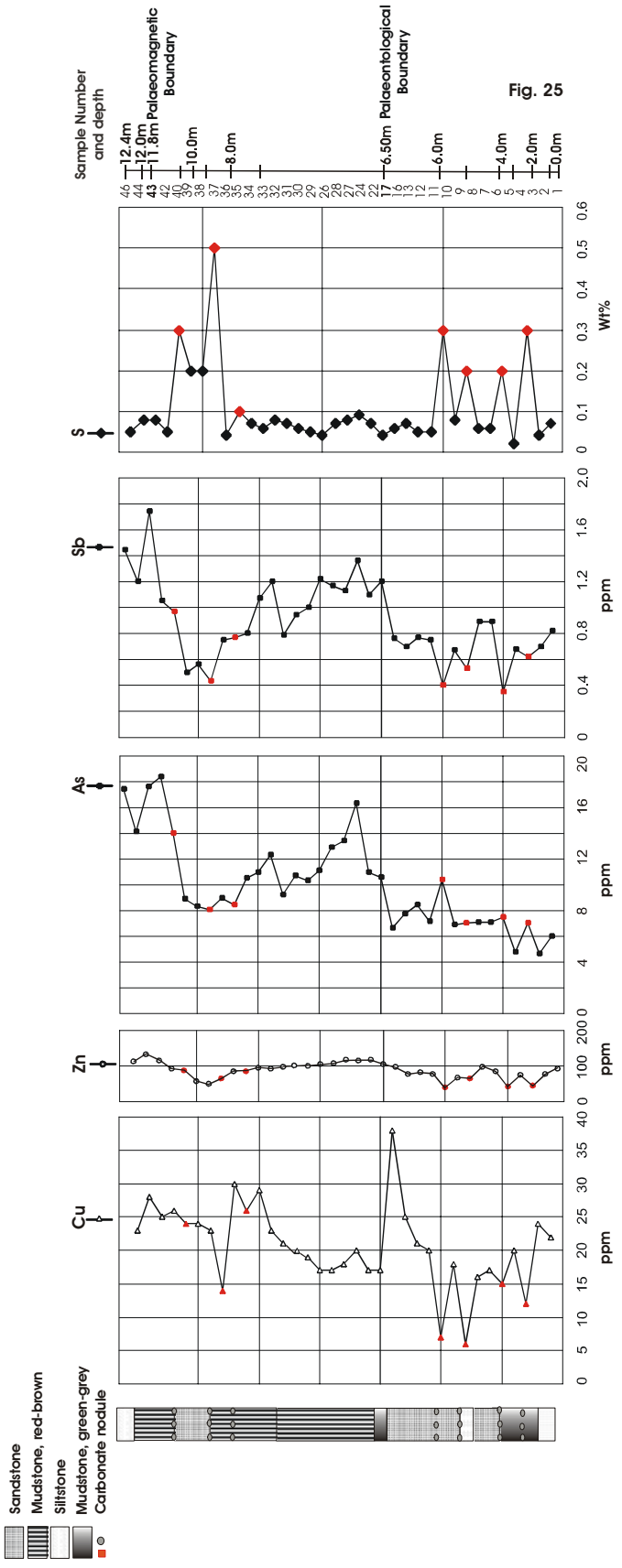

Sandstone
Mudstone, red-brown
Siltstone
Mudstone, green-grey
Carbonate nodule
Cu
ppm
Zn
ppm
As
ppm
Sb
ppm
S
Wt%
Sample Number and depth
12.4m
12.0m
11.8m Palaeomagnetic Boundary
10.0m
8.0m
6.50m Palaeontological Boundary
6.0m
4.0m
2.0m
0.0m

Fig. 25

Figure 25: *Chalcophile trace element abundance patterns (data in ppm) for the Commando Drift Dam section (compared to the S pattern). Red symbols indicate the carbonate nodular horizons.*

An increase in Cu concentration occurs at the first appearance of the green-grey mudstone samples (38 ppm), with a sharp decrease to average values at the palaeontologically defined boundary as the red-brown mudstones are encountered.

Arsenic (As) shows much variation and no apparent lithological constraint; no consistent changes in concentration are seen for the nodular horizons (increases are seen for PCD 3, 5 and 10, no change is seen for PCD 8 and PCD 40, and decreases are seen for PCD 35 and 37). Maximum variation is observed around the palaeomagnetically defined boundary, where the highest concentrations are seen. There appears to be an increasing trend from the first sample in the Permian to the last sample in the Triassic across the entire sequence, and this pattern is also observed for the antimony (Sb) concentrations (the pattern of which is generally similar to that of As).

3.3.2.1.4 Rare Earth Elements

Rare earth element (REE) values were obtained using INAA. REE concentrations were normalized to a composition of the C1 chondritic meteorites values (after Taylor and McLennan, 1985). C1 chondritic meteorites represent relatively unfractionated samples of the solar system dating from nuclear synthesis (Rollinson, 1993). REE concentrations are very irregular in the solar system, because of the different stabilities of atomic nuclei. REE with even atomic numbers are more abundant (as they are more stable) than those with odd atomic numbers, which then produces a zig-zag pattern on an abundance pattern diagram. Chondritic normalization is used to limit the natural variation in concentrations as

well as to measure any fractionation relative to chondritic meteorites (Rollinson, 1993).

Abundance patterns are very similar for all samples, but a few, small differences are noted (Figs 26-28). These anomalies were correlated to differences in the contents of heavy and light REE, and can be seen in the following ratios: La/Th (Fig. 27), La_N/Yb_N (Fig. 28), and La/Lu (Fig. 28). The ratios of the samples below and above the palaeontologically defined boundary showed no differences to ratio of the sample at the boundary. Additionally, there were no changes in the REE abundance patterns around the palaeomagnetically defined boundary.

The graph of La/Th (Fig. 27) indicates a lithological control on La or Th values. La/Th ratios are higher in the carbonate nodular horizons, except for those ratios of samples PCD 35 (at 7.2 m)and PCD 40 (at 11.1 m). Lanthanum concentrations (in ppm) are constant, and thus Th concentrations (Fig. 23) vary slightly at the levels of the carbonate nodular horizons. The Th concentrations decrease from background levels at the nodular horizons, but these variations are small.

Most samples in the sequence have La_N/Yb_N ratios of 9 to 10 and La/Lu ratios of 8.5 to 9.3 (Fig. 28). In those samples where the La_N/Yb_N ratio is higher, the concentration pattern has the same shape but falls below the average REE abundance pattern (PCD 1 – a representative of the rest of the sequence). The converse follows – where the ratio was lower, the REE abundance pattern has the same shape, but lies above the abundance pattern (Fig. 28). Thus the total REE content varies slightly throughout the section. For La/Lu (Fig. 28), a number of anomalies are seen, which mostly correspond to lithological differences. The La/Lu ratio represents the ratio of light REE to heavy REE.

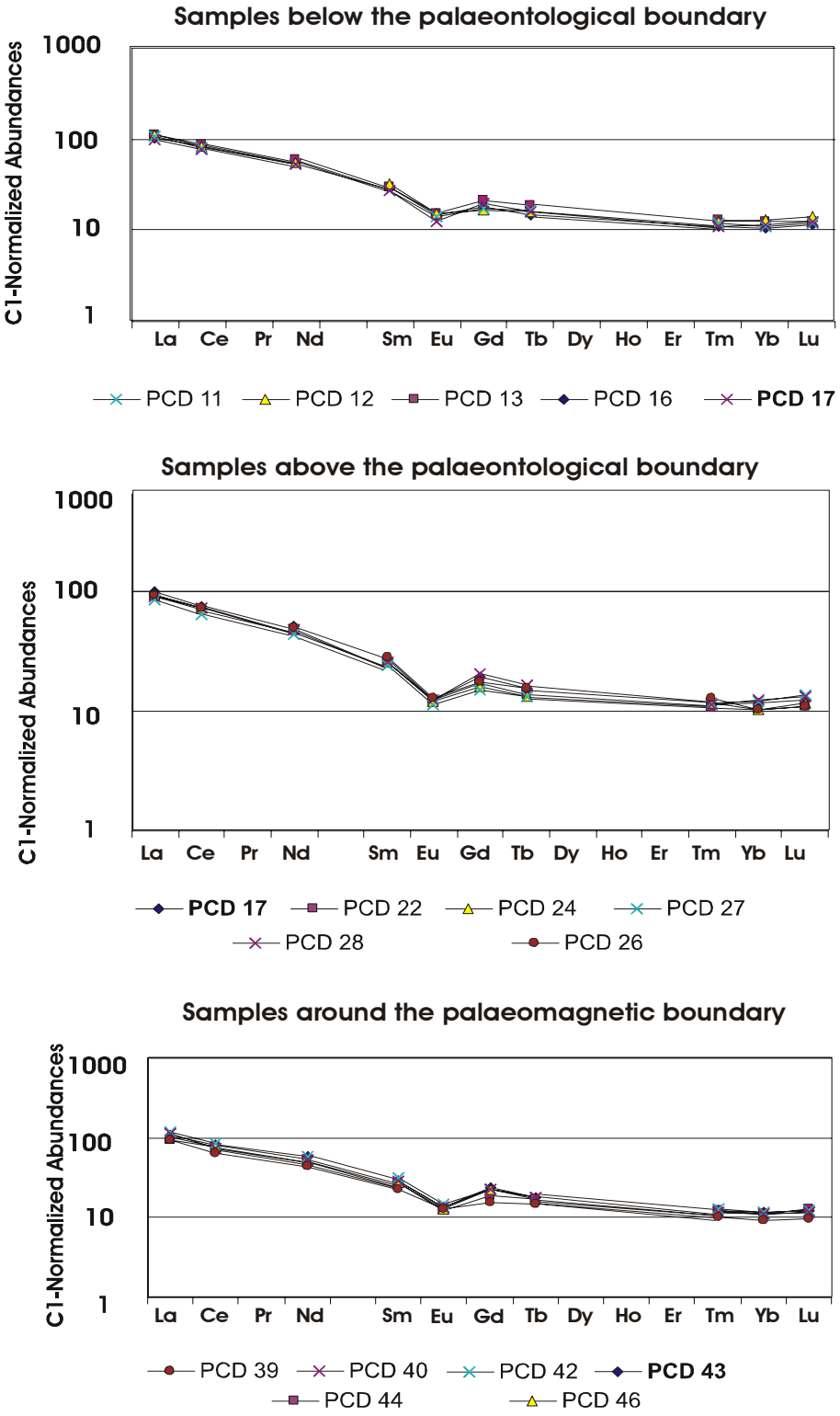


Figure 26: *Rare earth element abundance patterns for selected samples from the Commando Drift Dam section (data normalized after Taylor and McLennan, 1985).*

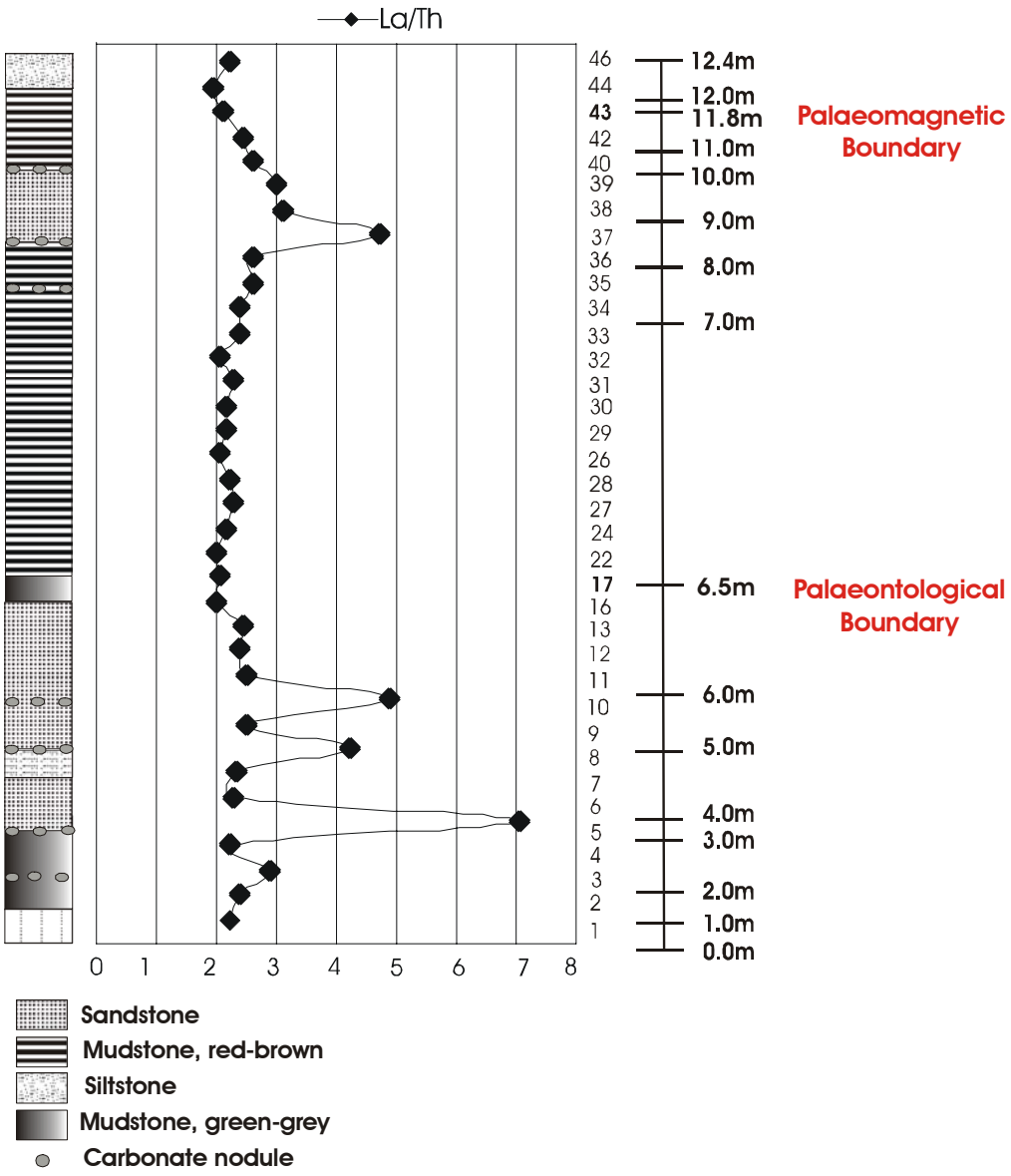


Figure 27: *La/Th ratios for the Commando Drift Dam section.*

The differences in the La/Lu ratio are not consistent, however – for PCD 10, a carbonate sample, there are more heavy REE, whereas for PCD 35, another carbonate, the light REE are enriched, which indicates that there is another factor, such as mobility due to weathering, controlling the REE composition. There are similar inconsistencies in the mudstones.

The most distinct peaks in the La/Lu values correspond to calcium carbonate horizons, or mudstones more enriched in calcium carbonate than the average sandstone/mudstone sample.

The samples do not show distinct differences in La/Lu ratio or in La_N/Yb_N below or above the P-Tr boundary. Cerium anomalies are not observed. Europium anomalies are always present, and are consistent in shape.

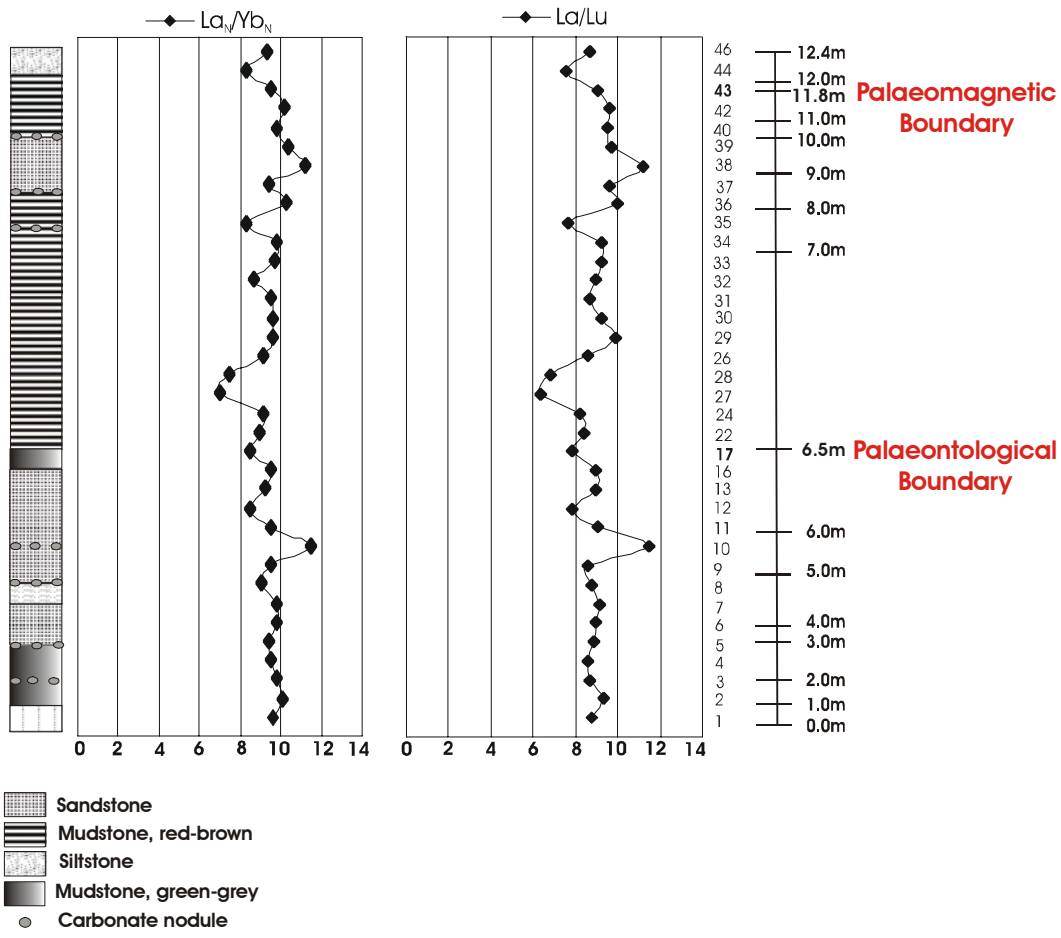


Figure 28: *La_N/Yb_N and La/Lu ratios for the Commando Drift Dam section.*

3.3.2.1.5 Geochemical Changes for the Commando Drift Dam Section

The palaeontologically defined boundary is characterized by the change of colour of sedimentary strata from green-grey to red-brown, and the corresponding increase in the content of Fe and the siderophile elements. The chalcophile elements do not show any consistent increase or decrease at the palaeontologically defined boundary. Increases in the concentrations of Rb, Sr, Cr, Ni, and Co are observed. For the palaeomagnetically defined boundary, a number of elements increase in concentration – particularly the siderophile elements, Cr and the chalcophile elements. Other elements show no changes at either boundary – notably Y, Nb, U, Zr and Au. Hf decreases at both boundaries, but this is probably accidental owing to random sampling of zircon. Zinc concentrations increase slightly at both boundaries, and in general Zn values remain nearly constant. Scandium and Cs show maxima at both boundaries, followed by decreasing values. REE abundance patterns do not change across either the palaeontologically defined or the palaeomagnetically defined boundaries, and any variation is attributed to lithological changes.

3.3.2.2 The Wapadsberg Section

All trace elements show much variation in the lower part of the sequence (up to sample PW 22, which is at 5.65 m), where alternating sandstones and siltstones are seen.

3.3.2.2.1 Lithophile Elements

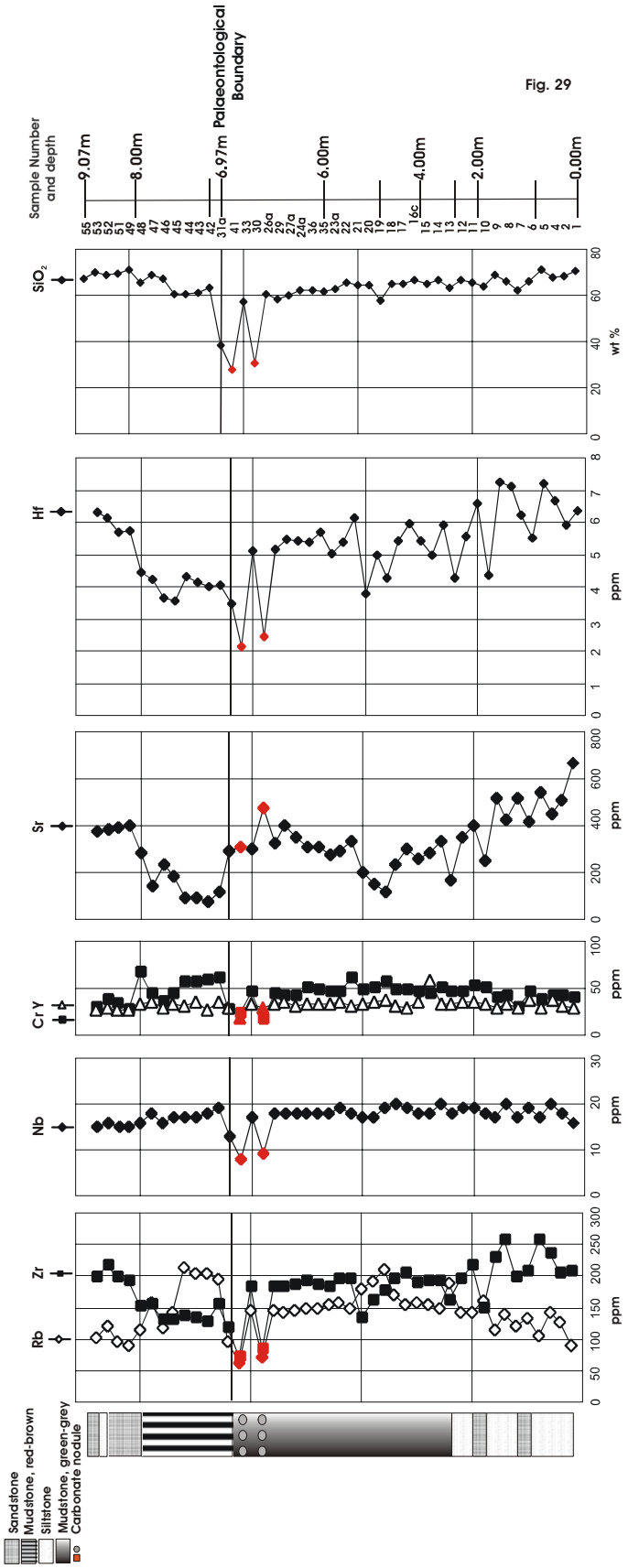
There are many similarities in the behaviour of the lithophile elements in the Wapadsberg section (Fig. 29) to those in the Commando Drift Dam section. The concentrations of Rb, Zr, Nb, Th, Hf and Ta are lowest within the carbonate nodular horizons. There are slight decreases in concentration for Y, Sc and Cs at these horizons. Uranium and chromium concentrations do not change at the carbonate nodular horizons.

Strontium concentrations show little change at the carbonate nodular horizons from average levels, and these changes are not consistent, which is also observed at the Commando Drift Dam section. After the boundary, Sr concentrations are lower than those seen before the boundary, and they gradually increase to average Sr values at 1.4 m above the boundary.

Rubidium shows a stronger lithological control than in the Commando Drift Dam section. Rubidium has highest concentrations in mudstones (greater than 150 ppm), followed by the siltstones and sandstones (100-140 ppm), and then the carbonate nodular horizons (71 ppm and 96 ppm). Zirconium concentrations are very variable and range from 150 to 250 ppm, whereas the related hafnium concentrations show a decreasing trend up sequence below the boundary, and then are slightly lower in concentration above the boundary, with a gradual recovery to average values 35 cm above the boundary. This may reflect a more consistent input of zircon into the Wapadsberg sequence, as opposed to the Commando Drift Dam sequence.

Chromium, Scandium and Cesium concentrations increase above the palaeontologically defined boundary indicating some correlation with Fe_2O_3. However, a slight increase in SiO_2 values is also noted; thus, correlation with both elements is possible. A maximum Cr concentration of 64.8 ppm is seen just above the palaeontologically defined boundary. Scandium contents reach a maximum of 19.6 ppm (from a general range of 11–15 ppm) at the palaeontologically defined boundary, and values return to 11.4 ppm at 44 cm above the palaeontologically defined boundary.

Thorium concentrations show more variation at Wapadsberg than at the Commando Drift Dam section, with distinct decreases of Th contents at the carbonate nodular horizons (from 12–19 ppm to 7-8 ppm).


Fig. 29
Sample Number and depth
9.07m
8.00m
Palaeontological Boundary
6.97m
6.00m
4.00m
2.00m
0.00m
55 53 52 51 49 48 47 46 45 44 43 42 41 33 30 26a 29 27a 24a 36 35 23a 22 21 20 19 18 17 16c 15 14 13 12 11 10 9 8 7 6 5 4 2 1
SiO2
wt %
Hf
ppm
Sr
ppm
Cr Y
ppm
Nb
ppm
Zr
Rb
ppm
Sandstone
Mudstone, red-brown
Siltstone
Mudstone, green-grey
Carbonate nodule

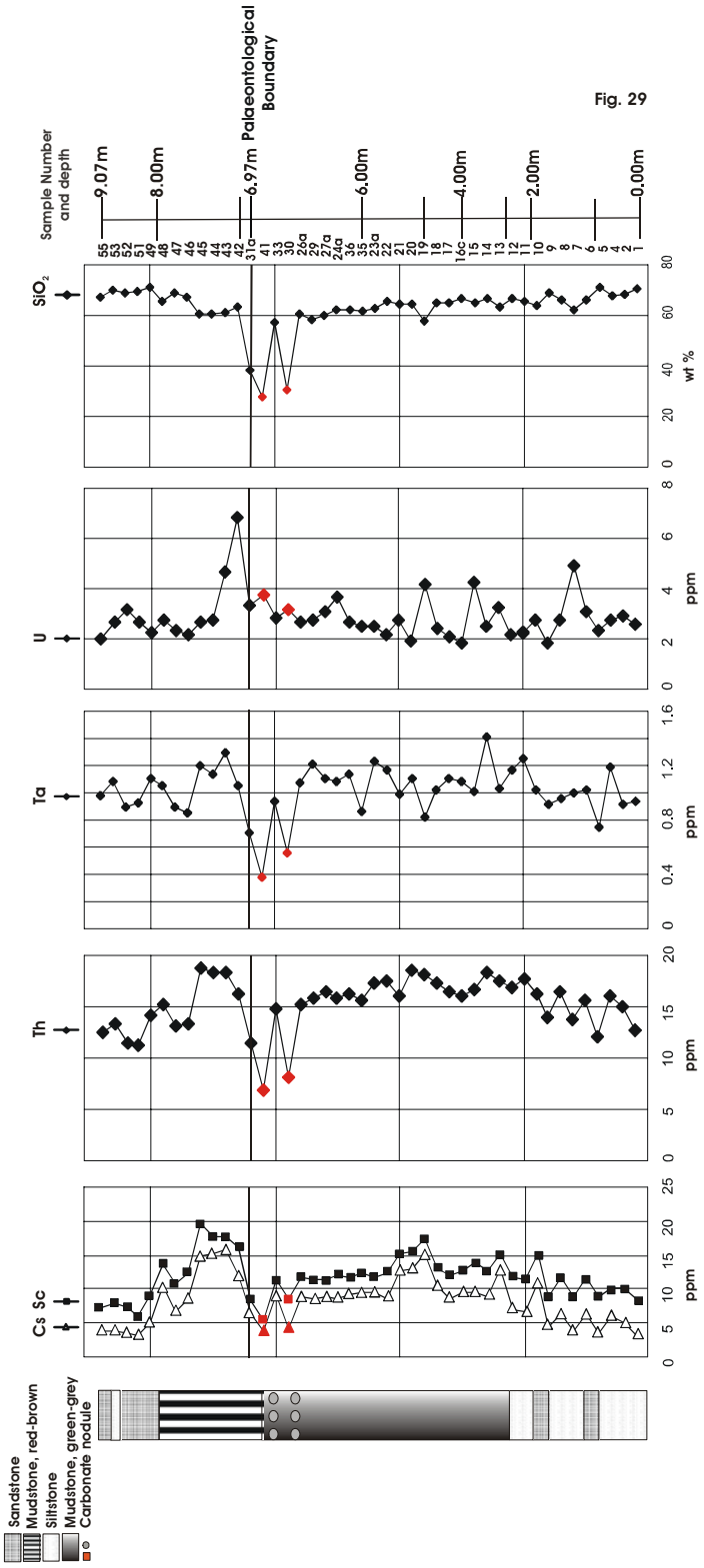

Fig. 29
Sample Number and depth
9.07m
8.00m
6.97m Palaeontological Boundary
6.00m
4.00m
2.00m
0.00m
SiO2
U
Ta
Th
Cs Sc
wt %
ppm
Sandstone
Mudstone, red-brown
Siltstone
Mudstone, green-grey
Carbonate nodule

Figure 29: *Lithophile trace element abundance patterns (data in ppm) for the Wapadsberg section (compared to the SiO_2 pattern). Red symbols indicate the carbonate nodular horizons.*

Thorium contents increase above the palaeontologically defined boundary, but return to section concentrations 35 cm above the boundary.

Yttrium, niobium and tantalum contents show little variation. Yttrium concentrations vary between 30 and 35 ppm, with decreases to 18 and 27 ppm at the first and second carbonate horizons, respectively, corresponding to the different CaO concentrations at these horizons.

3.3.2.2.2 Siderophile Elements

The variations in the concentrations of the siderophile elements are shown in Figure 30. Cobalt and vanadium concentrations both increase above the boundary. Nickel concentrations also slightly increase, but there is very little change from the average values observed below the boundary. There are decreases in the contents of Ni and V at the carbonate nodular horizons.

Nickel and vanadium, together with Fe_2O_3, all show anomalously high values for sample PW 19. This increase does not correspond to a change in lithology, and it is concluded that a particularly iron-rich rock (perhaps a lens of Fe-rich material, such as the red-brown mudstone) was probably sampled.

In the Wapadsberg section, the iron contents and corresponding siderophile element contents do not show such significant concentration changes as seen in the Commando Drift Dam section.

Au concentrations are almost all below the detection limit of 0.2 to 2 ppb. Concentrations above the detection limit are not above 5 ppb, and do not show any correlation with lithology. All Ir values are below the detection limit (see section 3.3.2.1.2).

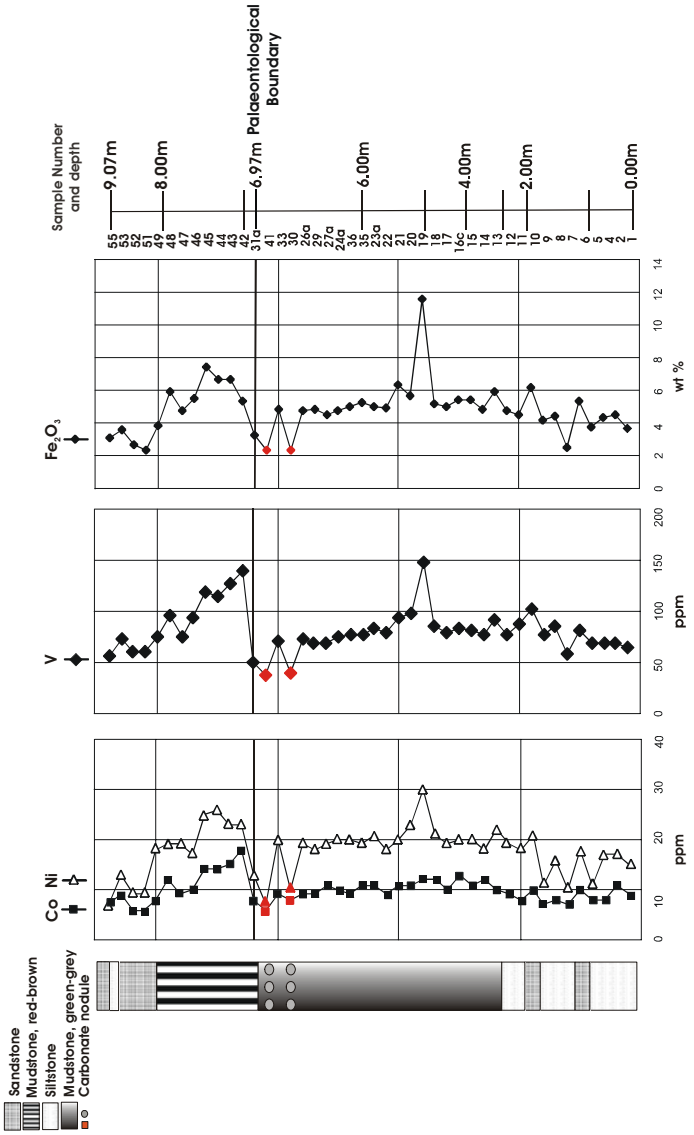


Figure 30: *Siderophile trace element abundance patterns (data in ppm) for the Wapadsberg section (compared to the Fe_2O_3 pattern). Red symbols indicate the carbonate nodular horizons.*

3.3.2.2.3 Chalcophile Elements

Sulphur concentrations vary within a small range except for a few anomalous values. There is a sharp increase in values with the first appearance of the mudstones, followed by a sharp decrease to average levels (PW 15). This pattern is not observed for the chalcophile trace elements (Fig. 31). There is another increase at the boundary in sulphur concentrations, which is also seen for Zn, Cu, Sb and As abundances, which decrease to lower average levels than seen below the boundary. There is no consistent pattern for the carbonate nodular horizons.

Zinc and copper concentrations are variable (Zn: 63–120 ppm; Cu: 15-35 ppm), whereas As concentrations show little variation (As: 5–10 ppm). Zinc and copper concentrations decrease at the carbonate nodular horizons, but this is not as significant a change as seen in the other elements. No changes in As concentrations are seen at the carbonate nodular horizons, and the pattern is similar to Sb. There are a number of anomalous values in the Cu and As concentration plots, but these do not show any correlation with the sulphur concentration values.

3.3.2.2.4 Rare Earth Elements

Rare earth element patterns for samples below, at and above the palaeontologically defined boundary are shown in Figure 32. As with the REE patterns from the Commando Drift Dam section, no differences between the samples are seen, except for the carbonate nodular horizon samples, which have relatively lower normalized values.

The La/Th graph of the Wapadsberg section (Fig. 33) indicates that, as in the Commando Drift Dam section, there is a lithological control. An anomalous value for sample PW 18 is also observed for the Fe_2O_3 contents (and corresponding siderophile elements concentrations), and this is hypothesized to represent an iron-rich layer.

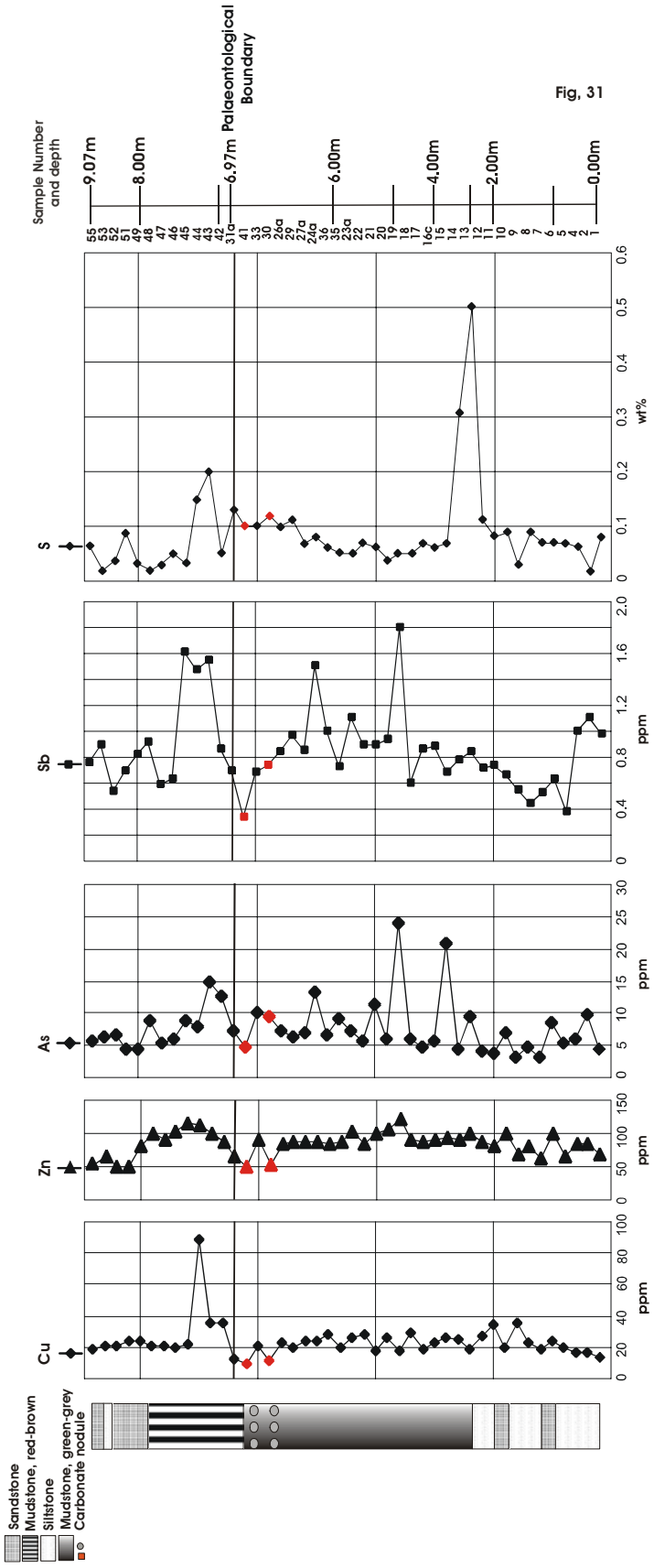

Fig, 31
Palaeontological Boundary
Sample Number and depth
9.07m
8.00m
6.97m
6.00m
4.00m
2.00m
0.00m
S
Sb
As
Zn
Cu
wt%
ppm
Sandstone
Mudstone, red-brown
Siltstone
Mudstone, green-grey
Carbonate nodule

Figure 31: *Chalcophile trace element abundance patterns (data in ppm) for the Wapadsberg section (compared to the S pattern). Red symbols indicate the carbonate nodular horizons.*

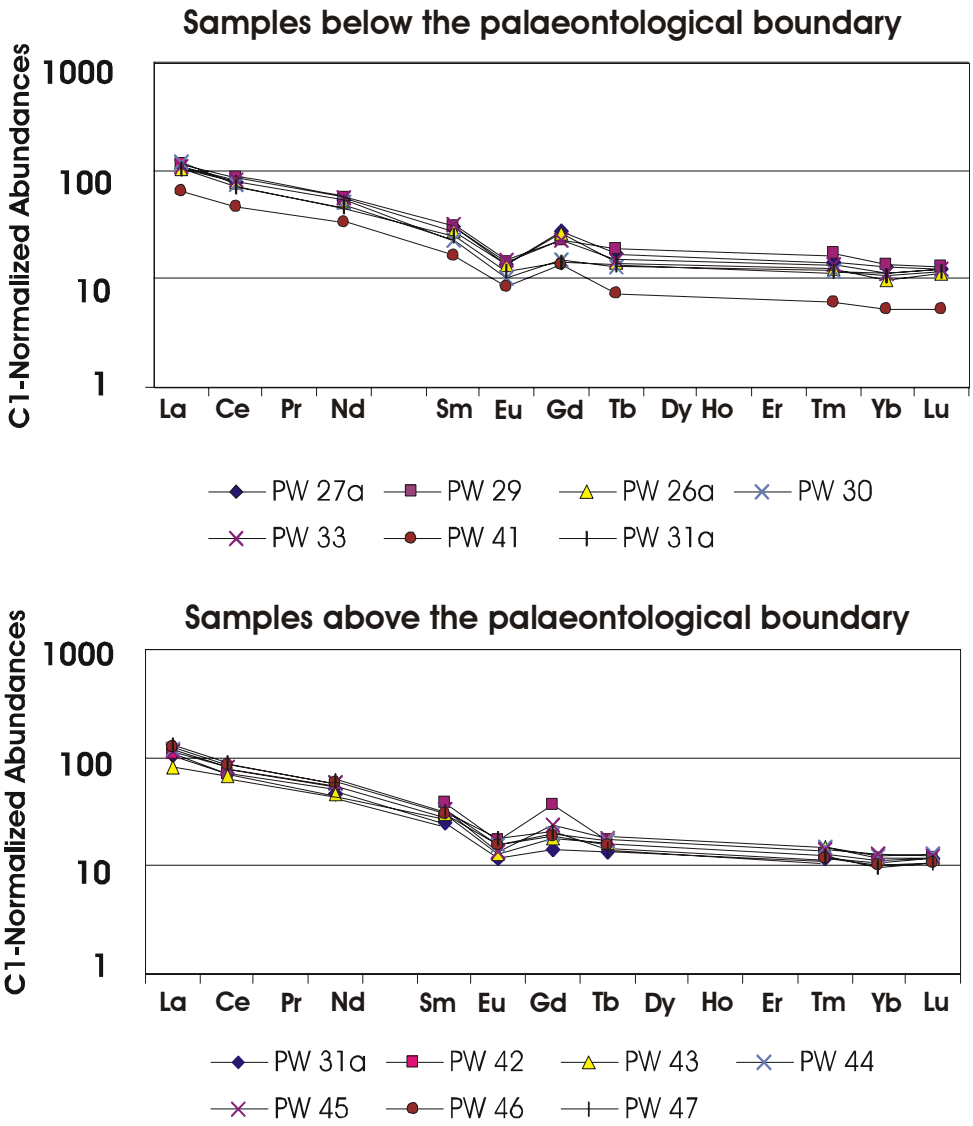


Figure 32: *Rare earth element abundance patterns for selected samples from the Wapadsberg section (data normalized after Taylor and McLennan, 1985).*

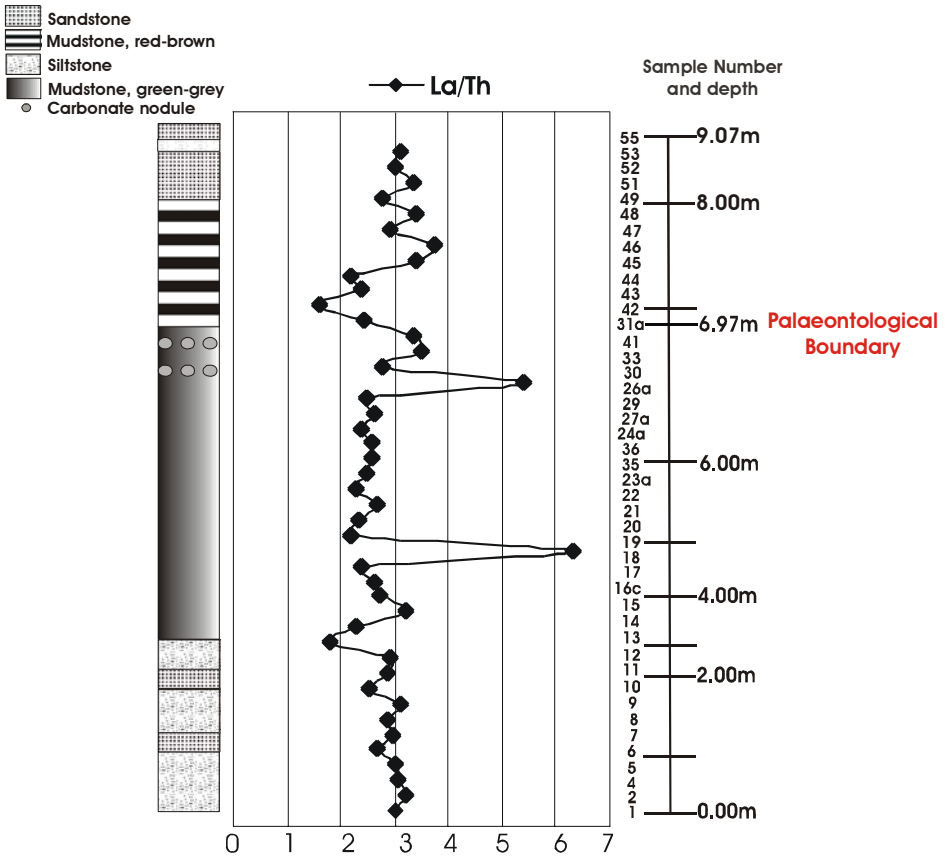


Figure 33: *La/Th ratios for the Wapadsberg section.*

In samples where a high Fe_2O_3 concentration is observed, La/Th ratios are higher, and this is reflected by the fact that La concentrations are higher than in the other samples, whereas Th concentrations remain constant. This is opposite to the pattern seen at Commando Drift Dam where La concentrations are constant, and Th concentrations vary. There is a decrease in this ratio just above the boundary, where Fe_2O_3 concentrations increase.

The majority of samples from the Wapadsberg section have a La_N/Yb_N ratio of 9 to 10 and a La/Lu ratio of 8.6 to 10 (Fig. 34). Increases in the ratios correspond to increases in the Fe_2O_3 concentration, mostly below the palaeontologically defined boundary. Where the Fe_2O_3 concentration and the REE ratios are high, light REE are associated with the Fe_2O_3

concentrations. There are some differences below and above the palaeontologically defined boundary. The La_N/Yb_N and La/Lu ratios below the boundary show a strong lithological control, in that the sandstones have lower ratios than the siltstones. The green-grey mudstones have less variable ratios, but show a similar pattern to the Fe_2O_3 concentration trends. Above the palaeontologically defined boundary, much oscillation in the values occurs, particularly in the red-brown mudstones.

The ratios of La/Th (Fig. 33), La_N/Yb_N (Fig. 34) and La/Lu (Fig. 34) show differences to those calculated for the Commando Drift Dam section. The carbonate nodular horizons show little difference from the other lithologies for these ratios, but can be distinguished from the other lithologies in the REE plots, as they have lower normalized abundances.

As with the Commando Drift Dam section, Cerium anomalies are not observed. Europium anomalies are always present, and are consistent in shape.

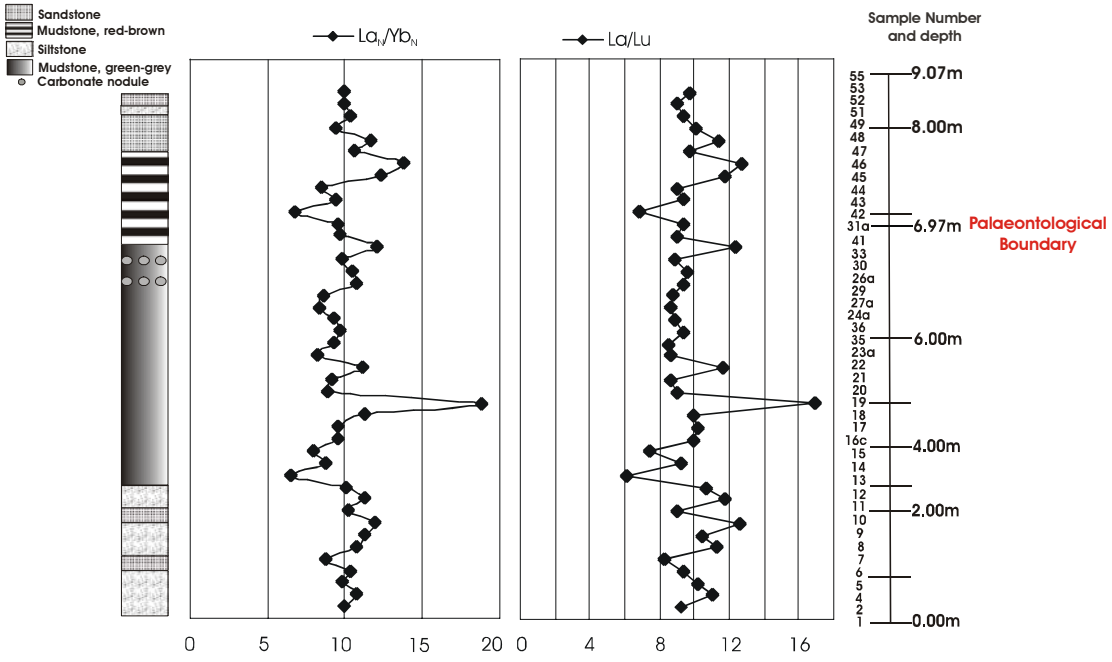


Figure 34: *La_N/Yb_N and La/Lu ratios for the Wapadsberg section.*

3.3.2.1.5 Geochemical Changes for the Wapadsberg Section

In the Wapadsberg section, changes in Fe_2O_3 content are not as marked as for the Commando Drift Dam section, and the siderophile elements follow the same trend, being somewhat enriched just above the boundary.

Changes across the P-Tr boundary of the Wapadsberg section include increases in the elemental concentrations of all the chalcophile elements, siderophile elements and the following lithophile elements: Cr, Sc, Cs, Th. The REE abundance patterns do not vary across the boundary, but the REE ratios show more variation than those for the Commando Drift Dam section, and they indicate a stronger lithological control, together with an association with Fe_2O_3 concentrations.

3.4 Stable Isotope Analysis

The Commando Drift Dam section, which is palaeontologically and palaeomagnetically constrained, was chosen for both sulphur and carbon isotopic analysis. Initially, a suite of samples spaced at large intervals was chosen, in order to detect if the sulphur and carbon isotopic ratios of the samples could be measured. A number of samples from below the palaeontologically defined boundary, at the palaeontological boundary, and at the palaeomagnetically defined boundary were analysed. However, sulphur concentrations turned out to be below the lowest limit of detection of 0.1 wt% (Table 6), so only carbon isotope results could be obtained.

3.4.1 Carbon Isotopic Ratios

A first suite of samples was analysed in order to determine whether the concentration of carbon was sufficient for isotopic analysis, and it was determined that this analysis could proceed. Concentrations of bulk carbon were high in the carbonate nodular horizons (over 7 wt%) and were between 0.05 and 0.2 wt% for other samples. Organic carbon

concentrations varied between 0.1 and 0.3 wt%. After the initial set of results was obtained (Fig. 35), it was concluded that the samples were not closely enough spaced to be able to constrain the variation pattern sufficiently. Additional samples would have to be analysed in order to permit our results to be comparable to those of de Wit et al. (2002) and Retallack et al. (2003). Tables 7 and 8 present the bulk and organic carbon isotopic data accumulated. Figure 36 shows the entire set of results for bulk carbon isotopic data for the Commando Drift Dam section. Organic carbon isotopic results are shown in Figure 37; apparent inorganic carbon isotopic results (Fig. 38) were calculated from: $\delta^{13}C_{Inorg} = \delta^{13}C_{bulk} - \delta^{13}C_{org}$.

The bulk carbon data (Fig. 36) are influenced by the presence of most of the carbonate nodular horizons, for which the seven values are lighter (-9.3 to -11.5 ‰) than those for the other lithologies (ca. -15 to -20 ‰ in the lower part of the sequence). Two carbonate horizons show values of -14.3‰ (PCD 40) and -15.7‰ (PCD 35) towards the top of the sequence, but these horizons still represent lighter ratios than the samples below and above them (Table 7). In general, for both the bulk carbon isotopic data (Fig. 36) and the inorganic carbon isotopic data (Fig. 38) a gradually decreasing trend is seen from the first sample (PCD 1) to the palaeontologically defined boundary (6.50 m). A slight negative excursion in the bulk carbon isotope values (in the range of -24.9 to -21.1‰) occurs at and just above the palaeontologically defined boundary. Above the boundary, increasing values (of ca. -15 to -19‰) are seen until 8.2 m. Towards the palaeomagnetically defined boundary, a gradual decrease of values is observed (of ca. -18 to -16‰), followed by an apparent return to previous average values (-20‰).

Table 6: *Sulphur concentrations for both the Commando Drift Dam and the Wapadsberg sections, as determined by XRF. Data in wt%.*

Sample No. Commando Drift Dam	**S (wt%)**	**Sample No. Wapadsberg**	**S (wt%)**
PCD 1	0.07	PW 1	0.08
PCD 2	0.04	PW 2	0.02
PCD 3	0.30	PW 4	0.06
PCD 4	0.02	PW 5	0.07
PCD 5	0.20	PW 6	0.07
PCD 6	0.06	PW 7	0.09
PCD 8	0.20	PW 8	0.03
PCD 9	0.08	PW 9	0.09
PCD10	0.30	PW 10	0.08
PCD 11	0.05	PW 11	0.08
PCD12	0.05	PW 12	0.11
PCD13	0.07	PW 13	0.50
PCD16	0.06	PW 14	0.31
PCD 17	0.04	PW 15	0.07
PCD 22	0.07	PW 16c	0.06
PCD 24	0.09	PW 17	0.07
PCD 27	0.08	PW 18	0.05
PCD 28	0.07	PW 19	0.05
PCD 26	0.04	PW 20	0.04
PCD 29	0.05	PW 21	0.06
PCD 30	0.06	PW 22	0.07
PCD 31	0.07	PW 23A	0.05
PCD 32	0.08	PW 35	0.05
PCD 33	0.06	PW 36	0.06
PCD 34	0.07	PW 24A	0.08
PCD 35	0.10	PW 27A	0.07
PCD 36	0.04	PW 29	0.11
PCD 37	0.50	PW 26A	0.10
PCD 38	0.20	PW 30	0.12
PCD 40	0.30	PW 33	0.10
PCD 42	0.05	PW 41	0.10
PCD 43	0.08	**PW 31A**	0.13
PCD 44	0.08	PW 42	0.05
PCD 46	0.05	PW 43	0.20
		PW 44	0.15
		PW 45	0.03
		PW 46	0.05
		PW 47	0.03
		PW 48	0.02
		PW 49	0.03
		PW 51	0.09
		PW 52	0.04
		PW 53	0.02
		PW 55	0.06

Table 7: *Bulk carbon isotopic data for samples from the Commando Drift Dam section. Errors are 1σ. Data are given as* $\delta^{13}C = \{(^{13}C/^{12}C$ *sample)/(*$^{13}C/^{12}C$ *standard) – 1} x 1000), expressed as per mil of the Vienna Pee Dee Belemnite standard (‰ PDB). Carbon concentrations in wt% are also shown, with standard deviations based on duplicate analyses.*

Sample No. Commando Drift Dam	**$\delta^{13}C$ (‰ $_{PDB}$)**		**C (wt%)**	
PCD 1	-20.90	±0.18	0.16	±0.01
PCD 2	-20.81	±0.43	0.12	±0.01
PCD 3	-9.28	±0.20	7.46	±0.09
PCD 4	-22.84	±0.12	0.10	±0.01
PCD 5	-10.15	±0.09	9.07	±0.06
PCD 6	-20.10	±1.43	0.13	±0.04
PCD 8	-10.15	±0.01	6.31	±0.4
PCD 9	-18.06	±0.32	0.96	±0.03
PCD10	-11.53	±0.17	8.29	±0.07
PCD 11	-18.52	±0.93	0.16	±0.02
PCD12	-20.17	±0.45	0.10	±0.01
PCD13	-16.38	±0.47	0.16	±0.01
PCD16	-24.88	±0.36	0.07	±0.01
PCD 17	-22.86	±1.61	0.04	±0.002
PCD 22	-22.41	±1.53	0.05	±0.004
PCD 24	-24.86	±0.92	0.05	±0.004
PCD 27	-21.10	±0.99	0.37	±0.04
PCD 28	-23.08	±1.32	0.05	±0.01
PCD 26	-21.46	±1.44	0.04	±0.01
PCD 29	-23.73	±1.30	0.05	±0.01
PCD 30	-22.75	±1.23	0.04	±0.004
PCD 31	-18.25	±1.44	0.09	±0.01
PCD 32	-22.48	±1.74	0.05	±0.01
PCD 33	-15.91	±0.17	0.31	±0.004
PCD 34	-18.59	±0.33	0.08	±0.01
PCD 35	-15.74	±1.22	1.06	±0.04
PCD 36	-15.77	±0.07	0.13	±0.06
PCD 37	-9.33	±0.35	6.22	±0.19
PCD 38	-17.80	±0.12	2.27	±0.05
PCD 40	-14.30	±0.46	1.50	±0.02
PCD 42	-16.30	±0.78	0.12	±0.01
PCD 43	-18.89	±0.80	0.44	±0.04
PCD 44	-23.04	±0.93	0.09	±0.002
PCD 46	-20.20	±0.81	0.46	±0.04

Table 8: *Organic carbon isotopic data from the Commando Drift Dam section. Errors are 1σ. Data are given as* $\delta^{13}C_{org}$, *expressed as per mil of the Vienna Pee Dee Belemnite standard (‰ PDB). Organic carbon concentrations in wt% are also shown, with standard deviations based on duplicate analyses.*

Sample No. Commando Drift Dam	**$\delta^{13}C_{org}$ (‰ PDB)**		**C (wt%)**	
PCD 1	-27.66	±0.38	0.21	±0.07
PCD 2	-27.96	±0.38	0.12	±0.01
PCD 3	-28.5	±0.41	0.12	±0.001
PCD 4	-28.2	±0.40	0.13	±0.001
PCD 5	-28.2	±0.33	0.08	±0.003
PCD 6	-27.8	±0.01	0.17	±0.001
PCD 8	-28.5	±0.08	0.12	±0.01
PCD 9	-28.4	±0.11	0.16	±0.001
PCD10	-28.8	±0.13	0.10	±0.002
PCD 11	-27.4	±0.04	0.21	±0.01
PCD12	-27.6	±0.81	0.09	±0.002
PCD13	-28.9	±0.64	0.11	±0.004
PCD16	-28.8	±0.54	0.15	±0.05
PCD 17	-27.4	±0.06	0.15	±0.01
PCD 22	-27.7	±0.02	0.33	±0.01
PCD 24	-28.0	±0.09	0.23	±0.01
PCD 27	-27.38	±0.25	0.25	±0.01
PCD 28	-26.62	±0.39	0.22	±0.03
PCD 26	-27.92	±0.33	0.24	±0.01
PCD 29	-28.72	±0.64	0.35	±0.03
PCD 30	-27.79	±0.01	0.31	±0.01
PCD 31	-27.66	±0.07	0.23	±0.01
PCD 32	-28.45	±0.13	0.30	±0.01
PCD 33	-28.31	±0.17	0.13	±0.02
PCD 34	-27.21	±0.29	0.20	±0.01
PCD 35	-27.67	±0.34	0.29	±0.004
PCD 36	-27.68	±0.76	0.13	±0.001
PCD 37	-27.92	±0.42	0.13	±0.05
PCD 38	-27.87	±0.11	0.11	±0.01
PCD 40	-28.19	±0.35	0.17	±0.01
PCD 42	-28.79	±0.23	0.15	±0.003
PCD 43	-28.03	±0.05	0.23	±0.04
PCD 44	-27.51	±0.07	0.18	±0.001
PCD 46	-27.28	±0.23	0.25	±0.01

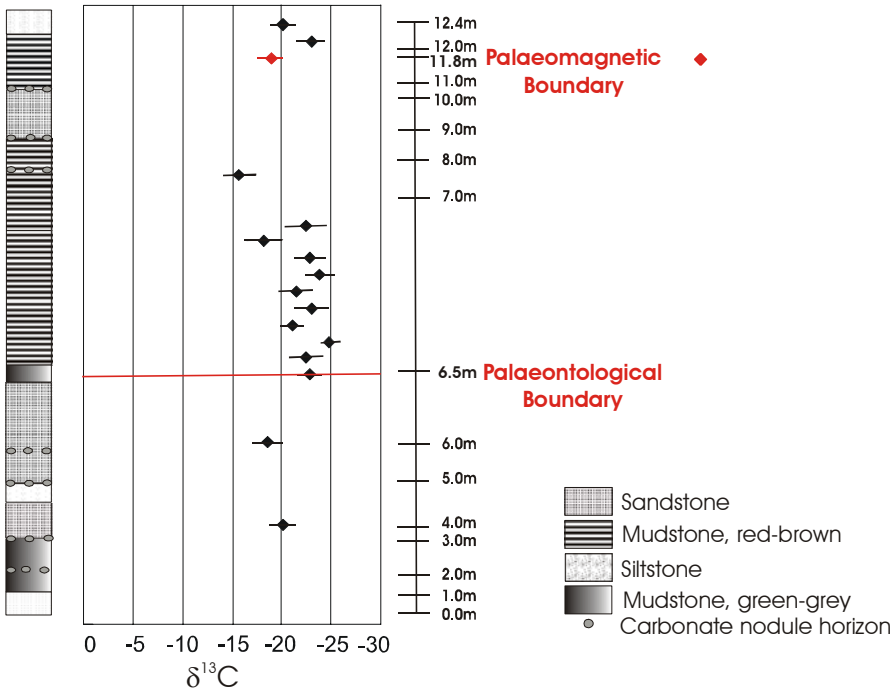


Figure 35: *Commando Drift Dam stratigraphic section: Initial results for bulk $\delta^{13}C$. Error bars shown represent 1σ standard deviations.*

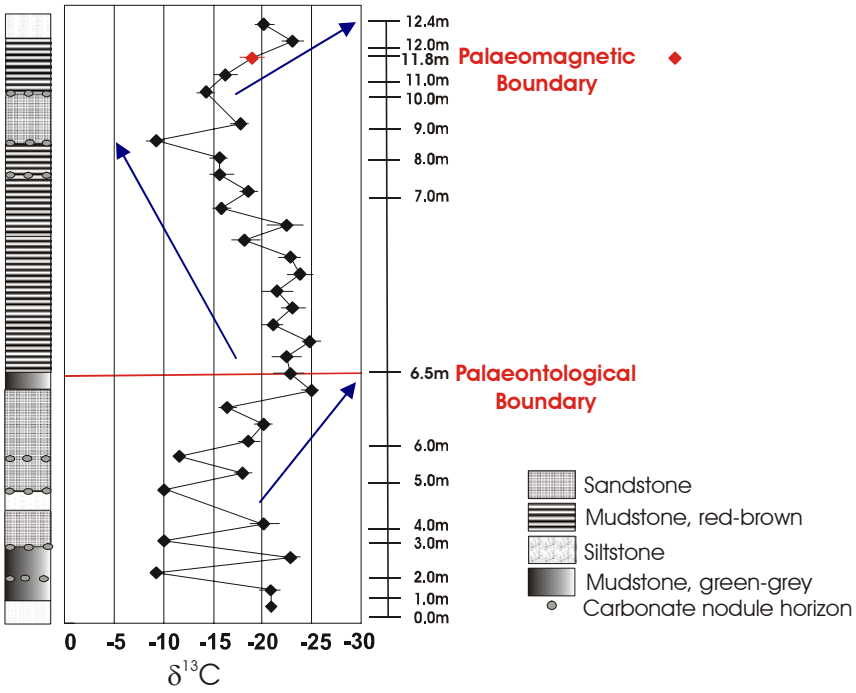


Figure 36: *Commando Drift Dam stratigraphic section: Full results for bulk $\delta^{13}C$. Error bars shown represent 1σ standard deviations.*

The organic carbon isotopic values (Fig. 37) vary only within a small range (-26.7 to -28.8‰) and do not display possibly significant trends. Thus, when both sets of data (as apparent inorganic carbon isotopic values) are considered together (Fig. 38), this shows that the inorganic carbon isotopic content must be changing more than the organic carbon isotopic content.

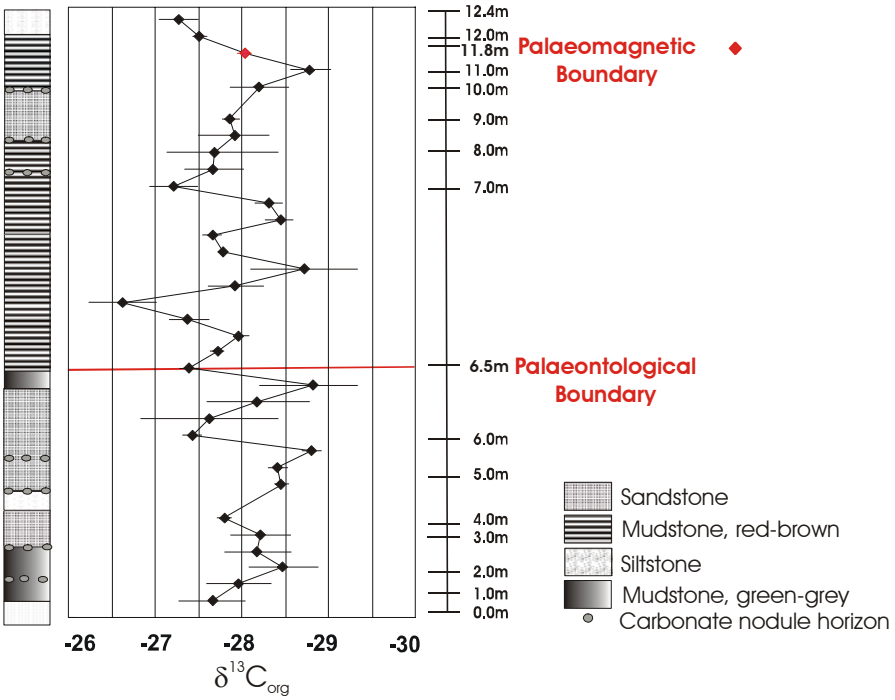


Figure 37: *Commando Drift Dam stratigraphic section: Results for organic $\delta^{13}C$. Error bars shown represent 1σ standard deviations.*

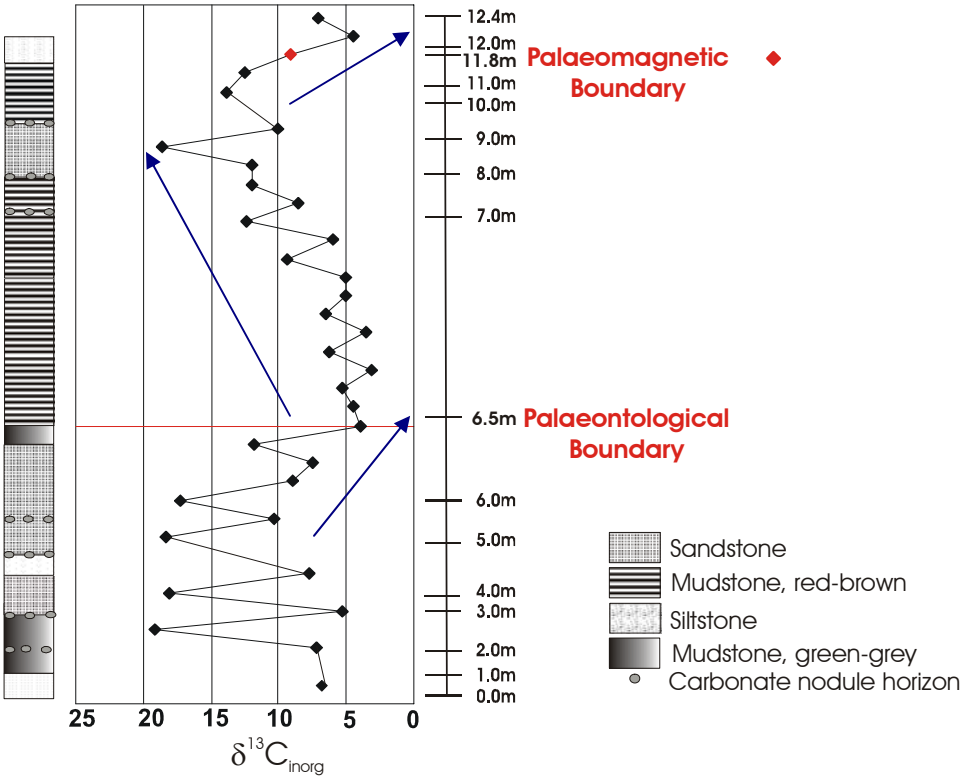


Figure 38: *Commando Drift Dam stratigraphic section: Apparent inorganic $\delta^{13}C$ variation, calculated as $\delta^{13}C_{bulk} - \delta^{13}C_{Org}$.*

Apparent inorganic carbon isotopic contents are slightly lower at and just above the palaeontologically defined boundary (ca. <5‰) compared to carbon isotopic values of 6-11‰ in the Permian samples – barring the carbonate nodule samples. Gradual recovery to average values (~6 ‰) is observed up to 8.2 m above the palaeontologically defined boundary. The presence of the carbonate nodular horizons is indicated by high inorganic carbon isotopic ratios of ~18 ‰. The apparent inorganic carbon isotopic content follows the same trends as the bulk carbon isotopic content, as indicated on Figs. 36 and 38.

CHAPTER FOUR: DISCUSSION AND CONCLUSION

Stratigraphic, sedimentological, petrographic and geochemical data and observations have been collected from the Commando Drift Dam and Wapadsberg sections to aid in the definition, placement and characterization of the continental P-Tr boundary in the southern Karoo Basin. The results are also used to evaluate the various hypotheses for the causes of environmental change at the time of the P-Tr boundary and associated mass extinction.

4.1 Stratigraphy and Sedimentology

Smith (1995), MacLeod et al. (2000), Smith and Ward (2001), de Wit et al. (2002), Retallack et al. (2003) and Ward et al. (2005) all used the Last Appearance Datum (LAD) of *Dicynodon lacerticeps* to constrain the P-Tr boundary in the Karoo Basin, and this has also been used in this study to mark the palaeontological boundary.

MacLeod et al. (2000), Retallack et al. (2003) and Ward et al. (2005) pointed out that this biostratigraphic placement of the P-Tr boundary is supported by carbon isotopic analyses, whereby the first of a number of negative excursions occurred at the level of "minimum vertebrate diversity" (MacLeod et al., 2000). Such carbon isotopic anomalies have been used to place the Permian-Triassic boundary at a number of localities world-wide (Morante, 1996; Krull and Retallack, 2000). A sharp, negative $\delta^{13}C$ excursion has been found at the position of the boundary (in both organic and inorganic carbon samples) at a number of marine sections, including the GSSP at Meishan, China (e.g., Wang et al., 1994; Yang et al., 1996). For sections in the Karoo Basin, MacLeod et al. (2000) reported carbon isotopic excursion ranges from ~3‰ to >10‰ less than background (MacLeod et al., 2000), but the most negative values

coincided with the position of the Permian-Triassic boundary and associated extinction.

The P-Tr boundary in the Karoo Basin is also marked by a change in fluvial style above the palaeontological boundary (first proposed by Smith, 1995, and subsequently by Ward et al., 2000; Smith and Ward, 2001; Hancox et al., 2002; Retallack et al., 2003), and this was observed during this study.

Hancox et al. (2002) examined sections at Senekal in the northern Karoo Basin. Below the suggested placement of the P-Tr boundary, a sequence dominated by mudstones is seen, that is fining-upward in character (Hancox et al., 2002). Above the P-Tr boundary, Hancox et al. (2002) found a 20 m sequence of cross-stratified sandstones, followed by a number of mudstone layers. The zone containing the palaeontological boundary was found to be erosive, and in some places a concretionary layer had been removed. Although the presence of the concretionary layer is in evidence in some places in the northern Karoo, as well as the change in fluvial style, there are a number of different characteristics to the southern Karoo sequences. The change in fluvial style is not gradational, and there is no thick sequence of red-brown mudstones or siltstones above the palaeontological boundary. Hancox et al. (2002) concluded that the temporal equivalent of the P-Tr boundary in the southern Karoo Basin is possibly represented by an unconformity surface in the north.

In this study, sections at both the Commando Drift Dam and Wapadsberg sites were studied (Figs 13 and 14). The strata consist predominantly of mudrock, with alternating sandstone and carbonate nodular horizons. Within the southern Karoo Basin, the boundary has previously been marked by a ~10 cm thick claystone breccia (e.g., Smith, 1995; Smith and Ward, 2001; Retallack et al., 2003).

Figure 39 shows detailed stratigraphic sections from sites in the southern Karoo Basin (Fig. 3), modified after Ward et al. (2005).

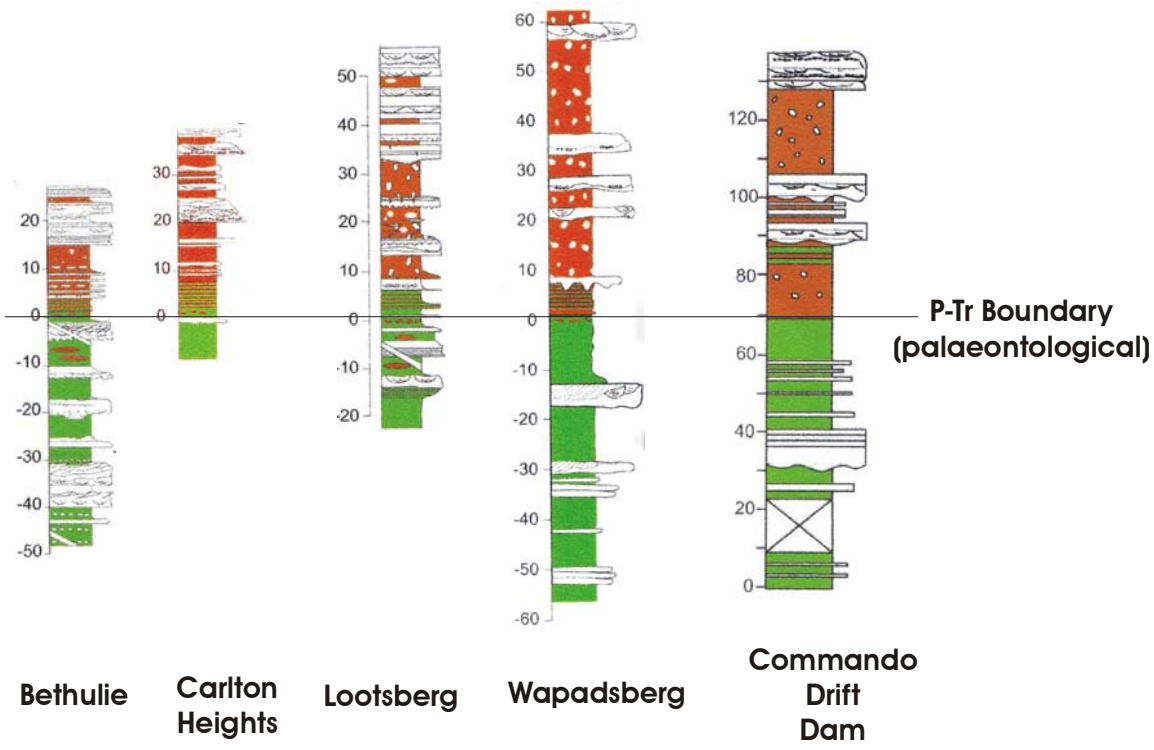


Figure 39: *Comparison of the stratigraphy of P-Tr sections in the southern Karoo Basin (modified after: Ward et al., 2005). Green indicates the green-grey mudstones; red indicates the red-brown mudstones. White indicates the sedimentological features of the sandstones and siltstones. Vertical scales in metres.*

The upper part of the sequence contains cross-stratified sandstones, and this continues upwards into the Katberg Formation. The most noticeable common feature of the sections is the change in colour from green-grey to red-brown mudstones at about the position of the P-Tr boundary. This change is gradual in most sections (Fig. 39), but can be sharp in places (e.g., Commando Drift Dam, Fig. 12), and may represent a change of the oxidation state of Fe^{2+} to Fe^{3+}, possibly caused by a change in the

groundwater redox conditions. The characteristics of the Commando Drift Dam and Wapadsberg sections (section 3.1; Figs 13 and 14) indicate that their stratigraphic records (and data sets obtained here; Fig. 39) are comparable to other studies undertaken in the southern Karoo Basin (e.g., Smith, 1995; Smith and Ward, 2001; Retallack et al., 2003; Ward et al., 2005).

The Wapadsberg and Commando Drift Dam sections were also studied by Ward et al. (2005), with similar observations to this study. All the stratigraphic sections in the southern Karoo Basin document similar lithological characteristics (Fig. 39), with the boundary placed at the base of the laminated event bed.

One of the major difference between the Wapadsberg section and the Commando Drift Dam section is that there are only two carbonate nodular horizons (compared to seven in the Commando Drift Dam section) just below the palaeontologically defined boundary and the event bed of Smith (1995) (Fig. 13). The distribution and characteristics of carbonate nodular horizons has been discussed as related to climate seasonality (Retallack et al., 2003 and references therein). Changes in the seasonality of the local climate may explain the different number of carbonate nodular horizons in the two sections. Additionally, there are differences in the number of carbonate nodular horizons between these sections and those examined by Retallack et al. (2003). Although Retallack et al. (2003) noted similar characteristics between those carbonate nodular horizons in the Permian as opposed to those carbonate nodular horizons in the Triassic, the variation in number of nodules indicates local, heterogeneous changes in the palaeoclimate.

4.2 Petrography

Petrographic study of thin sections of sandstones, siltstones and mudstones showed little textural and mineralogical differences below and above the palaeontologically-defined boundary, except for brecciation in a number of samples directly adjacent to the boundary (PCD 17 to PCD 27; PW 31 to PW 45). In particular large grains of plagioclase, microcline and particularly quartz are brecciated in samples from directly adjacent to the boundary (Fig. 16). This is seen for both the Commando Drift Dam and Wapadsberg sections.

Impact-diagnostic microdeformation of quartz (e.g., PDF's) is not observed. This would either imply that either an impact event did not take place at the Permian-Triassic boundary, or that, if an impact event did take place, it took place in quartz-poor crust. In order to rule out the impact hypothesis, geochemical observations have also been made.

In this study, an increase in chemical weathering, as indicated by the increasingly quartz-rich (increase of SiO_2) rock compositions (Johnson, 1991), is documented up sequence (Table 5; section 3.3.1). This was also observed by Retallack et al. (2003). With increased chemical weathering, feldspar and rock fragments are more readily weathered than quartz, and quartz abundance would increase.

4.3 Major and Trace Element Geochemistry

A major aim of this study was to investigate whether any geochemical change occurs across the palaeontologically-defined P-Tr boundary or the palaeomagnetic boundary of de Kock (2003) in the Commando Drift Dam section. The geochemical compositions of the rocks in the sections can be generally related to the lithological differences. Neither the

palaeontological nor the palaeomagnetically defined boundaries are marked by distinct differences in major element concentrations, except for the Fe_2O_3 content, which increases across both boundaries. For both the Commando Drift Dam and Wapadsberg sections, many of the major element concentrations are near constant in value and no substantial differences are seen (see section 3.3.1). The trace elements are far more variable, and some do show concentration differences at both the palaeontological and palaeomagnetically defined boundaries in the Commando Drift Dam section (see section 3.3.2.1).

4.3.1 The Commando Drift Dam Section

In the Commando Drift Dam section, the greatest variation in major and trace element concentrations relates to the appearance of the carbonate nodular horizons. Iron (as Fe_2O_3) contents also change up-sequence, with the major change being coincident with the position of the palaeontological boundary (Table 9, Fig. 19). The increase in concentration is directly related to a change in the oxidation state of iron from its reduced form (Fe^{2+}) to its oxidized form (Fe^{3+}), as indicated by the change in colour of the sedimentary rocks from green-grey to red-brown. This increase in concentration may be related to a change in the sedimentary provenance, aridification, climatic warming, or a diagenetic alteration effect such as the influx of iron-rich hydrothermal fluids. This change has previously been documented by Retallack et al. (2003), and noted by Ward (2004). The percentage of Fe_2O_3 once again increases (Fig. 19) at the palaeomagnetically defined boundary (after de Kock, 2003). This may have a similar origin to the increase in iron contents at the palaeontological boundary. At Commando Drift Dam, a number of trace element concentrations vary around both boundaries (Table 9). In general the variations are small and related to differences in the concentrations of the major elements with which they are associated.

Gradual changes in the trace element concentrations include Sc and Cs contents, which gradually decrease up sequence from the palaeontological to the palaeomagnetic boundary (Fig. 23). Strontium contents also show the same gradual change (Fig. 23) from below to the palaeontological boundary, and then again from above the palaeontological boundary to the palaeomagnetically defined boundary. Arsenic and Sb contents gradually increase across the entire sequence.

The palaeomagnetically defined boundary (de Kock, 2003) shows a number of distinct changes in terms of its geochemical signature relative to that below the boundary (Table 9; Figs 19, 23, 24 and 25): these are documented in Table 9.

4.3.2 The Wapadsberg Section

The Wapadsberg section shows great variation in the lower part of the sequence (section 3.3.1) for both major element and trace element concentrations. There appear to be more distinctive lithology-related chemical differences than observed at the Commando Drift Dam section between the sandstones, mudstones and siltstones, as well as the carbonate nodular horizons (section 4.1).

SiO_2 contents distinctively increase above the P-Tr boundary. The boundary sample shows intermediate SiO_2, CaO, MnO, MgO, and TiO_2 concentrations, (Fig. 21) but this may reflect the influence of the carbonate nodular layer in the sample immediately below (2 cm) the boundary sample (Table 9). Fe_2O_3 concentrations increase in relation to the background values at the boundary, with the concurrent change in colour of the mudstones from green-grey to red-brown (Fig. 21). The increase in Fe_2O_3 concentration in the Wapadsberg section is not as pronounced as in the Commando Drift Dam section, at ~2 wt% increase (~4 wt % for Commando Drift Dam). The siderophile element enrichment compared to

background levels is also not as pronounced as for the Commando Drift Dam section (Fig. 30). There is an anomalous value in Fe_2O_3 contents located nearly 1.97 m below the boundary, but this is attributed to a localized change in mineralogy (Fig. 30).

Trace element concentration changes (Table 9) across the palaeontological boundary of the Wapadsberg section are similar to those observed at Commando Drift Dam. Hafnium concentrations decrease gradually up sequence below the boundary.

Trace elements which increase across both sections include Zn, Sc, Cr, Cs and As. REE abundances do not change below, at or above the palaeontological or palaeomagnetically defined boundaries in either section (Figs 26-28, 32-34).

Gold concentrations were generally below the detection limit at both sections. Iridium concentrations from both the Commando Drift Dam and Wapadsberg sections are generally below the detection limit (utilizing INAA) in all samples (see sections 3.3.2.1.2 and 3.3.2.2.2). Consequently, it is not possible to test whether a significant enrichment has taken place at either boundary, without comprehensive low-level (high resolution) platinum group element analysis.

Geochemically, the P-Tr palaeontological boundary at the two sections in the southern Karoo Basin is not marked by distinct changes in the major and trace element contents. The well-defined changes that are observed along the sections are controlled by lithological changes. There are a number of gradual changes in concentration, particularly of the trace elements (see section 3.3.2), which could argue for gradual palaeoclimatic change up to the P-Tr boundary. If there were sudden changes in the palaeoclimate, these changes should be reflected by distinct concentration

changes of those elements affected by mobility. In both the Commando Drift Dam and Wapadsberg sections, Hf and Sr contents decrease at the palaeontological and palaeomagnetically defined boundaries, while the abundances of the siderophile, and many of the chalcophile, elements increase. The other trace elements, however, do not show consistent changes. The individual trace element changes are more likely to be controlled by element mobility, and alone should not be used to correlate sections in the southern Karoo Basin. Also, trace element changes are not consistent between the two sections (and are affected by processes such as weathering), and this cannot be used to correlate other continental sections worldwide.

The trace element changes across the palaeomagnetically defined boundary at the Commando Drift Dam section are similar to those observed across the palaeontological boundary. This, may, however, be an effect of weathering. Thus, the geochemical data cannot be used to correlate the change in palaeomagnetic signature in P-Tr sections worldwide, as local climatic variations (such as weathering) may provide the strongest control on the trace element compositions. Thus, the data cannot be used to ascertain the synchronicity of the marine and non-marine extinctions.

4.3.3 Comparison of Geochemical Data for Different Sections in the Karoo Basin

Hancox et al. (2002) found significantly different chemical signatures below and above the presumed palaeontological boundary at two sections in the northern Karoo Basin (Senekal; Fig. 3). They concluded that there may be an unconformity at the P-Tr boundary in the northern Karoo Basin. Hancox et al. (2002) present a first section showing relative depletion in Al_2O_3 and MgO contents with relative enrichments in Fe_2O_3 and Na_2O contents above the P-Tr boundary. There were no significant

changes in the concentrations of the siderophile elements, and Sc, V, Co, Ni, Rb and Cs were relatively depleted above the boundary. Higher Sr and Hf concentrations were observed above the palaeontological boundary.

Table 9: *Summary of geochemical changes across the palaeontological and palaeomagnetic boundaries for the Commando Drift Dam and the Wapadsberg sections.*

	Commando Drift Dam Palaeontological Boundary	**Commando Drift Dam Palaeomagnetic Boundary**	**Wapadsberg Palaeontological Boundary**
[Elements] Increase w.r.t. background values	Fe_2O_3, MgO, Rb, Cr, Ni, Co, As, Zn, Sc, Cs	Fe_2O_3, Cr, V, Sb, Zn, Sc, Cs	Fe_2O_3, MgO, Cr, Sc, Cs, Th, Co, V, Ni, Zn, Cu, Sb, As
[Elements] Decrease w.r.t. background values	Hf, Sr	Hf, Sr	Hf, Sr
No change in concentration	Au, Ir, Ta, Th, Y, Nb, U, Zr, REE	Au, Ir, Ta, Th, Y, Nb, U, Zr, REE	Au, Ir, Y, Nb, Ta, U, Zr, REE

In the second section of Hancox et al. (2002), relative depletion above the boundary in Fe_2O_3 and MgO contents was observed. Hancox et al. (2002) also noted slightly higher Cr concentrations and significantly higher Co concentrations at the boundary, in comparison to samples below the boundary. Enrichment in Sc, Co, Cr, Ni, Zn, As, Hf and Th contents was also seen for samples above the boundary.

Hancox et al. (2002) found that REE patterns were distinctly different below and above the boundary, for both their sections. Above the boundary, samples were characterized by relatively lower abundances of

the REEs and had a less pronounced Eu anomaly than the samples from below the boundary. The overall range of abundances was similar for both sections studied.

In this study, different geochemical signatures have not been observed across the P-Tr boundary, in contrast to the distinct differences observed by Hancox et al. (2002). There are a number of differences with respect to the observations made by Hancox et al. (2002) in the northern Karoo: In both the Commando Drift Dam and Wapadsberg sections, enrichment in Fe_2O_3 concentrations in samples above the palaeontological boundary is observed, together with an increase in MgO contents. This is in direct contrast to the second section at Senekal studied by Hancox et al. (2002). Enrichments in the siderophile trace elements as observed across the Commando Drift Dam boundary were not noted in the sections of Hancox et al. (2002). In the Commando Drift Dam and Wapadsberg sections, no REE variation along the profiles has been recorded.

Thus, the sections of Hancox et al. (2002) and this study are not directly comparable. Clearly, these spatially separated sections could involve sediment input from compositionally different sources. A small geological difference between provenance terranes could result in significant geochemical differences, potentially at the same stratigraphic level. This also re-emphasizes the reciprocal basin development model for the Karoo Basin (Catuneanu et al., 1998), which postulates that in a unitary basin without dynamic subsidence, flexurally induced subsidence will be out of phase in the proximal and distal sectors.

4.3.4 Palaeoclimatic Change Evaluated Using Geochemistry

The geochemical data do not offer support for either the wet to dry (Smith, 1995; see section 1.3.3) or dry to wet (Retallack et al., 2003; see section 1.2.4) palaeoclimatic models. The increase in Fe_2O_3 contents, and the

change in colour of the mudrocks from green-grey to red-brown, has traditionally been seen as indicating a more arid climate (Mader, 1990). However, many red beds have been noted in both arid (Mader, 1990) and humid palaeoclimates (Retallack, 1997; Retallack, 1999; Retallack and Krull, 1999) and may be a result of partial diagenesis. Thus, this dataset does not favour either palaeoclimatic change model, as the increase in Fe_2O_3 contents observed is compatible with both models, and the trace element data do not indicate any distinct palaeoclimatic change.

This study shows similarities with that of Retallack et al. (2003) in that there is an increase in SiO_2-rich compositions across the P-Tr boundary (see section 4.2). This may indicate an increase in chemical weathering or an increase in quartz sediment supply, or an increase in sorting of sediments. If this is an increase in either amount of quartz or the chemical weathering, it would indicate that the environment in the Triassic was warmer and wetter than in the Permian. In humid environments, quartz is less easily weathered than feldspars and rock fragments, and the proportion of quartz present increases (Suttner and Dutta, 1986). This observation supports the hypothesized change to a warm, wet environment. However, with the absence of carbonate nodular characteristics (e.g., spread and depth, compiled by Retallack et al., 2003), this study cannot support either palaeoclimatic model.

Molecular weathering ratios were calculated for the sections in this project (Figs 20 and 22), and were generally found to be constant for most lithologies except the carbonate nodular horizons. The ratio $Al_2O_3/(CaO+MgO+Na_2O+K_2O)$ shows some variation in both sections, which may have been caused by diagenetic alteration (see section 3.3.1). This variation was not observed by Retallack et al. (2003), whose molecular weathering ratios were constant.

4.4 Carbon Isotope Geochemistry

The relationship between the stable isotope record and the P-Tr boundary in non-marine sections is not well established. Differences in the size and placement of reported excursions in the Karoo Basin make interpretation and correlation difficult.

Thackeray et al. (1990) and Faure et al. (1995) performed broad sampling of the Lower Beaufort Group strata and fossils and found a negative carbon isotope trend of ~10‰ from stable Permian background values towards the palaeontologically defined boundary in the Karoo Basin. MacLeod et al. (2000) worked on a narrower stratigraphic interval and confining their analyses to the stable isotopes of carbonate nodules and therapsid tooth apatite, did not observe this broad trend, and found conflicting results from different boundary sections. In particular, at Doornplaats and Lootsberg, no changes were observed below and at the P-Tr boundary (MacLeod et al., 2000). This was attributed to diagenetic alteration (MacLeod et al., 2000), but could also be due to basinal fluid overprint of the stable isotope record (de Wit et al., 2002). A negative shift of ~10‰ in $\delta^{13}C_{carb}$ was, however, seen at the Bethulie site (Fig. 8), close to the palaeontologically defined boundary (MacLeod et al., 2000). MacLeod et al. (2000) used this to quantify the rapidity of the extinction event, and stated that the $\delta^{13}C$ event at Bethulie was neither geologically nor biologically instantaneous, and spanned a duration of greater than 1 million years. In contrast, Smith and Ward (2001) favoured the duration of the extinction to be sudden, based on the pattern of vertebrate extinctions.

De Wit et al. (2002) concluded that carbon isotopic signals could have been hidden in the southern Karoo Basin owing to basinal fluid flow driven by the formation of the Cape Fold Belt, on the southern active

convergent margin of Gondwana. De Wit et al. (2002) analysed organic matter preserved in carbonate nodules from Lootsberg (see Fig. 4) and assessed the work of MacLeod et al. (2000). At Lootsberg, a number of large negative organic carbon isotopic excursions ($\delta^{13}C_{org;}$ to -27‰ and -28‰) occur in the Late Permian, and a small negative spike (-30‰) is present around the palaeontological boundary above a background of -23 ± 2‰. De Wit et al. (2002) concluded that their results were comparable to those of Thackeray et al. (1990) based on therapsid tooth enamel, and Faure et al. (1995), who obtained carbon isotope signatures for coal-bearing strata. Retallack et al. (2003) arrived at similar conclusions as de Wit et al. (2002) and those made for the Bethulie site by MacLeod et al. (2000) (see section 1.2.3.4 for details).

The results of the present study include fluctuations in the bulk carbon isotopic record (Fig. 36). Three gradual changes in the bulk carbon isotope record have been identified: an initial decrease from the Late Permian to the palaeontological boundary, a second gradual increase following the palaeontological boundary (until 8.2 m above the initial sample), and finally, another gradually decreasing trend towards the palaeomagnetic boundary. There is a more pronounced negative carbon isotope excursion in the sample just below the palaeontological boundary.

This pattern is thought to represent a gradual environmental change, with one or more sudden changes around the palaeontological boundary, followed by some recovery, and then another more gradual environmental modification. Other studies have proposed a more sudden environmental change, caused by an asteroid impact at the P-Tr boundary (see section 1.2.1), but the close sample spacing of this study indicates a more gradual change. Other carbon isotope studies in the Karoo Basin have reached similar conclusions (Ward et al., 2005).

The organic carbon data (section 3.4; Fig. 37) show much oscillation, but within a small interval (2‰). The values of the variation, though, are comparable to the work of MacLeod et al. (2000), de Wit et al. (2002) (Fig. 40), Retallack et al. (2003) and Ward et al. (2005). Combining both the bulk carbon data and the organic carbon isotopic data, it is observed that calculated apparent inorganic carbon isotopic values show significant variation, and have positive carbon isotopic ratios. The apparent $\delta^{13}C_{inorg}$ patterns show the same data trends as observed for the bulk carbon isotopic ratios (Fig. 38), in that two gradually decreasing trends are seen towards the palaeontological and palaeomagnetic boundaries. An increasing trend follows the palaeontological boundary.

It must be emphasized that the present study has a small sample spacing (on the cm scale) in contrast to previous studies (MacLeod et al, 2000; de Wit et al., 2002) conducted with sample spacings over many metres. Additionally, most studies in the Karoo Basin have differed in terms of sampling and type of carbon isotope signature obtained (e.g., bulk, organic, carbonate), which makes any correlation between the various studies difficult. Figure 40 shows a comparison of the organic carbon isotope ratios of de Wit et al. (2002) and this work. Although these two studies were conducted over different vertical scales, it can be seen that the oscillations below, and at, the palaeontological boundaries are of similar magnitude.

4.5 Evaluation of Previous Models of the Extinction Event

Carbon isotope data, in addition to detailed geochemical and petrographic analysis, are used here to evaluate the various proposed external (bolide impact) vs. internal (volcanism, methane clathrate dissociation events) causes for the P-Tr mass extinction event.

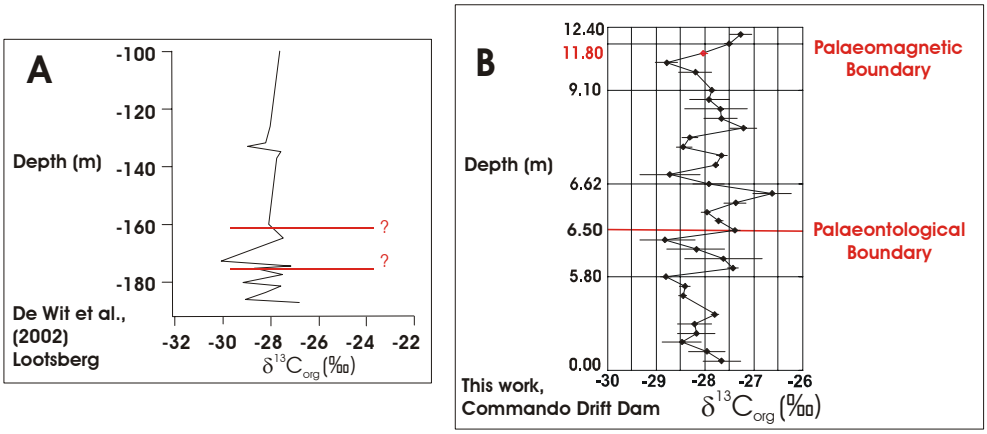


Figure 40: *Comparison of the carbon isotope signatures for* **A** *Lootsberg Pass (de Wit et al., 2002; the question marks represent the possible positions of the P-Tr boundary, as hypothesized by these authors), and* **B** *Commando Drift Dam (this study).*

Extinction by meteorite impact is not supported by this work as no planar deformation features (shock metamorphic features) in quartz have been found. INAA determined Ir concentrations are below the detection limit. Without additional high resolution platinum group element analysis, it is not possible to assess whether any enrichment is recorded in the southern Karoo Basin. In addition to searching for Ir enrichment, concentrations of the elements Cr, Co and Ni have been evaluated with regard to the P-Tr boundary level. These elements occur in concentrations that can be expected to occur in sedimentary rocks (Taylor and McLennan, 1985), and variations in the concentrations of Cr, Co and Ni are seemingly due to lithological changes (Figs 23, 24, 29 and 30). Nickel and chromium show some association with Fe_2O_3, and cobalt has near constant values for all lithologies for both sections (except for those at carbonate nodular horizons), indicating that enrichment in these elements did not take place at the palaeontological boundary.

These results are similar to the findings of Hancox et al. (2002), who did not find evidence for meteorite impact in their sections in the northern Karoo Basin either. However, these authors concluded that the P-Tr boundary may be represented by an unconformity surface in the northern Karoo. Other more recent studies on marine sections utilizing platinum group element (PGE) results, helium and osmium isotopic ratios also found no evidence for a large bolide impact at the P-Tr boundary (Koeberl et al., 2004).

Ward (2004) stated that the presence of red-beds at the P-Tr boundary indicated the process of oceanic anoxia, as there was conversion of Fe^{2+} to Fe^{3+}. The presence of red-beds at the tetrapod-defined palaeontological boundary in this study (and seen at other continental sections worldwide) supports this statement, but the red-beds may have been formed by another process, such as changes in pH rather than a redox reaction. Other options include humid pedogenic alteration, climatic warming, aridification, change in provenance, and hydrothermal alteration. There is possible evidence for hydrothermal alteration – microtextures within the carbonate nodular horizons, as revealed by cathodoluminescence (Fig. 17), that could be indicative of this process.

The size of the fluctuations in the carbon isotopic record measured for Commando Drift Dam are similar to those measured by de Wit et al. (2002) and Retallack et al. (2003), who both concluded that there must be some input from the dissociation of methane clathrates. As detailed in section 1.2.4, the carbon isotopic signal for volcanic input is substantially smaller than the carbon isotopic signals for methane clathrate dissociation. Due to the coincident timing of the Siberian Flood Basalts, the contribution of atmospheric carbon dioxide and other greenhouse gases (e.g., sulphur dioxide, methane, water vapour) cannot be ignored. In this study, a gradual decrease in the $\delta^{13}C$ is observed, with a more pronounced

negative excursion at the palaeontological boundary, which possibly indicates that an initial gradual input of anoxic material took place, followed by a later, more rapid influx of anoxic material. This material could be greenhouse gases, as these would have been produced from either a volcanic event or from the dissociation of methane clathrates. This agrees with the recent findings of Ward et al. (2005).

Multiple fluctuations in the carbon isotopic record in the sequence leading to the palaeontological boundary were interpreted by de Wit et al. (2002) to represent the episodic release of methane from clathrates located in the permafrost and along continental shelves. Methane (which is oxidized to carbon dioxide), a greenhouse gas, contributes to substantial global warming, in addition to other processes such as volcanically-induced global warming from the Siberian Traps. Such a greenhouse effect is thought to be part of the killing mechanism for the P-T extinction event

The marine GSSP (Meishan, China) also shows the same gradual decrease in organic carbon isotope values in the Late Permian (from +4 to 0‰), some recovery, and then a number of small excursions around the boundary, and just above it. This is similar to the pattern observed in this study (Figs 36–38). It indicates that the carbon isotopic record, as measured by de Wit et al. (2002), Ward et al. (2005) and in this study, is roughly comparable to the carbon isotope record seen at the marine GSSP of the Permian-Triassic boundary. Retallack et al. (2003) supported the conclusion of de Wit et al. (2002) and proposed that the size of the negative carbon isotope excursion in sites in the southern Karoo Basin can only be explained by the voluminous dissociation of methane clathrates from permafrost or continental shelves, events that could have been triggered by meteorite impact, volcanic eruption or submarine landslide (Krull et al., 2000).

These results agree with the findings and conclusions of MacLeod et al. (2000), de Wit et al. (2002) and Retallack et al. (2003), all of whom postulated that there may have been multiple sources for input of carbon dioxide, methane and other greenhouse gases into the atmosphere prior to the palaeontological extinction, as well as following the palaeontological extinction. It is possible that the mass extinction was caused by volcanism (the Siberian Traps) in addition to episodic methane clathrate dissociation associated with sea level fluctuations.

4.6 Conclusions

This study was aimed at characterization of the continental P-Tr boundary by examining two well-constrained sections across the boundary in the southern Karoo Basin using petrographic and geochemical analysis. The following conclusions have been reached:

(i) The P-Tr boundary in the southern Karoo Basin is marked by the LAD of *Dicynodon* and a colour change in the sedimentary rocks from green-grey to red-brown.

(ii) The P-Tr boundary is not marked by any major petrographic changes, and no impact diagnostic deformation is observed in quartz grains in boundary mudstones, as the grain size is too fine to preserve such effects. Some brecciation is seen in the sedimentary strata above the boundary. Iridium concentrations from both sections are generally below the detection limit (by INAA); thus it is not possible to test whether a large enrichment has taken place at the P-Tr boundary.

(iii) Major element profiles are dominated by the appearance of carbonate nodular horizons and an increase in Fe_2O_3 contents across both the palaeontological and palaeomagnetically defined boundaries. These,

together with other major element concentrations, largely control the trace element composition. The trace element compositions are also controlled by the effects of weathering (and are not comparable at the two sections).

(iv) Rare earth element normalized abundances do not change significantly across the palaeontological boundary, in contrast to the patterns observed in the northern Karoo Basin. The REE signatures may be different below and above the P-Tr boundary in the northern Karoo Basin, as different sedimentary provenances may have contributed to the section.

(v) An increase in the abundance of quartz across both sections has been observed in this study. This is interpreted to represent an increase in chemical weathering (Johnson, 1991). Retallack et al. (2003) also noted this increase, and used it, in addition to other observations, to suggest a palaeoclimate change from dry to wet in the Karoo Basin. Palaeoclimatic change in the Karoo Basin could not be conclusively evaluated in this study. Additional research into establishing whether a local palaeoclimatic change of wet to dry (Smith, 1995) or dry to wet (Retallack et al., 2003) needs to be undertaken.

(vi) Carbon isotopic data indicate a gradual atmospheric change in the Late Permian, followed by a more punctuated input of anoxic materials at the palaeontological boundary. This is followed by a recovery to background values, and then another gradual decrease in the carbon isotopic values, leading up to the palaeomagnetically defined boundary. The size of the carbon isotope excursions supports multiple inputs of carbon dioxide, methane and other greenhouse gases by the dissociation of methane clathrates, in addition to the contribution of such gases from the contemporaneous Siberian volcanic event.

CHAPTER FIVE: REFERENCES

Alvarez, L.W., Alvarez, W., Asaro, F. and Michel, H.V. (1980). Extraterrestrial cause for the Cretaceous-Tertiary extinction. Science **208**, p. 1095-1108.

Alvarez, W. and O'Connor, D. (1999). The Permian-Triassic Event: Progress and doubts. Catastrophic Events Conference, Lunar and Planetary Institute Contribution No. **1053**, Lunar and Planetary Institute, Houston, Texas, p. 3.

Alvarez, W. and O'Connor, D. (2002). Permian-Triassic boundary in the southwestern United States: Hiatus or continuity. *In* Catastrophic Events and Mass Extinctions: Impacts and Beyond (C. Koeberl and K.G. MacLeod, eds.). Geological Society of America Special Paper **356**, p. 385-394.

Arz, J.A., Alegret, L. and Arenillas, I. (2004). Foraminiferal biostratigraphy and paleoenvironmental reconstruction at the Yaxcopoil-1 drill hole, Chicxulub crater, Yucatán Peninsula. Meteoritics & Planetary Science **39**, p. 1099–1111.

Basu, A.R., Chakrabarti, R., Peterson, J., Poreda, R.J. and Becker, L. (2004). Laser raman spectroscopic confirmation of maskelynite in the Bedout Impact Breccia, offshore, northwest Australia. *In* AGU Abstracts, Fall Meeting, American Geophysical Union, Washington DC, Abstract No. B31E-06.

Becker, L., Poreda, R.J., Hunt, A.G., Bunch, T.E. and Rampino, M. (2001). Impact event at the Permian-Triassic boundary: evidence from extraterrestrial noble gases in fullerenes. Science **291**, p. 1530-1533.

Becker, L., Poreda, R.J., Basu, A.R., Pope, K.O., Harrison, T.M., Nicholson, C. and Iasky, R. (2004). Bedout: A possible End-Permian impact crater offshore of northwestern Australia. Science **304**, p. 1469-1476.

Benton, M.J. and Twitchett, R.J. (2003). How to kill (almost) all life: The End-Permian extinction event. Trends in Ecology and Evolution **18**, p. 358-365.

Benton, M.J., Tverdokhlebov, V.P. and Surkov, M.V. (2004). Ecosystem remodeling among vertebrates at the Permian-Triassic boundary in Russia. Nature **432**, p. 97-100.

Berner, E.K. and Berner, B.A. (1996). Global Environment: Water, Air, and Geochemical Cycles. Prentice-Hall, Englewood Cliffs, NJ, 376 pp.

Berry, W.B.N., Ripperdan, R.L. and Finney, S.C. (2002). Late Ordovician extinction: A Laurentian view. *In* Catastrophic Events and Mass Extinctions: Impacts and Beyond (C. Koeberl and K.G. MacLeod, eds.) Geological Society of America Special Paper **356**, p. 463-471.

Bhandari, N., Shukla, P. N., Ghevariya, Z. G., and Sundaram, S. M. (1996). K/T boundary layer in Deccan Intertrappeans at Anjar, Kutch. *In* The Cretaceous-Tertiary Event and Other Catastrophes in Earth History (G. Ryder, D. Fastovsky, and S. Gartner, eds.). Geological Society of America Special Paper **307**, p. 417–424.

Botha, J. and Smith, R.M.H. (2004). *Lystrosaurus* species composition across the Permian/Triassic Boundary in South Africa. *In* Geoscience Africa 2004, Abstract Volume, University of the Witwatersrand, Johannesburg, South Africa, p. 81.

Bowring, S.A., Erwin, D.H., Jin, Y.G., Martin, W.W., Davidek, K. and Wang, W. (1998). U/Pb zircon geochronology and tempo of the End Permian mass extinction. Science **280**, p. 1039-1045.

Brenchley, P.J. and Marshall, J.D. (1999). Relative timing of critical events during late Ordovician mass extinction: New data from Oslo. Acta Universitatis Carolinae, Geologica **43**, p. 187-190.

Brown, R.D. (2002). An impact centered near Cameroon at the time of the Permian extinction caused the fragmentation of Pangaea. *In* AGU Abstracts, Spring Meeting, American Geophysical Union, Washington DC, Abstract No. T22A-08.

CANMET (1994). Catalogue of Certified Reference Materials. Canadian Certified Reference Materials project 94-1E, CANMET, Ottawa, 82 pp.

Catuneanu, O., Hancox, P.J. and Rubidge, B.S. (1998). Reciprocal flexural behaviour and contrasting stratigraphies: A new basin development model for the Karoo retroarc foreland system, South Africa. Basin Research **10**, p. 417-439.

Chapman, C.R. (2005). Were Permian-Triassic extinctions sudden and caused by impact? *In 68th Annual Meteoritical Society Meeting,* Abstract #5139, Gatlinberg, Tennessee (CD Rom).

Cheng, Z. (1993). On the discovery and significance of the nonmarine Permo-Triassic transition zone at Dalongkou in Jimusar, Xinjiang, China. *In* The Nonmarine Triassic (S.G. Lucas and M. Morales, eds.). New Mexico Museum of Natural History and Science Bulletin **3**, p. 65-67.

Coplen, T.B. (1996). New guidelines for reporting stable hydrogen, carbon, and oxygen isotope-ratio data. Geochimica et Cosmochimica Acta **60**, p. 3359-3360.

Courtillot, V. and Besse, J. (1987). Magnetic field reversals, polar wandering, and core-mantle coupling. Science **237**, p. 1140-1147.

Courtillot, V., Besse, J., Vandamme, D., Montigny, R., Jaeger, J.J., Cappetta, H. (1986). Deccan food basalts at the Cretaceous/Tertiary boundary? Earth and Planetary Science Letters **80,** p. 361-374.

Courtillot, V., Gallet, Y., Rocchia, R., Féraud, G., Robin, E., Hofmann C, Bhandari, N. and Ghevariya, Z.G. (2000). Cosmic markers, $^{40}Ar/^{39}Ar$ dating and paleomagnetism of the KT sections in the Anjar Area of the Deccan large igneous province. Earth and Planetary Science Letters **182**, p. 137-156

De Kock, M.O (2003). Magnetostratigraphic studies in the main Karoo Basin (South Africa): Implications for mass extinction events and the supercontinent of Pangea. M.Sc. dissertation (unpubl.), Rand Afrikaans University, Johannesburg, 126 pp.

De Wit, M.J., Ghosh, J.G., de Villiers, S., Rakotosolofo, N., Alexander, J., Tripathi, A. and Looy, C. (2002). Multiple organic carbon isotope reversals across the Permo-Triassic boundary of terrestrial Gondwana

sequences: Clues to extinction patterns and delayed ecosystem recovery. Journal of Geology **110**, p. 227-240.

Dietz, R.S. (1986). Triassic-Jurassic extinction event, Newark basalts and impact-generated Bahama nexxus. Lunar and Planetary Institute Contribution No. **600**, Lunar and Planetary Institute, Houston, Texas, p. 1-10.

Erwin, D.H. (1993). The great Paleozoic crisis: Life and death in the Permian. Columbia University Press, New York, 327 pp.

Erwin, D. H. (1994). The Permo-Triassic extinction. Nature **367**, p. 231-236.

Erwin, D. H. (1996). Understanding biotic recoveries: Extinction, survival and preservation during the End-Permian mass extinction. *In* Evolutionary Paleobiology (D. Jablonski, D.H. Erwin and J.H. Lipps, eds.) University of Chicago Press, Chicago, p. 398-418.

Erwin, D. H. (2000). The End-Permian mass extinction and Early Triassic biotic recovery. Catastrophic Events Conference, Lunar and Planetary Institute Contribution No. **1053**, Lunar and Planetary Institute, Houston, Texas, p. 43-44.

Erwin, D.H. (2003). Impact at the Permo-Triassic Boundary: A Critical Evaluation. Rubey Colloquium Paper. Astrobiology **3**, p. 67-74.

Erwin, D.H., Bowring, S.A. and Yugan, J. (2002). End-Permian mass extinctions: A review. *In* Catastrophic Events and Mass Extinctions:

Impacts and Beyond (C. Koeberl and K.G. MacLeod, eds.). Geological Society of America Special Paper **356**, p. 363-383.

Farley, K.A. and Mukhopadhyay, S. (2001). An extraterrestrial impact at the Permian-Triassic Boundary? Science **293,** p. 2343a.

Farndon, J. (1994). Dictionary of the Earth. Dorling Kindersley Limited, London, 192 pp.

Faure, K., de Wit, M.J. and Willis, J.P. (1995). Late Permian global coal hiatus linked to ^{13}C-depleted CO_2 flux into the atmosphere during the final consolidation of Pangea. Geology **23**, p. 507-510.

Fowell, S.J., Cornet, B. and Olsen, P.E. (1994). Geologically rapid Late Triassic extinctions: Palynological evidence from the Newark Supergroup. *In* Pangaea: Paleoclimate, tectonics and sedimentation during accretion, zenith and break-up of a supercontinent (G.D. Klein, ed.). Geological Society of America Special Paper **288**, p. 197-206.

Gerlach, T.M. and Graeber, E.J. (1985). Volatile budget of Kilauea volcano. Nature **313**, p. 273-277.

Gibson, R.L. and Reimold, W.U. (2001). The Vredefort Impact Structure, South Africa: The scientific evidence and a two-day excursion guide. Memoir **92**, Council for Geoscience, South Africa, 111 pp.

Gill, R. (ed.) (1997). Modern Analytical Geochemistry. Longman Group UK Limited, 350 pp.

Glikson, A.Y. (2004). Comment on “Bedout: A possible End-Permian Impact Crater Offshore of Northwestern Australia”. Science **306**, p. 613b.

Goto, K., Tada, R., Tajika, E., Bralower, T.J., Hasegawa, T. and Matsui, T. (2004). Evidence for ocean water invasion into the Chicxulub crater at the Cretaceous/Tertiary boundary. Meteoritics & Planetary Science **39**, p. 1233–1247.

Govindaraju, K. (1989). 1989 compilation of working values and sample description for 272 geostandards. Geostandards Newsletter **13**, p. 1-113.

Gradstein, F.M., Ogg, J.G., Smith, A., et al. (2004). A geologic time scale 2004. Cambridge University Press, United Kingdom, 500 pp.

Grard, A., François, L.M., Dessert, C., Dupré, B. and Goddéris, Y. (2005). Basaltic volcanism and mass extinction at the Permo-Triassic boundary: Environmental impact and modeling of the global carbon cycle. Earth and Planetary Science Letters **234**, p. 207-221.

Grieve, R.A.F., Langenhorst, F. and Stöffler, D. (1996). Shock metamorphism of quartz in nature and experiment: II. Significance in geoscience. Meteoritics & Planetary Science **31**, p. 6-35.

Hallam, A. and Wignall, P.B. (1997). Mass Extinctions and Their Aftermath. Oxford University Press, Oxford, 320 pp.

Hallam, A., Grose, J.A. and Ruffell, A.H. (1991). Palaeoclimatic significance of changes in clay mineralogy across the Jurassic-Cretaceous boundary in England and France. Palaeogeography, Palaeoclimatology, Palaeoecology **81**, p. 173-187.

Hancox, P.J. (2000). The continental Triassic of South Africa. Zentralblatt für Geologie und Paläontologie Teil **I**, Heft 11-12, p. 1285-1324.

Hancox, P.J., Brandt, D., Reimold, W.U., Koeberl, C. and Neveling, J. (2002). Permian-Triassic boundary in the northwest Karoo Basin: Current stratigraphic placement, implications for basin development models, and search for evidence of impact. *In* Catastrophic Events and Mass Extinctions: Impacts and Beyond (C. Koeberl and K.G. MacLeod, eds.). Geological Society of America Special Paper **356**, p. 429-444.

Hayward, C.L. (1998). Cathodoluminescence of ore and gangue minerals and its application in the minerals industry. *In* Modern Approaches to Ore and Environmental Mineralogy (L.J. Cabri and D.J. Vaughan, eds.). Short Course Series **27**, Ottawa, Ontario 1998, p. 269-325.

Heller, F., Haihong, C., Dobson, J. and Haag, M. (1995). Permian-Triassic magnetostratigraphy – new results from South China. Physics of the Earth and Planetary Interiors **89**, p. 281-295.

Heymann, D., Chibante, L.P.F., Brooks, R.R., Wolbach, W.S., Smit, J., Korochantsev, A., Nazarov, M.A. and Smalley, R.E. (1996). Fullerenes of possible wildfire origin in Cretaceous-Tertiary boundary sediments. *In* The Cretaceous-Tertiary event and other catastrophes in Earth history. (G. Ryder, D. Fastovsky and S. Gartner, eds.). Geological Society of America Special Paper **307**, p. 453-464.

Hildebrand, A.R., Penfield, G.T., Kring, D.A., Pilkington, M., Camargo Z, A., Jacobsen, S.B. and Boynton, W.V. (1991). Chicxulub crater: A possible Cretaceous/Tertiary boundary impact crater on the Yucatán Peninsula, Mexico. Geology **19**, p. 867-871.

Hotinski, R.M., Bice, K.L., Kump, L.R., Najjar, R.G. and Arthur, M.A. (2001). Ocean stagnation and end-Permian anoxia. Geology **29**, p. 7-10.

Isozaki, Y. (1997). Permo-Triassic Boundary superanoxia and stratified superocean: Records from lost deep sea. Science **276**, p. 235-238.

Isozaki, Y. (2001). An extraterrestrial impact at the Permian-Triassic boundary? Science **293,** p. 2343a.

Ivanov, B.A. and Melosh, H.J. (2003). Impacts do not initiate volcanic eruptions: Eruptions close to the crater. Geology **31**, p. 869-872.

Jarosewich, E., Clarke, R.S. Jr. and Barrows, J.N. (eds.) (1987). The Allende meteorite reference sample. Smithsonian Contribution to Earth Science **27**, p. 1-49.

Jin, Y.G., Wang, Y., Wang, W., Shang, Q.H., Cao, C.Q. and Erwin, D.H. (2000). Pattern of marine mass extinction near the Permian-Triassic boundary in South China. Science **289**, p. 432-436.

Johnson, M.R. (1991). Sandstone petrography, provenance and plate tectonic setting in Gondwana context of the south-eastern Cape Karoo Basin. South African Journal of Geology **94**, p. 137-154.

Johnson, M.R. (ed.) (1994). Lexicon of South African Stratigraphy. Part 1: Phanerozoic Units. Council for Geoscience, South Africa, 56 pp.

Jones, A.P., Price, G.D., Price, N.J., DeCarli, P.S. and Clegg, R.A. (2002). Impact induced melting and the development of large igneous provinces. Earth and Planetary Science Letters **202**, p. 551-561.

Kaiho, K., Kajiwara, Y., Nakano, T., Miura, Y., Kawahata, H., Tazaki, K., Ueshima, M., Chen, Z. and Shi, G.R. (2001). End-Permian catastrophe by a bolide impact: Evidence of a gigantic release of sulfur from the mantle. Geology **29**, p. 815-818.

Kamo., S.L., Czamanske, G.K., Amelin, Y., Fedorenko, V.A., Davis, D.W. and Trofimov, V.R. (2003). Rapid eruption of Siberian flood-volcanic rocks and evidence for coincidence with Permian-Triassic boundary and mass extinction at 251 Ma. Earth and Planetary Science Letters **214**, p. 75-91.

Kearey, P. and Vine, F.J. (1996). Global Tectonics. Second Edition, Blackwell Science, Oxford, 333 pp.

Keller, G., Adatte, T., Stinnesbeck, W., Rebolledo-Vieyra, M., Fucugauchi, J.U., Kramar, U. and Stüben, D. (2004). Chicxulub impact predates the K-T boundary mass extinction. Proceedings of the National Academy of Science of the United States of America **101**, p. 3753–3758.

Kerr, R.A. (2004). Evidence of huge, deadly impact found off Australian Coast? Science **304**, p. 941.

King, G.M. (1990). Dicynodonts and the end Permian event. Palaeontologia Africana **27**, p. 31-39.

Kirschvink, J.L. and Ward, P.D. (1998). Magnetostratigraphy of Permian/Triassic boundary sediments in the Karoo of southern Africa. Journal of African Earth Sciences **27**, p. 124.

Kitching, J.W. (1977). The distribution of the Karroo vertebrate fauna. Bernard Price Institute Palaeontological Research, Memoir **1**, 131 pp.

Knoll, A.H., Bambach, R.K., Canfield, D.E. and Grotzinger, J.P. (1996). Comparative earth history and Late Permian mass extinction. Science **273**, p. 452-457.

Koeberl, C. (1993). Instrumental neutron activation analysis of geochemical and cosmochemical samples: A fast and reliable method for small sample analysis. Journal of Radioanalytical and Nuclear Chemistry **168**, p. 47-60.

Koeberl, C. (1994). Neutron Activation Analysis. *In* Advanced Mineralogy, Volume 2 Methods and Instrumentations: Results and Recent Developments (A.S. Marfunin, ed.). Springer Verlag, Berlin. p. 322-329.

Koeberl, C., Gilmour, I., Reimold, W.U., Claeys, P. and Ivanov, B. (2002). End-Permian catastrophe by bolide impact: Evidence of gigantic release of sulfur from the mantle: Comment. Geology **30**, p. 855-856.

Koeberl, C., Farley, K.A., Peucker-Ehrenbrink, B. and Sephton, M.A. (2004). Geochemistry of the end-Permian extinction event in Austria and Italy: No evidence for an extraterrestrial component. Geology **32**, p. 1053-1056.

Krull, E.S. and Retallack, G.J. (2000). $\delta^{13}C_{org}$ depth profiles from paleosols across the Permian-Triassic boundary: Evidence for methane release. Geological Society of America Bulletin **112**, p. 1459-1472.

Krull, E.S., Retallack, G.J., Campbell, H.J. and Lyon, G.L. (2000). $\delta^{13}C_{org}$ chemostratigraphy of the Permian-Triassic boundary in the Maitai Group, New Zealand: Evidence for high-latitudinal methane release. New Zealand Journal of Geology and Geophysics **43**, p. 21-32.

Krull, E.S., Lehrmann, D.J, Druke, D., Kessel, B., Yu, Y. and Li, R., (2004). Stable carbon isotope stratigraphy across the Permian-Triassic boundary in shallow marine carbonate platforms, Nanpanjiang Basin, South China. Palaeogeography, Palaeoclimatology, Palaeoecology **204**, p. 297-315.

Kump, L.R., Arthur, M.A., Patzkowsky, M.E., Gibbs, M.T., Pinkus, D.S. and Sheehan, P.M. (1999). A weathering hypothesis for glaciation at high atmospheric pCO_2 during the Late Ordovician. Palaeogeography, Palaeoclimatology, Palaeoecology **152**, p. 173-187.

Kvenvolden, K.A. (1998). A primer on the geological occurrence of gas hydrate. Geological Society of London Special Publication **137**, p. 9-30.

Leroux, H., Reimold, W.U. and Doukhan, J.-C (1994). A T.E.M. investigation of shock metamorphism in quartz from the Vredefort Dome, South Africa. Tectonophysics **230**, p. 223-239.

Looy, C.V., Twitchett, R.J., Dilcher, D.L., Van Konijnenburg-Van Cittert, J.H.A. and Visscher, H. (2000). Life in the end-Permian dead zone. Proceedings of the National Academy of Science of the United States of America **98**, p. 7879-7883.

Lozovsky, V.R. (1998). The Permian-Triassic boundary in the continental series of Eurasia. Palaeogeography, Palaeoclimatology, Palaeoecology **143**, p. 273-283.

MacLeod, K.G., Smith, R.M.H., Koch, P.L. and Ward, P.D. (2000). Timing of mammal-like reptile extinctions across the Permian-Triassic boundary in South Africa. Geology **28**, p. 227-230.

MacRae, C.S. (1999). Life Etched in Stone: Fossils of South Africa. The Geological Society of South Africa, Johannesburg, 305 pp.

Mader, D. (1990). Palaeoecology of the Flora in Buntsandstein and Keuper in the Triassic of Middle Europe. G. Fisher, Hannover, 1687 pp.

Maruoka, T., Koeberl, C., Hancox, P.J. and Reimold, W.U. (2003). Sulfur geochemistry across a terrestrial Permian-Triassic boundary section in the Karoo Basin, South Africa. Earth and Planetary Science Letters **206**, p. 101-117.

Matsumato, R. (1995). Causes of the $\delta^{13}C$ anomalies of carbonates and a new paradigm 'Gas Hydrate Hypothesis'. Journal of the Geological Society of Japan **101**, p. 902-924.

McCartney, K., Huffman, A.R. and Tredoux, M. (1990). A paradigm for endogenous causation of mass extinctions. *In* Global Catastrophes in Earth History (V.L. Sharpton and P.D. Ward, eds.). Geological Society of America Special Paper **247**, p. 125-138.

McDonald, I., Irvine, G.J., de Vos, E., Gale, A.S. and Reimold, W.U. (2005). Geochemical search for impact signatures in possible impact-

generated units associated with the Jurassic-Cretaceous Boundary in southern England and northern France. *In* Biological Processes Associated with Impacts (C. Cockell, I. Gilmour and C. Koeberl, eds.). Impact Studies Series, Springer, Berlin (in press).

McLean, D.M. (1981). Cretaceous-Tertiary extinctions and possible terrestrial and extraterrestrial causes. Proceedings of K-TEC Group Workshop **39**, National Museums of Canada.

Meteoritics and Planetary Science (2004), **39**, issues 6 and 7.

Morante, R. (1996). Permian and Early Triassic isotopic records of carbon and strontium in Australia and a scenario of events about the Permian-Triassic boundary. Historical Biology **11**, p. 289-310.

Mory, A.J., Iasky, R.P., Glikson, A.Y. and Pirajino, F. (2000). Woodleigh, Carnarvon Basin, Western Australia: a new 120 km diameter impact structure. Earth and Planetary Science Letters **177**, p. 118-128.

Mundil, R., Ludwig, K.R., Metcalfe, I. and Renne, P.R. (2004). Age and timing of the Permian mass extinctions: U/Pb dating of closed-system zircons. Science **305**, p. 1760-1763.

Ogg, J.G., Hasenyager, R.W., Wimbledon, W.A., Channell, J.E.T. and Bralower, B. (1991). Magnetostratigraphy of the Jurassic-Cretaceous boundary interval, Tethyan and English faunal realms. Cretaceous Research **12**, p. 455-482.

O'Keefe, J.D. and Ahrens, T.J. (1989). Impact production of CO_2 by the Cretaceous/Tertiary extinction bolide and the resultant heating of the Earth. Nature **338**, p. 247-249.

Olsen, P.E. (1999). Giant lava flows, mass extinctions, and mantle plumes. Science **284**, p. 604-605.

Olsen, P.E., Koeberl, C., Huber, H., Montanari, A., Fowell, S.J., Et-Touhami, M. and Kent, D.V. (2002). Continental Triassic-Jurassic boundary in central Pangea: Recent progress and discussion of an Ir anomaly. *In* Catastrophic Events and Mass Extinctions: Impacts and Beyond (C. Koeberl and K.G. MacLeod, eds.). Geological Society of America Special Paper **356**, p. 505-522.

Pálfy, J., Smith, P.L. and Mortensen, J.K. (2002). Dating the end-Triassic and Early Jurassic mass extinctions, correlative large igneous provinces, and isotopic events. *In* Catastrophic Events and Mass Extinctions: Impacts and Beyond (C. Koeberl and K.G. MacLeod, eds.). Geological Society of America Special Paper **356**, p. 523-532.

Petaev, M.I., Jacobsen, S.B., Basu, A.R. and Becker, L. (2004). Magnetic Fe, Si, Al-rich Impact Spherules from the P-Tr Boundary Layer at Graphite Peak, Antarctica. *In Lunar and Planetary Science XXXV*, Abstract #1216, Lunar and Planetary Institute, Houston (CD Rom).

Poort, R.J., Clement-Westerhof, J.A., Looy, C.V. and Visscher, H. (1997). Aspects of Permian palaeobotany and palynology. 17. Conifer extinction in Europe at the Permian-Triassic junction: Morphology, ultrastructure and geographic/stratigraphic distribution of *Nuskoisporites dulhuntyi*

(prepollen of *Ortiseia, Walchiaceae*). Reviews of Palaeobotany and Palynology **97**, p. 9-39.

Rampino, M.R. (1987). Impact cratering and flood basalt volcanism. Nature **327**, p. 468.

Rampino, M.R. (1992). A major Late Permian impact event on the Falkland Plateau. EOS (Transactions, American Geophysical Union) **73**, p. 336.

Rampino, M.R. (1999). Impact crises, mass extinctions and galactic dynamics: The case for a unified theory. *In* Large Meteorite Impacts and Planetary Evolution II (B.O. Dressler and V.L. Sharpton, eds.). Geological Society of America Special Paper **339**, p. 241-248.

Raup, D.M. and Sepkoski, J.J. Jr (1982). Mass extinctions in the marine fossil record. Science **215**, p. 1501-1503.

Raup, D.M. and Sepkoski, J.J. Jr (1986). Periodic extinction of families and genera. Science **231**, p. 833-836.

Reichow, M.K., Saunders, A.D., White, R.V., Pringle, M.S., Al'Mukhamedov, A.I., Medvedev, A.I. and Kirda, N.P. (2002). $^{40}Ar/^{39}Ar$ Dates from the West Siberian Basin: Siberian Flood Basalt Province Doubled. Science **296**, p. 1846-1849.

Reimold, W.U. and Koeberl, C. (2000). Comment on: "Woodleigh, Carnarvon Basin, Western Australia: a new 120 km diameter impact structure", by A.J. Mory, R.P. Iasky, A.Y. Glikson and F. Pirajino [Earth

Planet. Sci. Lett. **177** (2000), p. 118-128]. Earth and Planetary Science Letters **184**, p. 353-367.

Reimold, W.U., Kelley, S.P., Sherlock, S.C., Henkel, H. and Koeberl, C. (2005). Laser argon dating of melt breccias from the Siljan Impact Structure, Sweden: Implications for possible relationship to Late Devonian extinction events. Meteoritics and Planetary Science, (in press).

Renne, P.R., Zichao, Z., Richards, M.A., Black, M.T. and Basu, A.R. (1995). Synchrony and causal relations between Permian-Triassic boundary crises and Siberian Flood Volcanism. Science **269**, p.1413-1413.

Renne, P.R., Reimold, W.U., Koeberl, C., Hough, R. and Claeys, P. (2002). Comment on: "K-Ar evidence from illitic clays of a Late Devonian age for the 120 km diameter Woodleigh impact structure, Southern Carnarvon Basin, Western Australia", by I.T. Uysal, S.D. Golding, A.Y. Glikson, A.J. Mory and M. Glikson [Earth Planet. Sci. Lett. 192 (2001) 218-289]. Earth and Planetary Science Letters **201**, p. 247-252.

Renne, P.R., Melosh, H.J., Farley, K.A., Reimold, W.U., Koeberl, C., Rampino, M.R., Kelley, S.P. and Ivanov, B.A. (2004). Is Bedout an Impact Crater? Take 2. Science **306**, p. 610-612.

Retallack, G.J. (1997). A colour guide to paleosols. Wiley, Chichester, England, 175 pp.

Retallack, G.J. (1999). Postapocalyptic greenhouse paleoclimate revealed by earliest Triassic paleosols in the Sydney basin, Australia. Geological Society of America Special Bulletin **111**, p. 52-70.

Retallack, G.J. (2003). Soils and global change in the carbon cycle over geological time. *In* Treatise on Geochemistry Volume 5 (J. I. Denver, ed.). Surface and Ground Water, Weathering, and Soils, p. 581–605.

Retallack, G.J. and Krull, E.S. (1999). Landscape ecological shift at the Permian-Triassic boundary in Antarctica. Australian Journal of Earth Sciences **46**, p. 785-812.

Retallack, G.J., Seyedolali, A., Krull, E.S., Holser, W.T., Ambers, C.P. and Kyte, F.T. (1998). Search for evidence of impact at the Permian-Triassic boundary in Antarctica and Australia. Geology **26**, p. 979-982.

Retallack, G.J., Smith, R.M.H. and Ward, P.D. (2003). Vertebrate extinction across Permian-Triassic boundary in Karoo Basin, South Africa. Geological Society of America Bulletin **115**, p. 1133-1152.

Rollinson, H.R. (1993). Using Geochemical Data: Evaluation, Presentation and Interpretation. Longman Group UK Limited, Oxford, 352 pp.

Rubidge, B.S. (ed.) (1995). Biostratigraphy of the Beaufort Group (Karoo Supergroup), South Africa. South African Committee for Stratigraphy Biostratigraphic Series **1**, 45 pp.

Rubidge, B.S. and Hancox, P.J. (1999). The Karoo – A Palaeontological Wonderland. *In* An Introduction to South Africa's Geological and Mining Heritage (M.J. Viljoen and W.U. Reimold, eds.). Geological Society of South Africa and Mintek, Randburg, p. 83-91.

Sandberg, C.A., Morrow, J.R. and Ziegler, W. (2002). Late Devonian sea-level changes, catastrophic events, and mass extinctions. *In* Catastrophic Events and Mass Extinctions: Impacts and Beyond (C. Koeberl and K.G. MacLeod, eds.). Geological Society of America Special Paper **356**, p. 473-488.

Schindewolf, O.H. (1954). Über die möglichen Ursachen der grossen erdgeschichtlichen Faunenschnitte. Neues Jahrbuch für Geologie end Paläontologie Monatshefte, p. 457-465.

Sephton, M.A., Amor, K., Franchi, I.A., Wignall, P.B., Newton, R. and Zonneveld, J-P. (2002). Carbon and nitrogen isotope disturbances and an end-Norian (Late Triassic) extinction event. Geology **30**, p. 1119-1122.

Sepkoski, J.J. Jr (1986). Phanerozoic overview of mass extinctions *in* Patterns and processes in the history of life (D.M. Raup and D. Jablonski, eds.). Springer-Verlag, Berlin, p. 277-295.

Shukolyukov, A., Lugmair, G.W., Becker, L., Macisaac, C. and Poreda, R. (2004). Extraterrestrial chromium in the Permian-Triassic boundary at Graphite Peak, Antarctica. *In Lunar and Planetary Science XXXV*, Abstract #1875, Lunar and Planetary Institute, Houston (CD Rom).

Smit, J. (1981). A catastrophic event at the Cretaceous Tertiary boundary. PhD dissertation (unpubl.), University of Amsterdam, Holland.

Smit, J. (1990). Meteorite impact, extinctions and the Cretaceous Tertiary boundary. Geologie en Mijnbouw **69**, p. 187-204.

Smit, J., Van der Gaast, S. and Lustenhouwer, W. (2004). Is the transition impact to post-impact rock complete? Some remarks based on XRF scanning, electron microprobe, and thin section analyses of the Yaxcopoil-1 core in the Chicxulub crater. Meteoritics & Planetary Science **39**, p. 1113–1126.

Smith, R.M.H. (1993). Vertebrate taphonomy of Late Permian floodplain deposits in the southwestern Karoo Basin of South Africa. Palaios **8**, p.45-67.

Smith, R.M.H. (1995). Changing fluvial environments across the Permian-Triassic boundary in the Karoo Basin, South Africa, and possible causes of tetrapod extinctions. Palaeogeography, Palaeoclimatology, Palaeoecology **117**, p. 81-104.

Smith, R.M.H. and Ward P.D. (2001). Pattern of vertebrate extinctions across an event bed at the Permian-Triassic boundary in the Karoo Basin of South Africa. Geology **29**, p. 1147-1150.

South African Committee for Stratigraphy (SACS) (1980). Stratigraphy of South Africa. Part I (Compiler L.E. Kent), Lithostratigraphy of the Republic of South Africa, South Waest-Africa/Namibia, and the Republics of Bophuthatswana, Transkei, and Venda. Geological Survey South Africa Handbook **8**, 690 pp.

Steiner, M.B., Ogg, J., Zhang, Z. and Sun, S. (1989). The Late Permian/Early Triassic magnetic polarity time scale and plate motions of South China. Journal of Geophysical Research **94**, p. 7343–7363.

Steiner, M.B., Eshet, Y., Rampino, M.R. and Schwindt, D.M. (2003). Fungal abundance spike and the Permian-Triassic boundary in the Karoo Supergroup (South Africa). Palaeogeography, Palaeoclimatology, Palaeoecology **3036**, p. 1-10.

Stöffler, D. and Langenhorst, F. (1994). Shock metamorphism of quartz in nature and experiment: I. Basic observation and theory. Meteoritics **29**, p. 155-181.

Suttner, L.J. and Dutta, P.K. (1986). Alluvial sandstone composition and palaeoclimate. I Framework mineralogy. Journal of Sedimentary Petrology **56**, p. 329-345.

Tanner, L.H., Lucas, S.G. and Chapman, M.G. (2004). Assessing the record and causes of Late Triassic extinctions. Earth-Science Reviews **65**, p. 103-139.

Taylor, S.R. and McLennan, S.M. (1985). The Continental Crust: Its Composition and Evolution. Blackwell, Oxford, 312 pp.

Thackeray, J.F., van der Merwe, N.J., Lee-Thorpe, J.A., Sillen, A., Lanham, J.L., Smith, R.M.H., Keyser, A. and Monteiro, P.M.S. (1990). Changes in carbon isotope ratios in the Late Permian recorded in therapsid tooth apatite. Nature **347**, p. 751-753.

Twitchett, R.J., Looy, C.V., Morante, R., Visscher, H. and Wignall, P.B. (2001). Rapid and synchronous collapse of marine and terrestrial ecosystems during the end-Permian biotic crisis. Geology **29**, p. 351-354.

Uysal, I.T., Golding, S.D., Glikson, A.Y., Mory, A.J. and Glikson, M. (2001). K-Ar evidence from illitic clays of a Late Devonian age for the 120 km diameter Woodleigh impact structure, Southern Carnarvon Basin, Western Australia. Earth and Planetary Science Letters **192**, p. 218-289.

Visscher, H., Brinkhuis, H., Dilcher, D.L., Elsik, W.C., Eshet, Y., Looy, C.V, Rampino, M.R. and Traverse, A. (1996). The terminal Paleozoic fungal event: Evidence of terrestrial ecosystem destabilization and collapse. Proceedings of the National Academy of Science of the United States of America **93**, p. 2155-2158.

Vogt, P.R. (1972). Evidence for global synchronism in mantle plume convection, and possible significance for geology. Nature **240**, p. 338-342.

Wang, K., Geldsetzer, H.H.J. and Krouse, H.R. (1994). Permian-Triassic extinction: Organic $\delta^{13}C$ evidence from British Columbia, Canada. Geology **22**, p. 580-584.

Ward, P.D. (2004). The Greatest Catastrophe on Earth. Astrobiology Magazine **17**, 5 pp.

Ward, P.D., Montgomery, D.R. and Smith, R.M.H. (2000). Altered river morphology in South Africa related to the Permian-Triassic extinction. Science **289**, p. 1740-1743.

Ward, P.D., Botha, J., Buick, R., de Kock, M.O., Erwin, D.H., Garrison, G.H., Kirschvink, J.L. and Smith, R. (2005). Abrupt and gradual extinction among Late Permian land vertebrates in the Karoo Basin, South Africa. Science **307**, p. 709-714.

Weidlich, O., Kiessling, W. and Flügel, E. (2003). Permian-Triassic boundary interval as a model for forcing marine ecosystem collapse by long-term atmospheric oxygen drop. Geology **31**, p. 961-964.

White, R.V. (2002). Earth's biggest 'whodunnit': unraveling the clues in the case of the end-Permian mass extinction. Philosophical Transactions of the Royal Society London A **360**, p. 2963-2985.

White, R.V. and Saunders, A.D. (2005). Volcanism, impact and mass extinctions: incredible or credible coincidences? Lithos **79**, p. 299-316.

Wignall, P.B. (2001). Large igneous provinces and mass extinctions. Earth-Science Reviews **53**, p. 1-33.

Wignall, P.B. and Twitchett, R.J. (1996). Oceanic anoxia and the End Permian mass extinction. Science **272**, p. 1155-1158.

Wignall, P.B. and Twitchett, R.J. (2002). Extent, duration, and nature of the Permian-Triassic superanoxic event. *In* Catastrophic Events and Mass Extinctions: Impacts and Beyond (C. Koeberl and K.G. MacLeod, eds.). Geological Society of America Special Paper **356**, p. 395-413.

Yanagisawa, F. and Sakai, H. (1983). Thermal decomposition of barium sulfate-vanadium pentaoxide-silica glass mixtures for preparation of sulfur dioxide in sulfur isotope ratio measurements. Analytical Chemistry **55**, p. 985-987.

Yang, Z.Y., Sheng, J.Z. and Yin, H.F. (1996). The Permian-Triassic boundary: Global stratotype section and point (GSSP). Episodes **18**, p. 49-53.

Yin, H., Sweet, W.C., Glenister, B.F., Kotlyar, G., Kozur, H., Newell, N.D., Sheng, J.Y. and Zakharov, Y.D. (1996). Recommendations of the Meishan section as global stratotype section and point for basal boundary of Triassic system. Newsletter of Stratigraphy **34**, p. 81-108.

Appendix One

Commando Drift Dam Section:
Geochemical Data

Appendix Two

Wapadsberg Section:
Geochemical Data

Appendix Three

Conference Abstracts Related to the Project

Lunar and Planetary Science XXXV,
Houston, Texas, U.S.A.
15 – 19 March, 2004

Coney, L., Reimold, W.U., Hancox, P.J. and Koeberl, C. (2004). A mineralogical and geochemical study of the nonmarine Permian-Triassic boundary in the southern Karoo Basin, South Africa. *In Lunar and Planetary Science XXXV*, Abstract #1488, Lunar and Planetary Institute, Houston (CD Rom).

A MINERALOGICAL AND GEOCHEMICAL STUDY OF THE NONMARINE PERMIAN-TRIASSIC BOUNDARY IN THE SOUTHERN KAROO BASIN, SOUTH AFRICA L.Coney[1], W.U. Reimold[1], P.J. Hancox[1], and C. Koeberl[2] [1]Impact Cratering Research Group, School of Geosciences, Univ. Witwatersrand, Private Bag 3, Johannesburg, Wits 2050, South Africa; [2]Dept. of Geological Sciences, University of Vienna, A-1090 Vienna, Austria (ConeyL@science.pg.wits.ac.za)

Summary: Mineralogical and geochemical investigations across two nonmarine Permian-Triassic (P/Tr) boundary sections in the southern part of the main Karoo Basin have been undertaken in order to aid in our understanding of this complex extinction event.

Introduction: The end-Permian (251.4 ± 0.1 Ma) mass extinction is universally acknowledged as the most consequential of the five major Phanerozoic mass extinctions. More than 90% of marine species, ~70% of terrestrial vertebrates and ~90% of plant life were lost in a very short timespan [1,2]. The nature of the P/Tr boundary and the cause of the mass extinction have been the subject of international debate. Possible causes for the P/Tr extinction include: asteroid/comet impact; environmental change; oceanic anoxia or overturn; volcanism and synergistic combinations of the above [3]. Occurrences of planar deformation features in quartz in Australian and Antarctic sections have been reported [4] but not yet confirmed. Iridium concentrations do not show a clear anomaly as seen in K/T boundary sections. A $\delta^{13}C$ negative excursion has been seen to accompany some inconsistent Iridium anomalies in marine sections [1]. Becker et al. [5] supposedly found evidence for impact, but this has been solidly refuted [6,7]. Kaiho et al. [8] used the coincidence of sulphur and strontium isotopic data and strange metallic grains to suggest the event was caused by impact-triggered release of mantle-derived sulphur and strontium, but this was rejected by Koeberl et al. [9] based on a number of different arguments. Evidence proposed for an exogenic play at the P/Tr boundary therefore remains contentious.

Evidence for a volcanic cause includes the eruption of the Siberian Flood Basalts at the time of the mass extinction [10,11]. The eruptions would have introduced large volumes of carbon dioxide and sulphide/ate [11] into the atmosphere, which could have triggered extensive acid rain [16]. The observed $\delta^{13}C$ excursion could have been caused by rapid release of methane or carbon dioxide coincident with the volcanic event.

The boundary is now well documented in the marine realm, however far less is known about the pattern and duration of the extinction event in the nonmarine realm, and as to whether these events are truly synchronous.

The Karoo Basin, South Africa: The Karoo Basin is a large retro-arc foreland basin which accumulated sediment from the Carboniferous (300 Ma) through to the Early Jurassic (180 Ma) in southwestern Gondwana. The Karoo Basin also preserves a largely uninterrupted 100 million year palaeontological record which has aided in the biostratigraphic subdivision of the sequence. From the end of the Middle Permian on, deposition in the Karoo Basin was puerely nonmarine[12], and the basin preserves a number of P/Tr boundary sections. Hancox et al. [13] have shown that the extinction event in the north of the boundary is marked by an erosional unconformity, however the sequence is temporally complete in the southern, more proximal reaches of the basin.

Historically the P/Tr boundary in the Karoo Basin has been placed biostratigraphically at the contact between the *Dicynodon* and *Lystrosaurus* Assemblage Zones [14], however Smith and Ward [2] have shown that the boundary is better placed at the Last Appearance Datum (LAD) of *Dicynodon*. This is because the First Appearance Datum (FAD) of *Lystrosaurus* actually occurs in the Permian. Ward et al. [3] have also documented a change in fluvial style across the boundary. A changeover in climate from an arid and highly seasonal (Permian) to semi-arid and less seasonal (Triassic) climate has been proposed on the basis of observations of palaeosol types in sections crossing the boundary in the Karoo Basin [15]. This is, however, in contrast to Smith [16], who believed the changeover marked a general drying of the floodplain. Coupled with changes in the carbon isotopes this may indicate a greenhouse-effect following the mass extinction. Previous authors have documented a synchronous global negative shift in carbon isotopic composition [18], however other authors [19] question this.

Recently, a section at Commandodrift Dam in the southern Karoo Basin has given reliable palaeomagnetic signatures [20], with a reversed-normal magnetic signal present, which co-incides with the palaeontologically defined boundary at this locality.

This study: Due to the uncertainty regarding the nature of the mineralogical and geochemical signatures across the P/Tr boundary in the Karoo Basin, two sections were sampled in the southern Karoo Basin where the sequence is most temporally complete. The first section was sampled across the interval of DeKock's [20] study, and the second across a palaeontologically constrained boundary section at Wapadsberg.

Samples were taken at 2 cm intervals in the metre below and above the boundary, and in 25 to 50 cm

intervals for the rocks below and above these. Geochemical analysis of the samples was done by XRF Spectrometry and INAA for major and trace elements, and mass spectrometry for carbon isotopes. Petrographic work is still in progress.

Lithological results: Both sections straddle the stratigraphic interval between the uppermost Palingkloof Member of the Balfour Formation and the lowermost part of the Katberg Formation. The lower part of the sequence is dominated by drab greenish-grey fines with smooth surfaced carbonate nodule horizons, and lenticular sandstone bodies that document a predominantly meandering environment. At both sections the end of the Permian is marked by palaeosol development, and a laminated mudrock layer (referred to as an event bed by Smith and Ward [2]). Above this event horizon, the fines become redder and the sandstones more laterally continuous with gutter cast erosional bases, documenting a change in fluvial style to one of a lower sinuosity.

Geochemical results: The carbonate nodular horizons in the lower part of the sequence are clearly indicated by the geochemical data, where increases in CaO are seen, with corresponding decreases in SiO_2 and Al_2O_3. For the Commandodrift Dam section, siderophile elements and Fe_2O_3 show the most variation, increasing in concentration where the mudrocks change colour from greenish-blue to red, indicating a more oxidizing, or a more Fe-rich environment (see Figure 1). This is not observed in the Wapadsberg section. The Fe_2O_3 concentrations decrease once the rocks change lithology back to sandstones, and then it increases once again when more mudstones are encountered. The trace elements are far more variable, with Cu concentrations increasing substantially (by ~10 ppm) at the proposed boundary site at Commandodrift Dam and slightly above it at Wapadsberg. Ni also shows an increase from approximately 15 ppm to 27 ppm; this remains high for the next 48 cm, and then decreases to 11 ppm, once sandstones are encountered in both sections. Co contents show irregular variations with no major increases or decreases for any particular lithology. Iridium values (by INAA) are below the detection limit for almost all samples and no Ir anomaly is observed for the sections studied.

Discussion and Conclusion: The change in colour and nature of the paleosols across the boundary in the southwestern Karoo basin observed by Retallack et al. [15], from red to greenish grey, is the same as seen in the Commandodrift Dam section. Increasingly quartz-rich compositions following the boundary are seen, indicating increasing chemical weathering, and this observation corresponds to the findings of Retallack et al. [15], as well as Hancox et al. [12] in the northern basin near Senekal. The suggestion of extinction by the degassing of methane from shallow marine and permafrost clathrates, supported by [15], cannot be confirmed in our study. The geochemical results for the two sections are inconclusive with regard to a dramatic change in environmental conditions at the P/Tr boundary as chemical characteristics below and above the palaeontologically and palaeomagnetically defined boundary seem to be similar, with the only chemical difference caused by the local presence of carbonate nodules.

Acknowledgements: This work is funded through the Palaeo-Anthropology Scientific Trust (PAST), the Geological Society of South Africa, and the Barringer Family Fund for Meteorite Impact Research. Analytical work in Vienna was supported by the Austrian FWF, project Y58-GEO (to CK).

References:[1] Jin, Y.G. et al. (2000) *Science 289*, 432-435. [2] Smith, R.M.H. and Ward P.D. (2001) Geology *29*, 1147-1150. [3] Ward, P.D. et al. (2000) *Science, 289,*1740-1743. [4] Retallack, G.J. et al. (1998) Geology *26*, 979-982. [5] Becker, L. et al. (2001) Science *291*, 1530. [6] Farley, K.A. and Mukhopadhyay, S. (2001) Science *293*, 2343a. [7] Isozaki, Y. (2001) Science *293*, 2343a. [8] Kaiho, K. et al. (2001) Geology *29*, 815-818. [9] Koeberl, C. et al. (2001) Geology 30, 855-856. [10] Erwin, D. H. (2000) Catastrophic Events Conference, LPI Contrib. No. *1053*, 43-44. [11] Kamo, S.L. et al. (2003), EPSL *6737*, 1-17. [12] Hancox, P.J. (2000) Zbl. Geol. Paläont. Teil. *I*, 1285-1324. [13] Hancox, P.J. et al. (2002) Spec. Paper GSA *356*, 429-444. [14] Rubidge, B.S., ed., (1995) SACS Biostrat. Series *1*, 45p. [15] Retallack et al. (2003) GSABulletin *115*, 1133-1152. [16] Maruoka, T. et al. (2003) EPSL *206*, 101-117. [17] Smith, R.M.H. (1995) PPP 117, 81-104. [18] Sephton, M.A. (2002) GSA Spec. Paper *356*, 455-462. [19] de Wit, M.J. et al. (2002) J. Geology *110*, 227-240. [20] de Kock, M.O and Kirschvink, J.L., Gondwanian Research, in press.

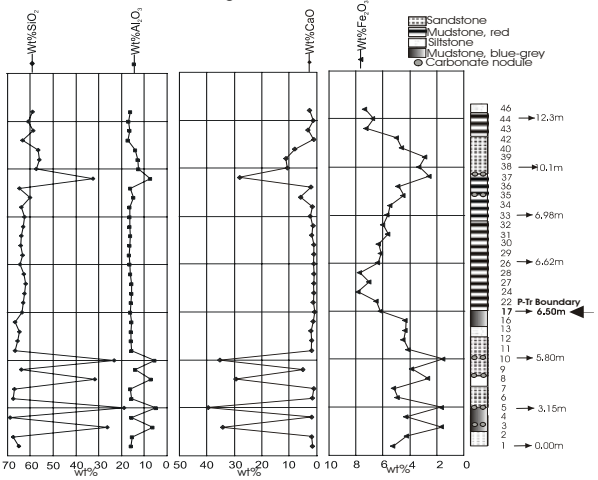


Figure 1

Geoscience Africa 2004,
Johannesburg, South Africa
12 - 16 July, 2004

Coney, L., Reimold, W.U., Hancox, P.J. and Koeberl, C. (2004). A mineralogical and geochemical investigation of the continental Permian-Triassic boundary in the southern Karoo Basin, South Africa. Geoscience Africa 2004, Abstract Volume, University of the Witwatersrand, Johannesburg, South Africa, pp. 132-134

A MINERALOGICAL AND GEOCHEMICAL INVESTIGATION OF THE CONTINENTAL PERMIAN-TRIASSIC BOUNDARY IN THE SOUTHERN KAROO BASIN, SOUTH AFRICA. L. Coney[1] , W.U. Reimold[1], P.J. Hancox[1] and C. Koeberl[2], [1]Impact Cratering Research Group, School of Geosciences, University of the Witwatersrand, Private Bag 3, Johannesburg, Wits 2050, South Africa, ConeyL@science.pg.wits.ac.za [2]Dept of Geological Sciences, University of Vienna, A-1090 Vienna, Austria.

Summary: Mineralogical and geochemical investigations across two nonmarine Permian-Triassic (P/Tr) boundary sections in the southern part of the main Karoo Basin have been undertaken in order to aid in our understanding of the P/Tr extinction event.

Introduction: The end-Permian (251.4 ± 0.1 Ma) mass extinction is universally acknowledged as the most consequential of the five major Phanerozoic mass extinctions. More than 90% of marine species, ~70% of terrestrial vertebrates and ~90% of plant life were lost in a very short timespan [1,2]. The nature of the P/Tr boundary and the cause of the mass extinction have been the subject of international debate. Possible causes for the P/Tr extinction include: asteroid/comet impact; environmental change; oceanic anoxia or overturn; volcanism and synergistic combinations of the above [3]. Occurrences of planar deformation features in quartz in Australian and Antarctic sections have been reported [4] but not yet confirmed. Iridium concentrations do not show a clear anomaly as seen in K/T boundary sections. A $\delta^{13}C$ negative excursion has been seen to accompany some inconsistent Iridium anomalies in marine sections [1]. Becker et al. [5] supposedly found evidence for impact, but this has been solidly refuted [6,7]. Kaiho et al. [8] used the coincidence of sulphur and strontium isotopic data and strange metallic grains to suggest the event was caused by impact-triggered release of mantle-derived sulphur and strontium, but this was rejected by Koeberl et al. [9] based on a number of different arguments. Evidence proposed for an exogenic play at the P/Tr boundary therefore remains contentious.

Evidence for a volcanic cause includes the eruption of the Siberian Flood Basalts at the time of the mass extinction [10,11]. The eruptions would have introduced large volumes of carbon dioxide and sulphide/ate [11] into the atmosphere, which could have triggered extensive acid rain [16]. The observed $\delta^{13}C$ excursion could have been caused by rapid release of methane or carbon dioxide coincident with the volcanic event.

The boundary is now well documented in the marine realm, however far less is known about the pattern and duration of the extinction event in the nonmarine realm, and as to whether these events are truly synchronous.

The Karoo Basin, South Africa: The Karoo Basin is a large retro-arc foreland basin that accumulated sediment from the Carboniferous (300 Ma) through to the Early Jurassic (180 Ma) in southwestern Gondwana. The Karoo Basin also preserves a largely uninterrupted 100 million year palaeontological record, which has aided in the biostratigraphic subdivision of the sequence. From the end of the Middle Permian on, deposition in the Karoo Basin was purely nonmarine [12], and the basin preserves a number of continental P/Tr boundary sections. Hancox et al. [13] have shown that the extinction event in the north of the basin is marked by an erosional unconformity, however the sequence is temporally complete in the southern, more proximal reaches of the basin.

Historically the P/Tr boundary in the Karoo Basin has been placed biostratigraphically at the contact between the *Dicynodon* and *Lystrosaurus* Assemblage Zones [14], however Smith and Ward [2] have shown that the boundary is better placed at the Last Appearance Datum (LAD) of *Dicynodon*. This is because the First Appearance Datum (FAD) of *Lystrosaurus* actually occurs in the Permian. Ward et al. [3] have also documented a change in fluvial style across the boundary. A changeover in climate from an arid and highly seasonal (Permian) to semi-arid and less seasonal (Triassic) climate has been proposed on the basis of observations of palaeosol types in sections crossing the boundary in the Karoo Basin [15]. This is, however, in contrast to Smith [16], who believed the changeover marked a general drying of the floodplain. Coupled with changes in the carbon isotope systematics this may indicate a greenhouse effect following the mass extinction. Previous authors have documented a synchronous global negative shift in carbon isotopic composition [18], however other authors [19] question this.

Recently, a section at Commandodrift Dam in the southern Karoo Basin has given reliable palaeomagnetic signatures [20], with a reversed-normal magnetic signal present, which coincides with the palaeontologically defined boundary at this locality.

This study: Due to the uncertainty regarding the nature of the mineralogical and geochemical signatures across the P/Tr boundary in the Karoo Basin, two sections were sampled in the southern Karoo Basin where the sequence is most complete. The first section was sampled across the interval of De Kock's [20] study at Commandodrift Dam, and the second across a palaeontologically constrained boundary section at Wapadsberg.

Samples were taken at 2 cm intervals in the metre below and above the boundary, and in 25 to 50 cm

intervals for the rocks below and above these. Geochemical analysis of the samples was done by XRF spectrometry and INAA for major and trace elements, and mass spectrometry for carbon isotopes. Petrographic work is still in progress.

Lithological results: Both sections straddle the stratigraphic interval between the uppermost Palingkloof Member of the Balfour Formation and the lowermost part of the Katberg Formation. The lower part of the sequence is dominated by drab greenish-grey fines with smooth-surfaced carbonate nodule horizons, and lenticular sandstone bodies that document a predominantly meandering environment. At both sections the end of the Permian is marked by palaeosol development, and a laminated mudrock layer (referred to as an event bed by Smith and Ward [2]). Above this event horizon, the fines become redder and the sandstones more laterally continuous with gutter cast erosional bases, documenting a change in fluvial style to one of lower sinuosity.

Geochemical results: The carbonate nodular horizons in the lower part of the sequence are clearly indicated by the geochemical data, where increases in CaO are seen, with corresponding decreases in SiO_2 and Al_2O_3. For the Commandodrift Dam section, siderophile elements and Fe_2O_3 show the most variation, increasing in concentration where the mudrocks change colour from greenish-blue to red, indicating a more oxidizing, or a more Fe-rich environment (see Figure 1). This is not observed in the Wapadsberg section. The Fe_2O_3 concentrations decrease once the rocks change lithology back to sandstones, and then it increases once again when more mudstones are encountered. The trace elements are far more variable, with Cu concentrations increasing substantially (by ~10 ppm) at the proposed boundary site at Commandodrift Dam and slightly above it at Wapadsberg. Ni also shows an increase from approximately 15 ppm to 27 ppm; this remains high for the next 48 cm, and then decreases to 11 ppm, once sandstones are encountered in both sections. Co contents show irregular variations with no major increases or decreases for any particular lithology. Iridium values (by INAA) are below the detection limit for almost all samples; thus, no Ir anomaly is observed for the sections studied.

Discussion and Conclusion: The change in colour and nature of the paleosols across the boundary in the southwestern Karoo basin observed by Retallack et al. [15], from red to greenish grey, is the same as seen in the Commandodrift Dam section. Increasingly quartz-rich compositions following the boundary are seen, indicating increasing chemical weathering, and this observation corresponds to the findings of Retallack et al. [15], as well as of Hancox et al. [12] in the northern basin near Senekal. The suggestion of extinction by the degassing of methane from shallow marine and permafrost clathrates, supported by [15], cannot be confirmed in our study. The geochemical results for the two sections are inconclusive with regard to a dramatic change in environmental conditions at the P/Tr boundary as chemical characteristics below and above the palaeontologically and palaeomagnetically defined boundary seem to be similar, with the only chemical difference caused by the local presence of carbonate nodules.

Acknowledgements: This work is funded through grants from the Palaeo-Anthropology Scientific Trust (PAST), the National Research Foundation (NRF), the Geological Society of South Africa, and the Barringer Family Fund for Meteorite Impact Research. Analytical work in Vienna was supported by the Austrian FWF, project Y58-GEO (to CK).

References:[1] Jin, Y.G. et al. (2000) *Science 289*, 432-435. [2] Smith, R.M.H. and Ward P.D. (2001) Geology *29*, 1147-1150. [3] Ward, P.D. et al. (2000) *Science, 289,*1740-1743. [4] Retallack, G.J. et al. (1998) Geology *26*, 979-982. [5] Becker, L. et al. (2001) Science *291*, 1530. [6] Farley, K.A. and Mukhopadhyay, S. (2001) Science *293*, 2343a. [7] Isozaki, Y. (2001) Science *293*, 2343a. [8] Kaiho, K. et al. (2001) Geology *29*, 815-818. [9] Koeberl, C. et al. (2001) Geology 30, 855-856. [10] Erwin, D. H. (2000) Catastrophic Events Conference, LPI Contrib. No. *1053*, 43-44. [11] Kamo, S.L. et al. (2003), EPSL *6737*, 1-17. [12] Hancox, P.J. (2000) Zbl. Geol. Paläont. Teil. *I*, 1285-1324. [13] Hancox, P.J. et al. (2002) Spec. Paper GSA *356*, 429-444. [14] Rubidge, B.S., ed., (1995) SACS Biostrat. Series *1*, 45p. [15] Retallack et al. (2003) GSABulletin *115*, 1133-1152. [16] Maruoka, T. et al. (2003) EPSL *206*, 101-117. [17] Smith, R.M.H. (1995) PPP 117, 81-104. [18] Sephton, M.A. (2002) GSA Spec. Paper *356*, 455-462. [19] de Wit, M.J. et al. (2002) J. Geology *110*, 227-240. [20] de Kock, M.O and Kirschvink, J.L., Gondwana Research, in press.

A Mineralogical and Geochemical Investigation of the Continental Permian-Triassic Boundary in the Southern Karoo Basin, South Africa.

L. Coney, W.U. Reimold, P.J. Hancox and C. Koeberl

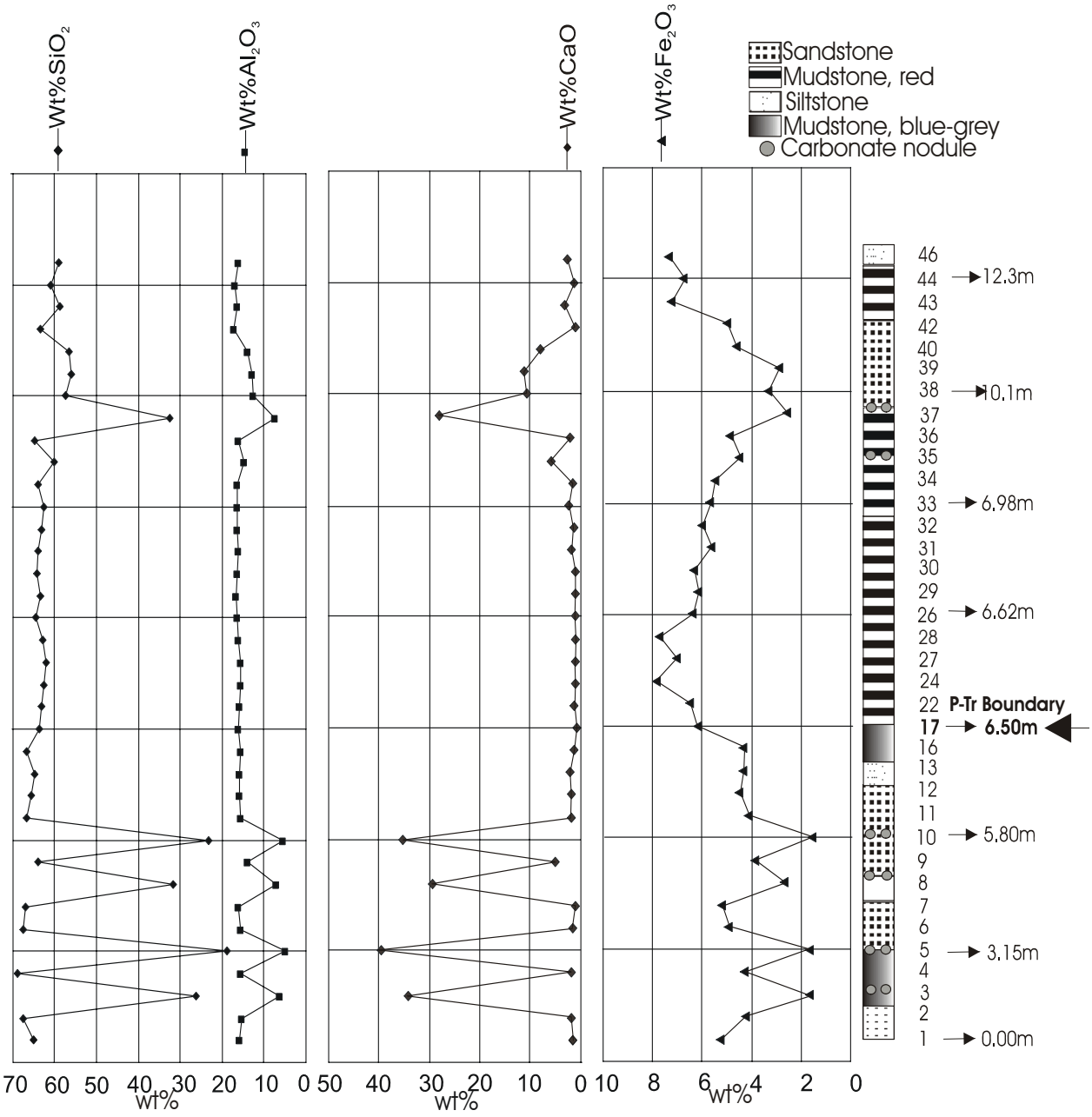


Figure 1: Geochemical Profiles across the P/Tr boundary section at Commandodrift Dam